FINAL REPORT

NASA NAG 5-328

Research Relative to Angular Distribution of Snow Reflectance / Snow Cover Characterization and Microwave Emission

Jeff Dozier — Principal Investigator
Robert E. Davis — Co-Principal Investigator

Center for Remote Sensing and Environmental Optics
University of California Santa Barbara
93106

Period: July 1, 1983 to Sept 30, 1987

INTRODUCTION

Remote sensing has been applied in recent years to monitoring snow cover properties for applications in hydrologic and energy balance modeling (e.g. Dozier, 1987). In addition, snow cover has been recently shown to exert a considerable local influence on weather variables (e.g. Namias, 1985; Dewey, 1987; Walsh, 1987). Of particular importance is the potential of sensors to provide data on the physical properties of snow with high spatial and temporal resolution. Visible and near-infrared measurements of upwelling radiance can be used to infer near-surface properties through the calculation of albedo. Microwave signals usually come from deeper within the snow pack and thus provide depth-integrated information, which can be measured through clouds and does not rely on solar illumination (Burke et al., 1984; Foster et al., 1984). Fundamental studies examining the influence of snow properties on signals from various parts of the electromagnetic spectrum continue in part because of the promise of new remote sensors with higher spectral and spatial accuracy. Information in the visible and near-infrared parts of the spectrum comprise nearly all of the available data with high spatial resolution. Current passive microwave sensors have poor spatial resolution and the data are problematic where the scenes consist of mixed landscape features, but they offer timely observations that are independent of cloud cover and solar illumination.

In interpreting remote sensing signals from snow, discrete scatterer models have been used with inferences about the connection between model parameters and the physical properties of the snow cover. Such models use Mie theory to describe the scattering and absorbing properties of the snow particles and radiative transfer theory to describe the radiation intensity field at various depths in the pack. Whereas these theoretical models treat the snow as homogeneous layers of spheres, the snow cover actually consists of layers of irregular grains, bonded to each other, and often separated by horizontal crusts and ice lenses. It is well known that the scattering and absorbing properties of a snow layer can be mimicked by selecting suitable sphere sizes. Much of our effort has been to obtain a set of data about the snow properties, microscopic and macroscopic, so that different characterizations of the snow cover can be tested.

Experimental Objectives

This report is the result of experimental study toward three objectives. Most of the work has proceeded concurrently except for the snow season 1986-1987, when no microwave measurements were taken.

1. Measure the Angular Variation of Spectral Reflection from Snow

All radiation of importance to the energy balance of a snow cover is contained in the spectral region (0.3–50 μm). In this study snow reflectance was measured for the visible and near-infrared wavelength range 0.3 to 1.1μm with two different instruments. Reflection from snow is moderately anisotropic, so measurements must be made at many view angles and azimuths, for a variety of sun angles. The variation

measuring the liquid water content of snow based on the dilution of fluorescing dye (Davis and Dozier, 1984).

As our confidence in measuring liquid water in snow and the energy budget of the pack rose (Davis et al., 1984; Davis et al., 1985; Perla et al., 1987), we began developing techniques to sample and observe undisturbed microstructure in snow, with the help of Dr. Ron Perla, Environment Canada. During the winter 1984-1985, samples of snow were collected during measurement scans of snow reflectance and microwave emission, returned to a cold room, and prepared for section analysis. This technique requires much practise and adaptation to a particular cold facility and equipment. Many data sets were collected using the slow-scan spectrometer over different snow and solar conditions. In addition, many sets of microwave data (at $35GHz$) were collected for a range of snow properties and snowpack structures using a hand-held radiometer borrowed from NASA/GSFC.

During the summer and fall 1985, the microwave data and stereological measurements of snow microstructure were analyzed and interpreted. This work resulted in the dissertation of Robert Davis, and publication of the findings (Davis, 1986; Davis et al., 1987). Also during this time it was determined that the scan time of the visible and near-infrared spectrometer was prohibitive to collecting a complete observation of snow reflectance for given illumination conditions. The scan rate for the instrument was twenty minutes, too long for the usual atmospheric changes at the Mammoth Mountain study plot. (See accompanying technical draft.)

In the winter, 1985-1986, the technique for measuring snow microstructure was improved substantially by introducing the pore filler then quick freezing the sample in the field, which reduces the chances of disturbing delicate snow structures. Data were obtained on many consecutive days so that the changes in near-surface snow microstructure were closely monitored with coincident reflectivity and energy balance data. Other improvements to the technique resulted in a few publications on methodology (Perla et al., 1986; Dozier et al., 1987a; Davis et al., 1987; Dozier et al., 1987b).

The angular distribution of solar reflectance was measured in April, 1986 using a new instrument borrowed from NASA/GSFC, and brought to Mammoth by Dr. Al Chang and Ken Brown of GSFC. Spectral data are acquired in 256 bands (wavelengths 0.4–1.1μm) and the integration time for a target like snow is less than a second. Although data were collected for only a short period of the season, the fast scan rate allowed many observations for a given snow condition.

The snow season at the Mammoth study plot started late in the 1986-1987 snow water year, with very little snow until mid-February. The instruments borrowed from NASA/GSFC arrived in late February, and radiometric measurements were collected from this time until mid-May, when the most of the snowpack had ablated. The AC power line to the site was cut by a snowcat in early March, which limited radiometric measurements because of limited battery power and prompted moving the site during the summer 1987. Snow property measurements were made from snow pits to guide the sampling for specimens for microstructure analysis. Results from analysis of stereologic measurements for the two winters were

presented at the 1987 Fall meeting of the American Geophysical Union and are presented herein. Results of the work on snow reflectance were presented the Fourth International Colloquim on Spectral Signatures in Remote Sensing and are also included in this report. Continuing work with this data set will examine near-surface grain growth in snow, its relationship to simple meteorologic parameters, and the albedo of snow.

Snow Cover Characteristics

All of the work reported here was performed on snow at a study plot where the pack remained undisturbed during the season, and there was little lateral variation in the snow cover over the plot. The snow study plot lies at about 2,900m on Mammoth Mountain, California on flat terrain, with relatively little vegetation. The site was instrumented for measuring the components of the energy balance over snow and the heat and mass budget in the snow pack (Davis et al., 1980, 1984). Snow properties other than temperature, settlement, and runoff were measured manually by visiting the site.

Modern theories on physical processes in snow require parameters describing the microstructure of snow as well as the classical measurements depth, density, etc. Snow is a network of ice grains interconnected in a complex structure whose properties are constantly changing as a strong function of density. However, the snow properties important to its radiometric response depend on the microstructure at any density (Mätzler et al., 1980; Colbeck, 1982). For discrete scatterer modeling the critical properties are the equivalent grain size and number density for dry snow, with the addition of the liquid water content for wet snow.

The assumption of isotropy of microstructural features – the arrangement, shape, and packing of snow crystals and pore space – in seasonal snow is common in modeling the transfer of radiation, heat, and water vapor. However, the microstructure of seasonal snow and firn may exhibit strong orientation, resulting from vertical temperature and vapor density gradients and from loading stresses. Bader et al. (1939) noticed that in shallow snow packs there might be some preferred orientation in the growth of individual particles and that the resultant three-dimensional patterns might be useful topics for future study (Bader, 1962). Keeler (1969) recognized that the fabric of snow, the mutual relationship between particles in the aggregate and the orientation of individual particles, is probably the single most fundamental property. Kry (1975) used measurements from section planes to analyze snow samples prepared by seiving snow into containers in the laboratory, and subjected to metamorphism at low temperature gradients. He reported that the assumption of isotropy of grain and grain bond location and orientation was satisfied to within 10 percent for equilibrium-metamorphosed snow in a density range of 270–340$Kg\ m^{-3}$. Slightly longer ice-intercept lengths were noted parallel to the direction of deformation, but these were disregarded in his analysis. Kry used randomly placed test grids on orthogonal planes prepared from the same sample, and therefore did not test directional dependence of stereological parameters.

Snow Pack Density

Profiles of density were measured with a 1000cm^3 cutter and an electronic top-loading balance. The empty cutter is tared on the balance so that the readout in grams converts easily to Kgm^{-3}. Four or more samples were taken for a given layer, usually at least 50cm apart, providing a meter-scale index of snow layer variability, and providing a check on the densities obtained from stereologic analysis. The densities obtained from the stereologic analysis were checked against the densities of the specimens prepared. The

density profiles in the field were measured every 10cm, and since the vertical dimensions of the cutter are the same, the profile data contains no gaps.

For two winter seasons, the average densities of the pack were sampled spatially to evaluate lateral variations of the snow cover. Measurements of average density were made with a Mt. Rose snow sampler, sometimes called a Federal sampler. A point sample of snow water equivalent is obtained from the net weight of the snow in the sample tube, and the average density from the quotient of the net weight divided by the depth. Examinations of the bias of the Mt. Rose sampler suggested by Letvak (1978) and carried out by Farnes et al., (1982) and this study show that the tube can have a positive bias of more than 10percent. Therefore, the measurements were calibrated with a snow pit the same day that samples were obtained from locations around the study site.

Liquid Water Content

Much effort has been spent developing techniques to measure snow wetness for correlation with microwave remote sensing data. Information is needed about the liquid mass or volume fraction and the shape of the liquid water inclusions. Measurement of the snow liquid water content in the field must be a quick and simple procedure to be successful. The two most promising principles for measuring snow wetness are direct measurement of the snow liquid water fraction and dielectric measurements in radio and microwave frequencies, relying on the sharp dielectric contrast between liquid water and ice (Colbeck, 1978). Currently all of the techniques in use involve destructive sampling, including the dielectric techniques (Denoth et al., 1984). Measurements of the structure of the liquid inclusions in snow have only been done by inference, using measurements of the real part of the dielectric constant and mixing or empirical formulae (Denoth, 1980, 1982).

Measurements of snow liquid water content were obtained using the dilution method. The dilution method has been refined and tested for accuracy and repeatability (Davis and Dozier, 1984; Perla and LaChapelle, 1984; Davis et al., 1985) and compared with freezing calorimetry, alcohol calorimetry, and a dielectric method (Boyne and Fisk, 1987). The tests show that the the methods are equivalent, but that the dilution method is the one of the most rapid, requiring about 5 minutes per sample,

The dilution method relies on the dilution of an aqueous solution when it is mixed with wet snow. The concentration change forms the basis for measurement. A stock solution of mass S and impurity concentration C_s is mixed thoroughly into a wet snow sample of mass M, with unknown water mass W. The solution is at 0°C and mixing is in an insulated container, so that melt or refreezing is minimized. The impurity concentration in the stock solution is small enough so that freezing point depression is negligible, but large enough to be well above the impurity concentration C_w in the liquid water in the snow sample. The mixture of stock solution and snow liquid water has impurity concentration C_m:

$$C_m = \frac{S\,C_s + W\,C_w}{S + W} \tag{1}$$

of snow albedo and emission is attributable to a number of parameters; size, shape and packing of the snow particles, the spectral and angular distribution of the propagating radiation field, the amount and distribution of impurities, departures from an optically thick homogeneous layer, and the liquid water content.

2. Quantify Snow Cover Characteristics

Because the response of snow to electromagnetic energy and thermodynamic gradients is controlled by the properties of the ice and water phases, most of the measurement effort was concentrated on analysis of snow properties, microstructure, stratigraphy and wetness. Stereological measurements were made from sections prepared from snow specimens, temperature profiles in the snow cover were monitored, snow wetness was measured, and the traditional snow pit observations were made (e.g. density). From these data we calculate: effective parameters for input to radiative transfer models, thermal properties to identify conditions governing metamorphic processes and thereby changes in radiative properties, and lateral variation in key parameters.

3. Measure the Angular Variation of Microwave Emission

The signal from snow in the microwave part of the spectrum contains information about the emissivity and volume scattering, which are controlled by the microscopic and macroscopic structure of the pack, and its liquid water content. This portion of the research was devoted to obtaining measurements of microwave emission of snow at 35 GHz. Measurements were acquired at a variety of angles at horizontal and vertical polarization during snow accumulation, metamorphism and melt. The emission data are be used to test existing and modified radiative transfer models that use Mie scattering theory.

Overview of Studies

This study started in July, 1983 with the goals of developing better methods for measuring snow properties, designing experimental configurations for observing the radiometric responses of snow, and improving techniques to monitor the components of the energy balance over snow. During the first year of the study, preliminary attempts were made to measure solar reflectance from snow by trying out a spectrometer borrowed from NASA/GSFC. Other work included upgrading the micrometeorological study site, mostly by redesigning instrument arrays to withstand severe winter environmental conditions. This was prompted by the failure of some sensor support structures.

The following winter, 1983-1984, marked the beginning of earnest efforts, with the help of Dr. Al Chang and NASA engineer Ken Brown, to evaluate an instrument to measure the angular distribution of snow reflectance. Data logging capability was upgraded at the snow study site to allow more rapid scanning of up and down looking hemispheric radiometers. This was necessary in order to monitor solar radiation, which sometimes changed markedly during a reflectance scan. Redundant data channels were also added to prevent potential data loss. During this winter we also began using a new technique for

This can be solved for W and divided by the snow mass M to give the liquid water mass fraction x_w. Typically $x_w \times 100$ is in the range 0 to 30%:

$$x_w \equiv \frac{W}{M} = \frac{S}{M} \frac{1 - \frac{C_m}{C_s}}{\frac{C_m}{C_s} - \frac{C_w}{C_s}} \tag{2}$$

The absolute concentrations C_s, C_m, and C_w are not needed, only their ratios. The volume fraction of liquid water θ_w can be obtained

$$\theta_w = x_w \frac{\rho_s}{\rho_i} \tag{3}$$

If mixing of the stock solution is complete, errors in the dilution method result from errors in the measurements of S, M, C_m/C_s, and C_w/C_s.

Snow Microstructure

Snow samples were obtained from snow pits at the same time conventional snow properties were observed. In addition to the field description, micrographs of selected snow samples were used with reference grids to obtain estimates of the grain average diameter.

Each sample of snow was subdivided into specimens of about 3×3×5 cm, carefully avoiding the edges of the blocks. Sections were prepared from the specimens according to recently reported procedures. Micrographs were then taken of the sections with a Nikon HFX photomicroscope using Kodak Ektachrome 400 35 mm slide transparency film. A fiberoptic ring illuminator was used to provide a cool light source, almost coaxial to the main optic tube of the photomicroscope. The lighting arrangement produces bright reflection from the pore filler and maximum light penetration into the exposed ice grains, which appear darker.

The micrographs were digitized with 8-bit brightness levels as 512×512 pixels using a frame-grabber video digitizer, part of a Model 70F image computer from International Imaging Systems. The classification procedure starts by calculating the snow density corresponding to most values of the brightness level threshold. By comparing the calculated densities to those measured independently for the snow specimen, this relationship guides the user in determining a threshold brightness value. Next a visual threshold is determined, which best replicates the micrograph appearance with a real-time density slicing operation while the image is displayed on the monitor.

The classified images are processed with a line sampling technique that results in three measurement parameters and their distributions:

1) Point density P_P, the number of pixels falling on ice profiles divided by the total number of pixels.

2) Intercept number density N_L, the number of ice-pore and pore-ice transitions.

3) Ice intercept lengths L, the distances between pore-ice and ice-pore transitions.

All of these are ratio estimates of statistical parameters and are subject to the standard estimates of error, which become smaller with increasing numbers of sample estimates.

Volume density is equal to the point density, i.e. the ice volume fraction θ_i:

$$\theta_i = V_V = P_P = \frac{P_i}{P_T} \tag{4}$$

P_i is the number of pixels falling on ice, and P_T is the total number of pixels. The snow density is $\rho_s = \rho_i P_P$, where $\rho_i = 917\,\mathrm{kg\,m^{-3}}$ is the density of ice.

Surface density, or surface area per containing volume, is

$$S_V = 2N_L = 2\frac{N_i}{L_T} \tag{5}$$

where N_L is the intercept density of the grain boundaries, N_i is the number of profile boundary intersections, and L_T is the length of the line scan.

Results

Figure 1 shows density data from bulk measurements for the last four winters, obtained from snow pits. The lines drawn are based on best visual fit. Density profiles for dry snow in the early winter for all years studied show trends with depth similar to the empirical models proposed by Bader (1963), Herron and Langway (1980), Ling (1985) and others. The model of Ling (1985), for example, requires only that the density of the surface be known and a maximum representative density for the time of season.

$$(\rho - \rho_o)/(\rho_m - \rho_o) = 1 - e^{-(z/H)} \tag{6}$$

The density at the surface is ρ_o, the maximum density is ρ_m, z is the depth, and H is a characteristic length scale (fitting parameter). This model shows promise for characterization of snow densities over wide areas from few measurements. Near the base of the pack, it is common to find a layer or zone of lower density, presumably because of depth hoar formation while the pack is thin. In general, the density reaches a constant value in the lower two thirds of the pack by March, except for frequent lower values near the snow-soil surface (Figure 1). In the spring, the snow has usually attained a uniform density if it is freely draining except for the near-surface zone.

The density measurements obtained for three winters at the study plot show that old snow layers, buried more than 1m in the pack show little lateral variation prior to melt. Layers of new snow exhibited

significant variation, depending on storm characteristics such as wind. An example of snow pit data showing five density profiles taken about 0.6 – 0.8m apart in Table 1 illustrates these observations.

TABLE 1 : Snow Pit, March 11, 1987

(all densities expressed as kgm^{-3})

Depth(cm)	Dens. 1	Dens. 2	Dens. 3	Dens. 4	Dens. 5	Stand Dev.
00-10	294	318	329	324	332	13.5
10-20	354	323	344	371	356	15.8
20-30	303	308	317	295	340	15.5
30-40	361	349	378	381	359	12.1
40-50	335	344	337	341	336	3.4
50-60	334	344	331	332	333	4.7
60-70	327	316	310	314	314	5.7
70-80	324	317	307	311	314	5.8
80-90	283	287	288	318	312	14.7
90-100	290	280	281	282	284	3.6
100-110	218	225	244	240	245	10.9
110-120	202	200	205	210	209	3.9
120-133	205	207	218	217	206	5.7

Table 2 shows measurements from the Mt. Rose snow sampler taken adjacent to the pit.

TABLE 2 : Mt. Rose SWE Sample, March 11, 1987

MEASURE	SAMP. 1	SAMP. 2	SAMP. 3	SAMP.4
DEPTH (cm)	132	130.8	129.5	127
SWE (cm)	41.4	41.7	38.1	40.64

Comparison between the average densities derived from the two methods shows that the Mt. Rose sampler had a positive bias of almost 4percent. Data from both winters 1985-1986 and 1986-1987 show that the bias can be related to the total absolute snow water equivalent SWE at the Mammoth site by

$$SWE \equiv SWE_{mr}(-0.005) + 0.131 \tag{7}$$

where SWE is the estimated snow water equivalent, and SWE_{mr} is the measurement from the Mt. Rose Sampler. We are currently examining methods use a value of average density and depth, determined from Mt. Rose measurements, in modeling the profiles of density over an area.

Measurements performed on sections from 1985 to 1987 show that planes cut parallel to the snow stratigraphy exhibit little, if any, anisotropy in the parameter L, while some snow types show

inhomogeneity in sections cut vertically, which was not apparent from snow pit observations. The section images were measured in orthogonal directions and counting measures tabulated to calculate L. Figure 2 shows the ratio of L measured vertically $\overline{L_v}$ to $\overline{L_h}$, the same parameter measured horizontally as a function of depth in the snow pack. The apparent vertical elongation of snow fabric is most prominent around depths of about 0.25m. There were no significant correlations found between this feature and the magnitude or direction of the imposed temperature gradients or the densities, except that most samples were old snow with intermediate densities (220–380kgm^{-3}). This figure also shows that most sampling for microstructure analysis was done in the near-surface layers.

Figures 2 and 3 show examples of sections illustrating these trends, one cut parallel to the snow stratigraphy and one cut vertically.

Introduction

Measurements of microwave emission from a snow pack contain information about the snow's liquid water content (Chang et al., 1985), water equivalent (Chang et al., 1982), grain size and geometry, and temperature (Colbeck, 1982a; Denoth, 1982a; Chang, 1984). The propagation and attenuation of microwaves in snow are controlled by the effective dielectric function. Emission and scattering formulations generally characterize the snow as a collection of scatterers embedded in a homogeneous background, or as a medium described by a randomly fluctuating dielectric constant (Fung, 1982; Fung and Eom, 1982; Tiuri, 1982; Schanda et al., 1983; Tiuri et al., 1984; Jin and Kong, 1985; Sadiku, 1985; Stogryn, 1985, 1986). Problems with applying such models result from the disparity between the radiative parameters used in the models and the physical properties of snow measured by experimentalists. Moreover, we lack reliable measurements of the complex refractive index of ice at many frequencies in the microwave spectrum (Foster et al., 1984; Warren, 1984; Sihvola et al., 1985).

The major difficulty in experimentally testing both discrete scatterer and random medium models is that the snow property observations made by field scientists are usually inadequate to determine the theoretical model parameters to allow comparison with radiometric measurements (Eom et al., 1983; Davis et al., 1987). For random medium models the correlation functions and the mean and variance of the permittivity are related to the average ice profile dimensions and volume fractions that can be derived from plane-section micrographs (Vallese and Kong, 1981; Perla, 1982; Perla et al., 1986). It can therefore be assumed that these parameters are related to the actual dimensions and volume fractions in snow, but the use of section measurements in field tests of random medium models or discrete scatterer models is rare. For discrete scatterer models only limited experiments (this study) have demonstrated that the equivalent spheres and number density are related to actual grain dimensions and volume fractions.

Experimental Design

Snow property measurements were carried out coincident with observations of microwave brightness temperature at the study plot.

The radiometer used to make the 35 GHz brightness temperature measurements is a periodically calibrated, AC coupled, total power type. The manufacturer's specifications are given in Table 3. The calibrate command signals are provided by external circuitry as an operate-calibrate duty cycle of about 8 to 1. The output during the calibration part of the cycle is a signal that represents the physical temperature at the waveguide termination, which affects the gain of the receiver. The operating frequency of 35 GHz varies less than 100 MHz from −10°C to +45°C. For single samples, during nominal operation the maximum error at target temperature 299K is about +3K and at target temperature 98.5K is about −2.5K. Samples were collected at a rate of about $9\,s^{-1}$ using software-controlled 12-bit A/D conversion in a portable

computer. These were averaged for each scan to reduce the error in brightness temperature determination. External calibrations were done by viewing the clear sky, an ambient-temperature Eccosorb target, and an Eccosorb target immersed in liquid nitrogen.

Table 3. Microwave Radiometer Specification Summary

Radiometer Type	Periodically calibrated, ac coupled dc radiometer with switched automatic gain control
RF Center Frequency	35 GHz
I-F Bandwidth (B)	600 MHz
Overall Receiver Noise Figure	7 dB DSB
Output Filter Bandwidth	150 Hz
Temperature Sensitivity (ΔT_{min})	1.5 K maximum
Temperature Measurement Range	0 to 500 K
Temperature Measurement Error	$\pm[0.05\|300-T_s\|+6]K_{max}$ for $0 \le T_s \le 500K$ (T_s = radiometric temperature of source)
Operating Temperature	$-25°C$ to $+55°C$

The radiometer was hand-held about 1m above the snow. When the snow was dry, as verified by temperature measurements, the brightness temperature observations consisted of views at zenith angles ranging from 0° to 70° in 10° increments for both horizontal and vertical polarizations. The observations compared with the model for each date are averages of two or more scans. When the snow surface was wet, detected by a surface radiant thermometer and wetness measurements, the radiometer was held at fixed angles as the surface water content changed as well as being scanned over a range of angles. Once the snow was wet throughout, only fixed angles were measured.

The microwave radiation emerging from the snow pack results from natural emission of radiation because of atomic and molecular vibration. The emitted spectral radiance L_ν at temperature T, frequency ν, and look angle $\cos^{-1}\mu$ is the product of the spectral emissivity $E_\nu(\mu)$ and Planck's equation:

$$L_\nu(T,\mu) = E_\nu(\mu)\,\beta_\nu(T) \tag{8}$$

where

$$\beta_\nu(T) = \frac{2h\nu^3}{c^2(e^{h\nu/kT}-1)} \tag{9}$$

The constants in Planck's equation are:

h 6.63×10^{-34}Js Planck's constant

k	$1.38\times10^{-23}\mathrm{JK}^{-1}$	Boltzmann's constant
c	$3\times10^{8}\mathrm{ms}^{-1}$	speed of light

If $E_\nu(\mu)$ is known, the Planck equation can be solved for the monochromatic brightness temperature T_B

$$T_B(\nu,\mu) = \frac{h\nu}{k \ln\left[\dfrac{e^{h\nu/kT} + E_\nu(\mu) - 1}{E_\nu(\mu)}\right]} \tag{10}$$

Because of the low absorption of ice in the microwave, the emissivity depends on the dielectric composition and physical structure of the snow pack integrated over a depth of at least 1 m for near-nadir viewing. However, as the snow becomes wet, the contribution to the emitted radiation from the near surface layers increases dramatically.

At microwave frequencies, the exponential function in the above equations can be replaced by its first-order Taylor series expansion. Therefore the Planck equation reduces to

$$\hat{\beta_\nu}(T) = 2c^{-2}k\nu^2 T \tag{11}$$

and equation (10) reduces to

$$T_B(\nu,\mu) = E_\nu(\mu)T \tag{12}$$

In the radiative transfer equation (Chandrasekhar, 1960), then, radiance terms can be replaced by brightness temperature. The brightness temperature of a snow pack can be found by solving the radiative transfer equation.

$$\mu \frac{dT_B(\tau_\nu,\mu)}{d\tau_\nu} = -T_B(\tau_\nu,\mu) + J(\tau_\nu,\mu) \tag{13}$$

$T_B(\tau_\nu,\mu)$ is the monochromatic brightness temperature at optical depth τ_ν in direction $\cos^{-1}\mu$. $J_\nu(\tau_\nu,\mu)$ is the source function, which accounts for scattering of diffuse radiation from other directions and for emitted radiation.

$$J_\nu(\tau_\nu,\mu) = \frac{\omega_\nu(\tau_\nu)}{2}\int_{-1}^{1} T_B(\tau_\nu,\mu')P_\nu(\tau_\nu;\mu,\mu')\,d\mu' + \tag{0q}$$

$$[1-\omega_\nu(\tau_\nu)]T(\tau_\nu)$$

ω_ν and P_ν are the single-scattering albedo and phase function; these are generally piecewise continuous functions of depth for a nonuniform medium. The optical thickness of a layer is

$$\tau_\nu = Nz\sigma_{ext}(\nu) = \frac{3\theta_i z Q_{ext}(\nu)}{4r} \tag{15}$$

N is the number density of scatterers of radius r, z is the layer thickness, $\sigma_{ext}(\nu)$ is the extinction cross section, θ_i is the volume fraction of ice, and $Q_{ext}(\nu)$ is the extinction efficiency. The parameters used in the Mie calculations are the radius of the equivalent sphere r for the layer and the relative index of refraction Low values of g allow us to assume the scattering is isotropic.

Equation 13 is solved numerically by the invariant embedding technique via recurrence relations (Chang and Choudhury, 1978), The technique is based on the principle that the radiation emerging from a plane-parallel medium is invariant with respect to the addition or subtraction of layers of arbitrary thickness. The model accounts for Fresnel reflection at the snow surface by treating the medium as a mixture of air, ice, and water, so an estimate of the bulk complex dielectric function of the snow ε is also required. By this method brightness temperatures T_B are calculated for horizontal and vertical polarizations and various view angles using parameters that have been estimated from the snow property measurements.

In the case of a ground based radiometer looking down at the snow at angle $\cos^{-1}\mu$, the power received or apparent temperature T_{AP} sensed, is a combination of the brightness temperature of the target T_B and the the component of radiation emitted by the sky and reflected by the target in the direction of the radiometer.

$$T_{AP}(\mu) = T_B(\mu) + (1 - E_\nu) T_{SC}(\mu) \tag{16}$$

The contribution from the sky is small for viewing angles near nadir, but it can become significant for high angles. Therefore we assume $T_{AP} \approx T_B$ for viewing angles less than about 60°.

Input Parameters for Emission Modeling

The microwave emission model uses Mie theory to compute the average absorption and scattering properties of each layer. This requires that the irregular snow grains can be mimicked by some sort of equivalent sphere, and requires an approximation of the relative refractive index of the grains. In the cases where we treat the background as air, the refractive index is that of pure ice. Adjustments to the relative refractive index compensating for the close proximity of the particles treat the background as a mixture of air and ice, and liquid water in the case of wet snow. The properties of the mixture are estimated using structure parameters from section analysis, snow density measurements, and snow wetness measurements.

Equivalent Spheres

That the irregular grains of ice in snow can be approximated by equivalent spheres in the microwave has been shown by Mugnai and Wiscombe (1980). For the range of size parameters encountered in this study there is little difference between the scattering and absorbing parameters for nonspherical and even concave particles and those of the equivalent spheres tested. In addition, Mungai and Wiscombe (1980) find that size averaging tends to reduce the spherical-nonspherical differences as does averaging for orientation.

In microwave modeling it has been generally assumed that the equivalent sphere has the same diameter as the snow grains. Whether this refers to the mean grain diameter, to the mean maximum diameter, or to some other dimension is unclear in most studies. For example, thin section micrographs are presented in Mätzler et al., (1980) to illustrate the ice phase variation in a snow cover and the mean intercept length is referred to as "mean grain diameter." But in most other studies, field estimation or measurements from photomicrographs seem to use mean maximum grain diameter (e.g. Stiles and Ulaby, 1980).

The measurements from the section micrographs in this study consider structure parameters; the measurements from the field and the disaggregated snow samples only allow estimates of caliper dimensions. In terms of stereological models using section measurements (e.g. Weibel, 1979), the object phase, ice, can have any shape, can be interconnected, and can have concave surfaces, but no particle parameters are directly measured and ratio estimates must suffice

In approximating the scattering properties of snow, the section information is transformed to a model of discrete particles with uniform size and spherical shape. The conversion procedures tested are: (1) the sphere of equal mean chord length, (2) the sphere of equal volume-to-surface ratio, (3) the sphere of equal mean diameter to grains in micrographs, and (4) the sphere of equal mean diameter to snow pit estimates. The section data are limited to conversions (1) and (2) and the particle parameter measurements are limited to conversions (3) and (4).

For the conversion of stereologic information to equal-chord-length spheres we assume that the mean intercept length of the ice profiles is related to the mean chord length of the equivalent sphere weighted by the probability that different parts of the sphere would be cut by the section. That is, we assume that the mean intercept length of the profiles is equal to the mean intercept lengths of circles that would form the profiles of the equivalent spheres. The relationship between the average radius of random circles cutting spheres of equal size and the true radius of the spheres is (Weibel, 1979):

$$R_L = \frac{4}{\pi}\bar{r} \tag{17}$$

R_L is the sphere radius and $\bar{r}$ is the average radius of the circular section profile. Similarly it can be shown that the average radius and mean intercept length of the circles are related by

$$\bar{r} = \frac{2}{\pi}\bar{L} \tag{18}$$

$\bar{L}$ is the mean intercept length. Thus

$$R_L = \frac{8}{\pi}\bar{L} = 0.81\,\bar{L} \tag{19}$$

The surface density S_V and the volume density V_V are used to calculate the radius of the sphere of equal volume-to-surface ratio

$$R_V = 3\left[\frac{V_V}{S_V}\right] \tag{20}$$

The diameter-equivalent sphere can be obtained from the particle information by using the mean diameters from the particle observations from the microscope and field.

$$R_{DM} = \frac{\overline{D_M}}{2} \tag{21}$$

and

$$R_{DF} = \frac{\overline{D_F}}{2} \tag{22}$$

$\overline{D_M}$ is the mean estimated grain diameter from the micrographs of disaggregated grains, $\overline{D_F}$ is the mean estimated grain diameter from the field observations. R_{D_M} and R_{D_F} are the radii of the equivalent spheres.

For the wet snow cases, the samples returned from the field were frozen so that the section and disaggregate parameters represent the combined dimensions of the ice and water. We assume that the field measurements of particle dimensions also incorporate the liquid inclusions. Therefore the equivalent-spheres, of which part is ice and part is water, are described by a total radius r_T. Furthermore, for volumetric water fractions $\theta_w \leq 0.07$, we assume that during the measurements no liquid drained from the layer where the average liquid fraction was measured.

To estimate the sizes of the ice spheres and water inclusions from r_T, θ_i and θ_w, it is necessary to use a relationship that makes some assumption about where melt takes place on the grains. For simplicity we assume that melt occurs uniformly around the equivalent spheres. Since the total radius r_T of the spheres is estimated from the samples it is necessary to calculate the radius of the ice cores r_i for different water contents

$$r_i = r_T \left[\frac{\theta_i}{1.091\theta_w + \theta_i} \right]^{1/3} \tag{23}$$

The central ice spheres decrease in radius and number density as the snow liquid water content increases.

We consider two configurations of the ice and liquid water in approximating the average radiative properties. The first characterization treats the equivalent spheres as ice covered by a thin layer of water (Chang et al., 1980). While this treatment is questionable for low water contents because equilibrium thermodynamics constrains the liquid to occur as menisci between grains (Colbeck, 1979), and it is inconsistent with mixing formulae comparisons to dielectric measurements, it is used to illustrate the effect of different ice-water geometry. The problem of scattering from concentric spheres was solved by Aden and Kerker (1951), and is not repeated here.

The second characterization treats the ice and water separately. The size of the ice spheres as melt progresses is calculated using equation 23, and the water is assumed to occur as small menisci approximated by a spherical shape held between two ice spheres. This is a more realistic treatment since the liquid

water in snow nestles between the grains, but it assumes complex shapes. However, the very small Mie sizes of the inclusions and the high absorption of water in the microwave allow us to use equivalent spheres with some confidence (Mugnai and Wiscombe, 1980). The ratio of the number of water spheres to the number of ice spheres is arbitrarily selected based on Colbeck's (1979) suggestion that wet seasonal snow may be dominated by two-grain bonds. Thus the radius of the water sphere r_w can be calculated from the number density of ice spheres N and the liquid water volume fraction θ_w

$$r_w = \left[\frac{3\theta_w}{2N\pi} \right]^{1/3} \tag{24}$$

Once the radius of the water spheres is determined, the relative refractive index of the spheres is calculated and the combined scattering and absorption properties of the layer are estimated according to Dozier and Warren (1982).

$$\overline{Q_{ext}} = \frac{S_{ice} Q_{ext}{}^{ice} + S_{water} Q_{ext}{}^{water}}{S_{ice} + S_{water}} \tag{25}$$

$$\overline{Q_{sca}} = \frac{S_{ice} Q_{sca}{}^{ice} + S_{water} Q_{sca}{}^{water}}{S_{ice} + S_{water}} \tag{26}$$

$$\bar{\omega} = \overline{Q_{sca}} / \overline{Q_{ext}} \tag{27}$$

where S_{ice} and S_{water} are the geometric cross sections of ice and water respectively. Equation 15 is used to calculate the optical depth by adding the contributions of ice and water.

The refractive index of ice at frequency 35 GHz ($\lambda = 8.57$ mm) is interpolated from the data compiled by Warren (1984). While the real part of the refractive index of ice is independent of temperature, and is 1.78 at $\nu = 35$ GHz, the imaginary part is temperature dependent, varying from 3.5×10^{-3} at -1°C to 1.4×10^{-3} at -20°C. This affects $Q_{ext}{}^{ice}$ and therefore the single scattering albedo ω. The refractive index of water is interpolated from the data of Lane and Saxton (1952): $m^{wat} = 3.95 + i\,2.44$.

The radiative transfer model assumes that scattering occurs at discrete locations and takes place independently. This assumption is generally not questioned when the scatterers are widely spaced relative to the wavelength, but doubts arise when the separations between the particles become less than the wavelength, and particularly when the particles are in mutual contact. In some of the model runs we attempt to compensate for the effects of close particle spacing using the method proposed by Gate (1973). The real part of the relative refractive index of the Mie spheres is divided by the effective refractive index of the surrounding medium. For dry snow

$$m_{re}{}^{med} = \theta_i \, m_{re}{}^{ice} + \theta_a \, m_{re}{}^{air} \tag{28}$$

and for wet snow

$$m_{re}{}^{med} = (\varepsilon_{ws}')^{1/2} \tag{29}$$

The estimation of the dielectric function of wet snow ε_{ws}' is discussed in the next section. Here we only adjust the real part of the index of refraction of the equivalent spheres and assume that there is no effect on the imaginary part. Since the wavelength is large, the medium immediately surrounding the spheres is assumed to have the same constituent mix as the bulk.

Generalizing the Parameters

Some of the snow pit observations show many layers with quite different properties. Rather than increase the model complexity to accommodate several layers, we average the parameters into two layers. The averaging scheme is based on the optical thickness of the layer and its optical depth:

$$\bar{x} = \frac{\sum_{i=1}^{n} x_i \left[\frac{\tau_{i+1}-\tau_i}{2}\right] \exp\left[-(\tau_{i+1}+\tau_i)/2\right]}{\sum_{i=1}^{n} \left[\frac{\tau_{i+1}-\tau_i}{2}\right] \exp\left[-(\tau_{i+1}+\tau_i)/2\right]} \tag{30}$$

where x is the parameter being averaged. This weighting scheme has the effect of decreasing the contribution from deeper layers. We average the temperature of the snow pack and the single scattering albedos for all model calculations.

Dielectric Properties of the Medium

Numerous experimental relationships and mixing rules have been proposed to calculate the dielectric functions of dry and wet snow. Since snow is a mixture, the bulk dielectric function represents contributions from the constituents. Some dielectric models may be linearized functions of density and wetness. Others are mixing formulae using the permittivities of air, ice, and liquid water and their volume fractions, or more theoretical relations accounting for the microscopic structure of the ice and liquid water. Sihvola et al. (1985) review various dielectric models and experimental results. Considering the data available we will avoid considerations requiring detailed information about the shape of the constituents, though it is recognized that no physical insight can be obtained from empirical formulae.

The complex dielectric function ε of a medium is related to the complex refractive index m

$$\varepsilon = \varepsilon' + i\,\varepsilon'' = (m_{re} + i\,m_{im})^2 \tag{31}$$

For dry snow we sum the refractive indices of air and ice weighted by volume fraction, and square the result to obtain the real and imaginary parts of the dielectric function.

$$\varepsilon_{ds} = (\theta_i\, m_{re}{}^{ice} + \theta_a\, m_{re}{}^{air} + i\,\theta_i\, m_{im}{}^{ice})^2 \tag{32}$$

where θ_a is the volume fraction of air, and $m^{air} = 1$. This gives the real and imaginary parts with one calculation and shows good agreement with other formulae. The values for the imaginary part of the dielectric function may be inaccurate because the measurements of loss in snow show a large variation and

because the imaginary part of the dielectric function of ice is not well determined.

Recent measurements (Hallikainen et al., 1986; Tiuri et al, 1984) show that the dielectric behavior of wet snow is dominated by Debye relaxation spectra for liquid water with a relaxation frequency of about 8.8 GHz. We use the empirical relationships of Tiuri et al. (1984) in which the dielectric effect of liquid water is superposed on the dielectric properties of dry snow.

$$\Delta\varepsilon' = \varepsilon_{ws}' - \varepsilon_{ds}' \tag{33}$$

$$\Delta\varepsilon' = (0.10\,\theta_w + 0.80\,\theta_w^{\,2})\varepsilon_w' \tag{34}$$

$$\varepsilon_{ws}'' = (0.10\,\theta_w + 0.80\,\theta_w^{\,2})\,\varepsilon_w'' \tag{35}$$

where ε_w' and ε_w'' are the real and imaginary parts of the dielectric function of water. These are given by the Debye relaxation spectra

$$\varepsilon(\nu) = \varepsilon_\infty + \frac{\varepsilon_s - \varepsilon_\infty}{1 + i\nu/\nu_0} \tag{36}$$

Substituting,

$$\varepsilon_w' = 4.9 + \frac{82.8}{1 + (\nu/\nu_0)^2} \tag{37}$$

and

$$\varepsilon_w'' = \frac{82.8(\nu/\nu_0)}{1 + (\nu/\nu_0)^2} \tag{38}$$

where 82.8 is the difference between the high frequency limit and the static dielectric function of water, ν is the frequency under consideration (35 GHz) and $\nu_0 \simeq 8.8$ GHz is the relaxation frequency. These values agree well with interpolated experimental data from Lane and Saxton (1952).

Results

The brightness temperature of the 35*GHz* signal increases with liquid water in a thin surface melting layer over dry snow. Spheres with equal volume-to-surface ratio and equal mean chord lengths underestimate the volume scattering in snow at 35 GHz as shown in Figures 4 and 5 for new snow conditions and in Figures 6 and 7 for mixed snow conditions. Equal-diameter spheres overestimate the scattering, resulting in brightness temperatures lower than the measurements, also shown in the figures listed above.

The adjustment to the relative refractive index to account for the close spacing and contact of the ice grains causes a reduction in the amount of scattering. Therefore only the model parameters using the larger equivalent spheres from the particle measurements have been modified. Figures 8 through 11 show the results for new snow and mixed snow conditions. The corrections improve the correspondence between the model and the radiometric measurements considerably, although the model shows poor agreement with

the horizontally polarized data. Alternatively, the data could probably be matched by finding equivalent sphere sizes somewhere between those tested, rather than by adjusting the refractive index of the spheres. Thus what constitutes the best equivalent sphere conversion is unresolved. Also, the possible dependence of the appropriate equivalent sphere size on frequency remains unaddressed. More accurate microwave measurements are needed for at least two frequencies.

The concentric shell geometry of liquid water in snow yields higher emissivities and better model results than the separate-sphere configuration for liquid water contents greater than about 0.05, while at lower liquid water contents the separate-sphere treatment gives better results. Whereas the model calculations for the early melt case are set up by selecting two dry snow characterizations from runs using measurements from previous days, then adding a wet snow layer to the top, the model calculations for the wet spring snow use a single layer. Figure 12 illustrates the results for a low liquid water content. It shows that the separate–sphere geometry of water and ice gives better model results, but at $\theta_w \geq 0.05$ the concentric–shell treatment of liquid water gives better results, as shown in Figure 13. This trend is reenforced by the spring data, which are better simulated with a concentric shell model (Figure 14). This result may reflect the change in dielectric behavior observed at lower frequencies (Denoth, 1982) when the snow undergoes a transition between the pendular and funicular saturation regimes or it may be an artifact of the characterization of wet snow.

REFERENCES

Aden, A. L. and M. Kerker, Scattering of electromagnetic waves from two concentric spheres, *Journal of Applied Physics*, *22*, 1242-1246, 1951.

Bader, H., *The physics and mechanics of snow as a meterial*, Monograph II-B, vol. AD 474576, 79 pp., U. S. Army Cold Regions Research and Engineering Laboratory, 1962.

Bader, H., Theory of densification of dry snow on high polar glaciers, in *Ice and Snow; Properties, Processes, and Applications*, edited by W. D. Kingery, vol. II, pp. 351-376, Massachusetts Institute of Technology, 1963.

Bader, H., R. Haefeli, E. Bucher, J. Neher, O. Eckel, Ch. Thams, and P. Niggli, *Der Schnee und seine Metamorphose (Snow and its Metamorphism)*, Translation 14, 313 pp., U.S. Snow, Ice and Permafrost Research Establishment, Wilmette, IL, 1939.

Boyne, H. S. and D. Fisk, A comparison of snow liquid water measurement techniques, *Water Resources Research*, *23*, 1833-1836, 1987.

Burke, H. K., J. Clinton, and J. C. Barnes, Determination of snowpack properties from satellite passive microwave measurements, *Remote Sensing of Environment*, *15*, 1-20, 1984.

Chandrasekhar, S., *Radiative Transfer*, 393 pp., Dover, New York, 1960.

Chang, A. T. C., Microwave emissions from snow, *Technical Memorandum 86177*, 33 pp., NASA Goddard Space Flight Center, Greenbelt, MD, 1984.

Chang, A. T. C. and B. J. Choudhury, Microwave emission from polar firn, *Technical Paper 1212*, NASA Scientific and Technical Information Office, Washington, DC, 1978.

Chang, A. T. C., J. L. Foster, M. Owe, D. K. Hall, and A. Rango, Passive and active microwave studies of wet snowpack properties, *Nordic Hydrology*, *16*, 57-66, 1985.

Chang, A. T. C., A. Rango, and J. C. Shiue, Remote sensing of snow properties by passive microwave radiometery: GSFC truck experiment, in *Microwave Remote Sensing of Snowpack Properties*, edited by A. Rango, NASA Conference Publication 2153, pp. 169-186, NASA Goddard Space Flight Center, Greenbelt, MD, 1980.

Colbeck, S. C., The difficulties of measuring the water saturation and porosity of snow, *Journal of Glaciology*, *20*, 189-201, 1978.

Colbeck, S. C., Grain clusters in wet snow, *Journal of Colloid and Interface Science*, *72*, 371-384, 1979.

Colbeck, S. C., The geometry and permittivity of snow, in *Snow Symposium I*, Special Report 82-17, pp. 113-132, U. S. Army Cold Regions Research and Engineering Laboratory, Hanover, NH, 1982.

Davis, R. E., Snow property measurements correlative to microwave emission at 35 GHz, Ph.D. Thesis, 94 pp., Department of Geography, University of California, Santa Barbara, CA, 1986.

Davis, R. E. and J. Dozier, Snow wetness measurement by fluorescent dye dilution, *Journal of Glaciology, 30*, 362-363, 1984.

Davis, R. E., J. Dozier, and A. T. C. Chang, Snow property measurements correlative to microwave emission at 35 GHz, in *Proceedings of the 1986 International Geoscience and Remote Sensing Symposium*, ESA SP-254, pp. 915-920, European Space Agency, Paris, 1986.

Davis, R. E., J. Dozier, and A. T. C. Chang, Snow property measurements correlative to microwave emission at 35 GHz, *IEEE Transactions on Geoscience and Remote Sensing, GE-25*, 751-757, 1987.

Davis, R. E., J. Dozier, E. R. LaChapelle, and R. Perla, Field and laboratory measurements of snow liquid water by dilution, *Water Resources Research, 21*, 1415-1420, 1985.

Davis, R. E., J. Dozier, and D. Marks, Micrometeorological measurements and instrumentation in support of remote sensing observations of an alpine snow cover, *Proceedings of the Western Snow Conference, 51*, 161-164, 1984.

Davis, R. E., J. Dozier, and R. Perla, Measurement of snow grain properties, in *Seasonal Snowcover: Physics, Chemistry, Hydrology*, edited by W. J. Orville-Thomas and H. G. Jones, NATO ASI Series C: Mathematical and Physical Sciences Vol. 211, pp. 53-74, D. Reidel, Dordrecht, 1987.

Davis, R. E. and D. Marks, Undisturbed measurement of the energy and mass balance of a deep alpine snowcover, *Proceedings of the Western Snow Conference, 48*, 62-67, 1980.

Denoth, A., The pendular-funicular liquid transition in snow, *Journal of Glaciology, 25*, 93-97, 1980.

Denoth, A., Effect of grain geometry on electrical properties of snow at frequencies up to 100 MHz, *Journal of Applied Physics, 53*, 7496-7501, 1982.

Denoth, A., The pendular-funicular liquid transition and snow metamorphism, *Journal of Glaciology, 28*, 357-364, 1982.

Denoth, A., A. Foglar, P. Weiland, C. Mätzler, H. Aebischer, M. Tiuri, and A. Sihvola, A comparative study of instruments for measuring the liquid water content of snow, *Journal of Applied Physics, 56*, 2154-2160, 1984.

Dewey, K. F., Snow cover - atmospheric interactions, in *Large Scale Effects of Seasonal Snow Cover*, edited by B. E. Goodison, R. G. Barry, and J. Dozier, IAHS Publication No. 166, pp. 305-314, International Association of Hydrological Sciences, Wallingford, UK, 1987.

Dozier, J., Recent research in snow hydrology, *Reviews of Geophysics, 25*, 153-161, 1987.

Dozier, J., R. E. Davis, and R. Perla, On the objective analysis of snow microstructure, in *Avalanche Formation, Movement and Effects*, edited by B. Salm and H. Gubler, IAHS Publication No. 162, pp. 49-59, International Association of Hydrological Sciences, Wallingford, UK, 1987.

Dozier, J., R. E. Davis, and R. Perla, Snow microstructure measurements using stereology, in *Snow Property Measurement Workshop*, edited by P. R. Kry, Technical Memorandum 140, pp. 59-69,

National Research Council of Canada, Ottawa, 1987.

Dozier, J. and S. G. Warren, Effect of viewing angle on the infrared brightness temperature of snow, *Water Resources Research, 18*, 1424-1434, 1982.

Foster, J. L., D. K. Hall, A. T. C. Chang, and A. Rango, An overview of passive microwave snow research and results, *Reviews of Geophysics and Space Physics, 22*, 195-208, 1984.

Fung, A. K., A review of volume scatter theories for modeling applications, *Radio Science, 17*, 1007-1017, 1982.

Fung, A. K. and H. J. Eom, Application of a combined rough surface and volume scattering theory to sea ice and snow backscatter, *IEEE Transactions on Geoscience and Remote Sensing, GE-20*, 528-536, 1982.

Gate, L. F., Light-scattering cross sections in dense colloidal suspensions of spherical particles, *Journal of the Optical Society of America, 63*, 312-317, 1973.

Hallikainen, M. T., F. T. Ulaby, and M. Abdelrazik, Dielectric properties of snow in the 3 to 37 GHz range, *IEEE Transactions on Antennas and Propagation, AP-34*, 1329-1339, 1986.

Herron, M. M. and C. C. Langway, Firn densification: an empirical model, *Journal of Glaciology, 25*, 373-385, 1980.

Jin, Y.-Q. and J. A. Kong, Strong fluctuation theory for scattering, attenuation, and transmission of microwaves through snowfall, *IEEE Transactions on Geoscience and Remote Sensing, GE-23*, 754-760, 1985.

Keeler, C. M., The growth of bonds and the increase of mechanical strength in a dry seasonal snowpack, *Journal of Glaciology, 8*, 441-450, 1969.

Kry, P. R., Quantitative stereological analysis of grain bonds in snow, *Journal of Glaciology, 14*, 467-477, 1975.

Lane, J. A. and J. A. Saxton, Dielectric dispersion of pure polar liquids at very high radio-frequencies, *Proceedings of the Royal Society of London, A-213*, 400-408, 1952.

Mätzler, C., E. Schanda, R. Hofer, and W. Good, Microwave signatures of the natural snow cover at Weissfluhjoch, in *Microwave Remote Sensing of Snowpack Properties*, edited by A. Rango, NASA Conference Publication 2153, pp. 203-223, NASA Goddard Space Flight Center, Greenbelt, MD, 1980.

Mugnai, A. and W. J. Wiscombe, Scattering of radiation by moderately nonspherical particles, *Journal of the Atmospheric Sciences, 37*, 1291-1307, 1980.

Namias, J., Some empirical evidence for the influence of snow cover on temperature and precipitation, *Monthly Weather Review, 113*, 1542-1553, 1985.

Perla, R., Preparation of section planes in snow specimens, *Journal of Glaciology*, *28*, 199-204, 1982.

Perla, R., R. E. Davis, J. Dozier, and E. R. LaChapelle, Dilution method for measuring liquid water in snow: field tests in a subalpine snowpack, in *Snow Property Measurement Workshop*, edited by P. R. Kry, Technical Memorandum 140, pp. 71-78, National Research Council of Canada, Ottawa, 1987.

Perla, R. and J. Dozier, Observations on snow structure, in *Proceedings, Sixth International Snow Science Workshop*, pp. 182-187, Mountain-Rescue, Aspen, CO, 1984.

Perla, R., J. Dozier, and R. E. Davis, Preparation of serial sections in dry snow specimens, *Journal of Microscopy*, *142*, 111-114, 1986.

Perla, R. and E. R. LaChapelle, Dilution method for measuring liquid water in snow, *Proceedings of the Western Snow Conference*, *52*, 80-85, 1984.

Sadiku, M. N. O., Refractive index of snow at microwave frequencies, *Applied Optics*, *24*, 572-575, 1985.

Sihvola, A., E. Nyfors, and M. Tiuri, Mixing formulae and experimental results for the dielectric constant of snow, *Journal of Glaciology*, *31*, 163-170, 1985.

Stiles, W. H. and F. T. Ulaby, Microwave remote sensing of snowpacks, *Contractor Report 3263*, 404 pp., NASA Goddard Space Flight Center, Greenbelt, MD, 1980.

Stogryn, A., Strong fluctuation theory for moist granular media, *IEEE Transactions on Geoscience and Remote Sensing*, *GE-23*, 78-83, 1985.

Stogryn, A., A study of the microwave brightness temperature of snow from the point of view of strong fluctuation theory, *IEEE Transactions on Geoscience and Remote Sensing*, *GE-24*, 1986.

Tiuri, M., A. H. Sihvola, E. G. Nyfors, and M. T. Hallikainen, The complex dielectric constant of snow at microwave frequencies, *IEEE Journal of Oceanic Engineering*, *OE-9*, 377-382, 1984.

Tiuri, M. E., Theoretical and experimental studies of microwave emission signatures of snow, *IEEE Transactions on Geoscience and Remote Sensing*, *GE-20*, 51-57, 1982.

Vallese, F. and J. A. Kong, Correlation function studies for snow and ice, *Journal of Applied Physics*, *52*, 4921-4925, 1981.

Walsh, J. E., Large scale effects of seasonal snow cover, in *Large Scale Effects of Seasonal Snow Cover*, edited by B. E. Goodison, R. G. Barry, and J. Dozier, IAHS Publication No. 166, pp. 3-14, International Association of Hydrological Sciences, Wallingford, UK, 1987.

Warren, S. G., Optical constants of ice from the ultraviolet to the microwave, *Applied Optics*, *23*, 1206-1225, 1984.

Weibel, E. R., *Stereological Methods, 1, Practical Methods for Biological Morphometry*, 415 pp., Academic Press, New York, 1979.

Figure 1. Composite density profiles for January 1, March 1, and May 1 (left to right) taken from data from three winters.

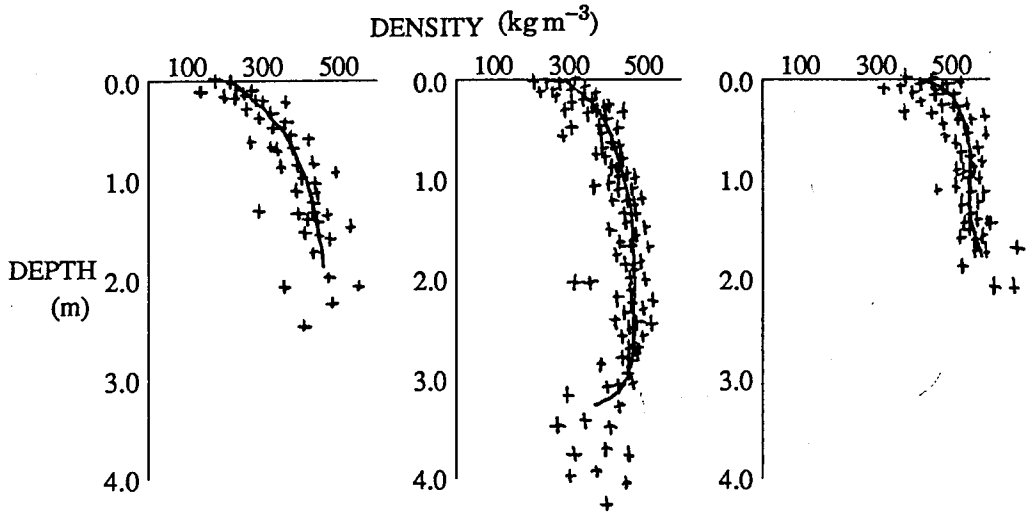

Figure 2. Relationship between snow sample depth and the ratio of the mean intercept length measured vertically L_v and the mean intercept length measured horizontally L_h.

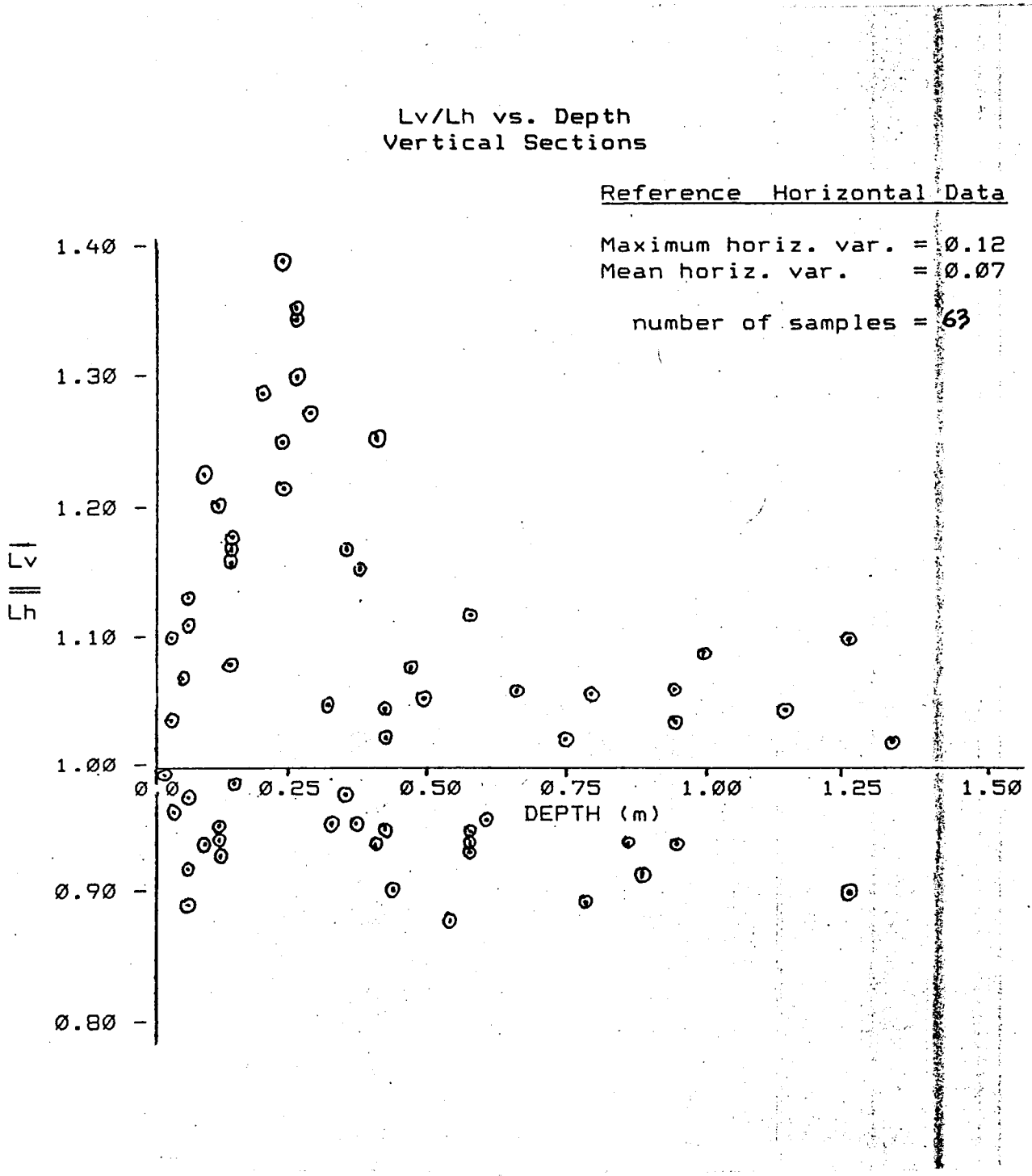

Figure 3. Section image from spring, 1987, cut parallel with the snow strata. This image exhibits little preferential orientation ($L_v/L_h = 0.97$).

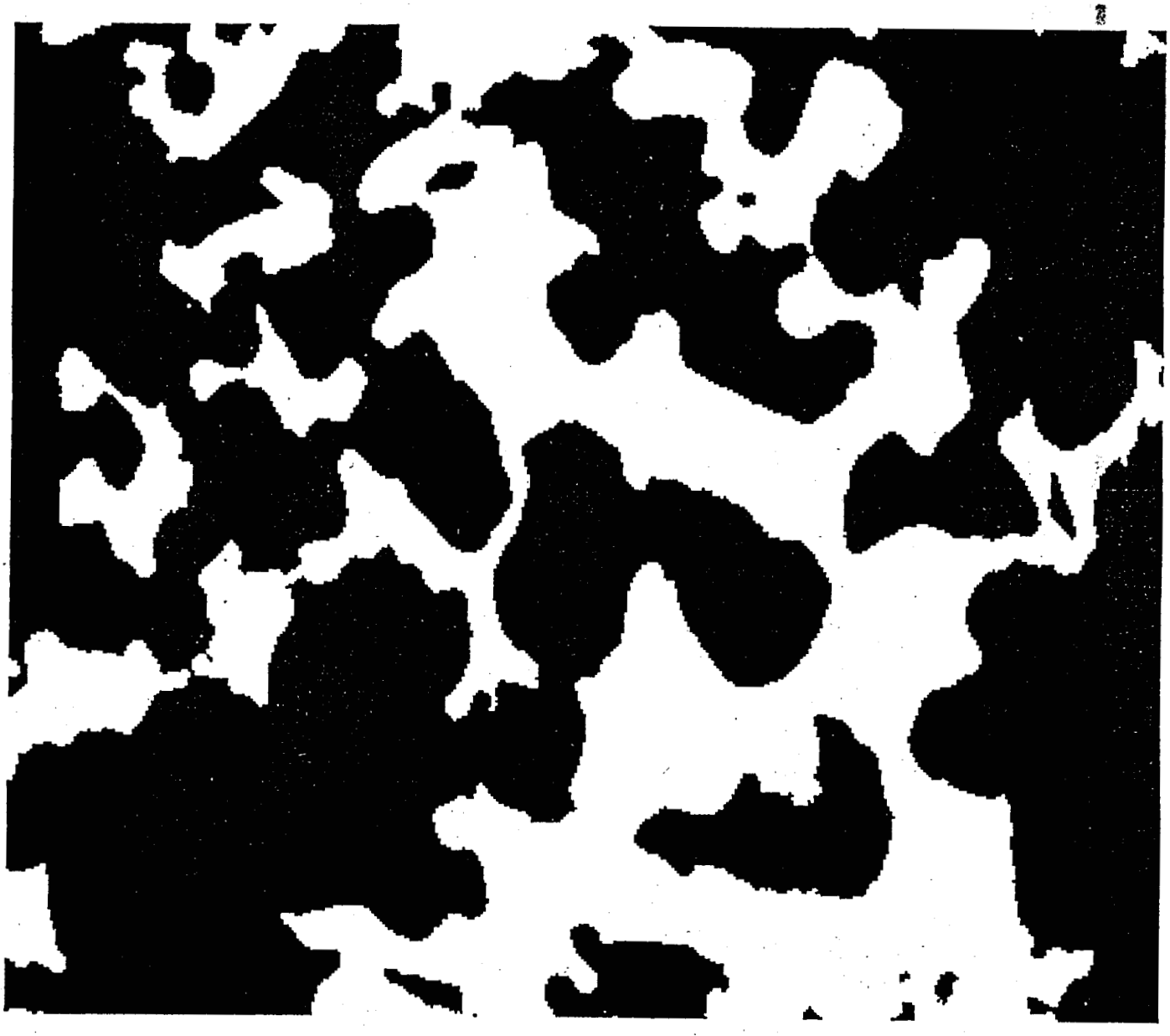

Figure 4. Section image from spring, 1987, cut perpendicular to the snow strata. This image exhibits preferential orientation ($L_v/L_h = 1.27$).

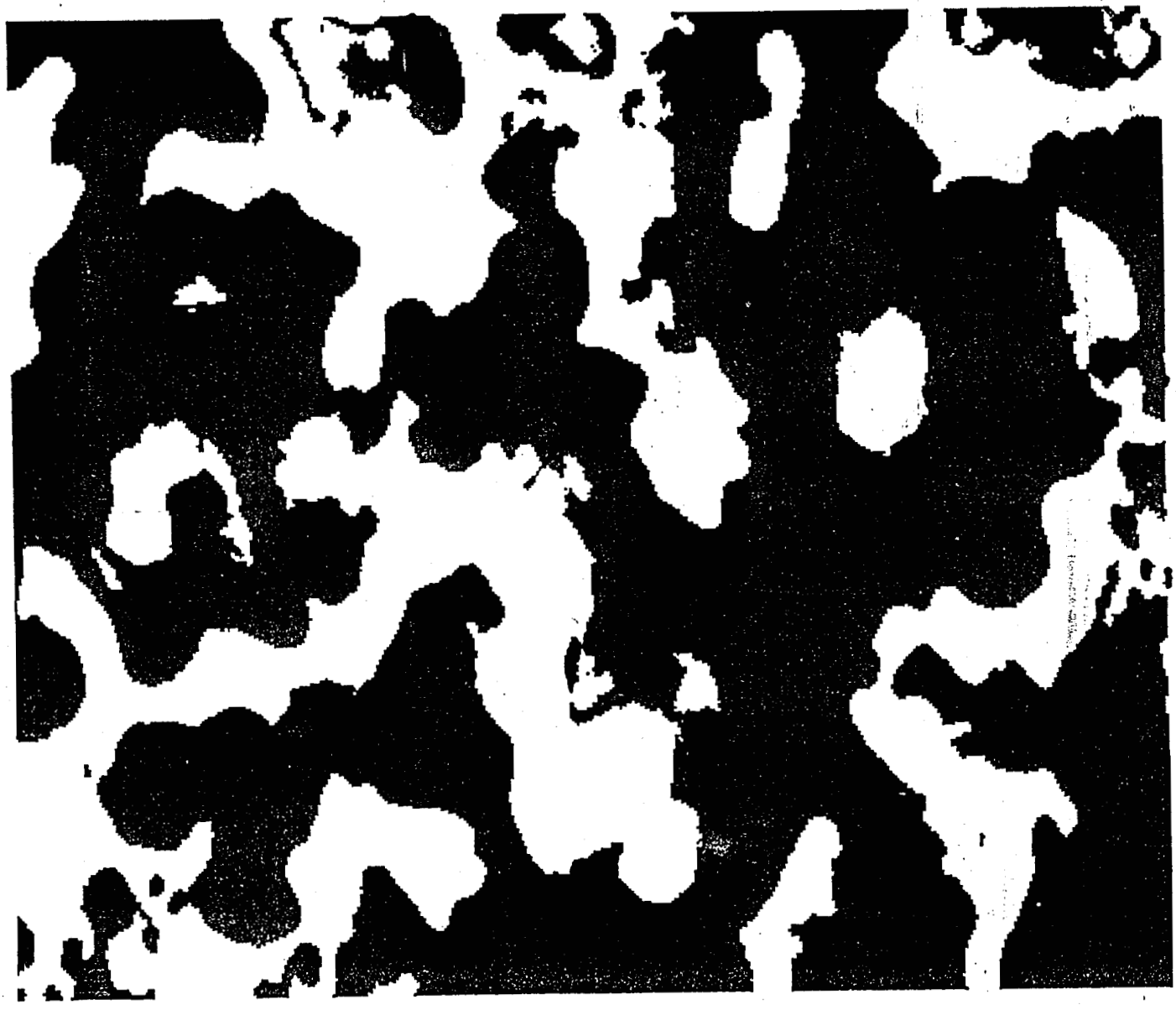

Figure 5. Results for 2/10/85, symbols represent measurements, and lines represent results from a single-layer model. Units of T_B are Kelvins and view angle is expressed in degrees from vertical.

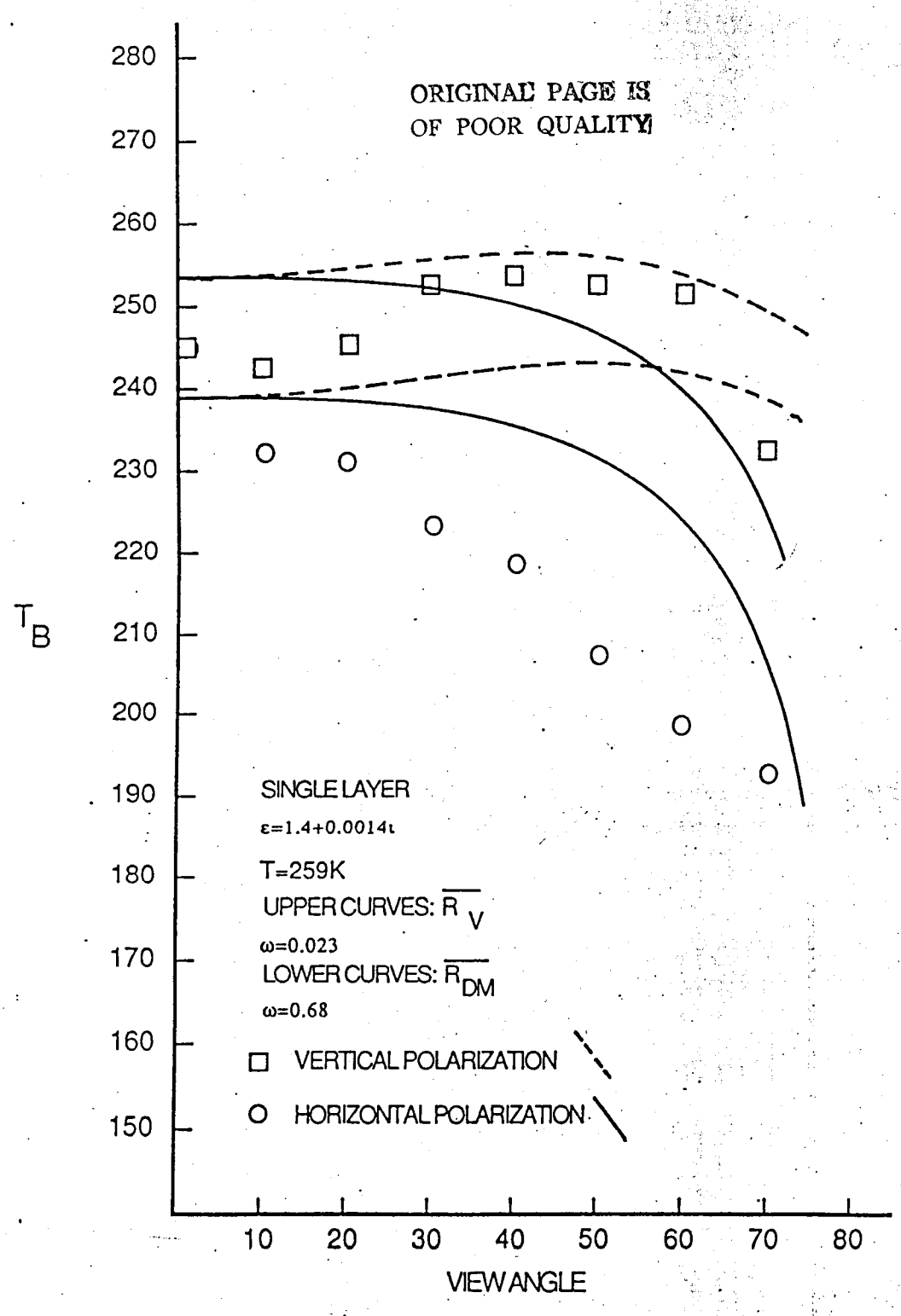

Figure 6. Results for 2/11/85. Section analysis showed slight grain growth since 2/10/85, and average snow temperature increased.

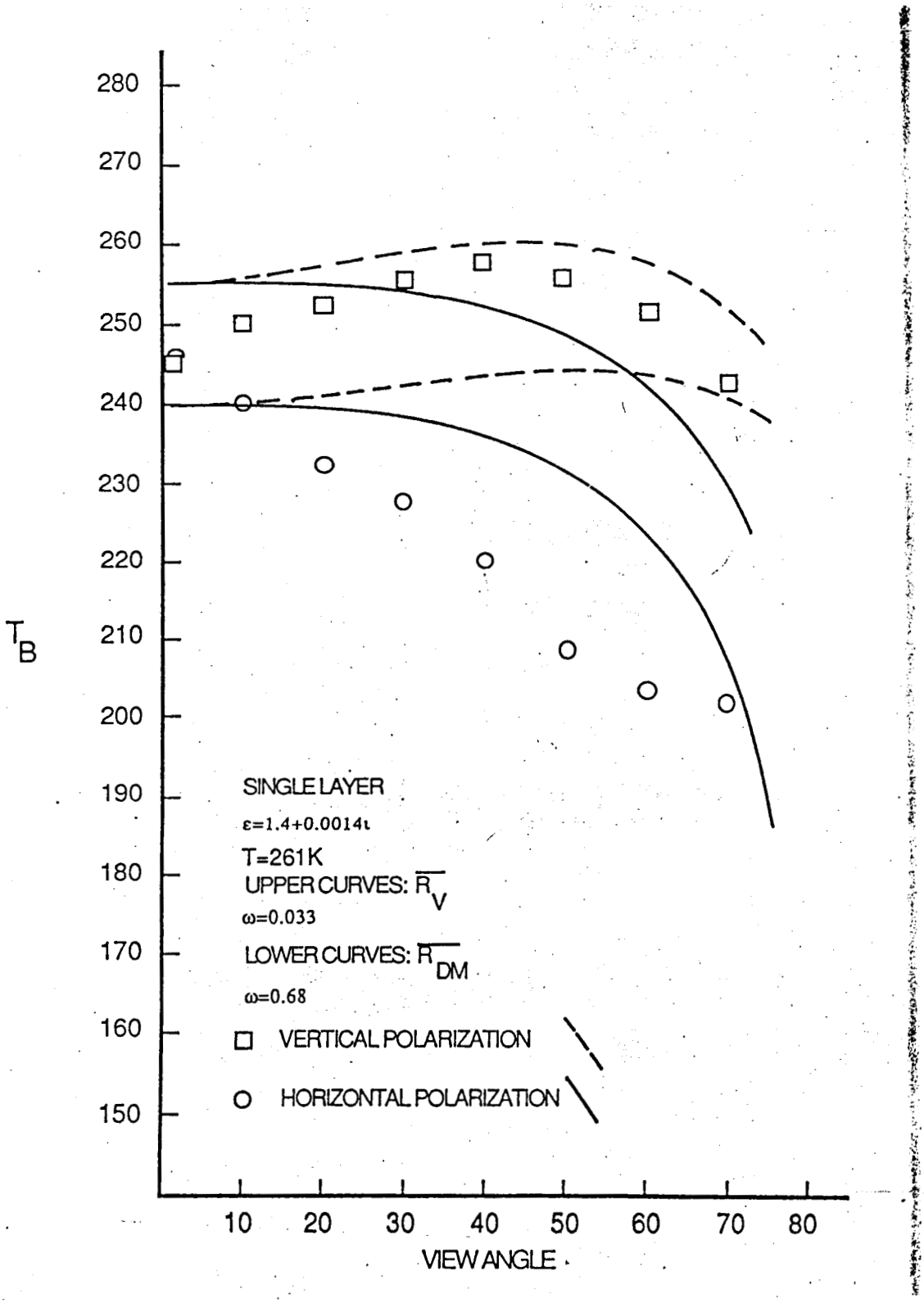

Figure 7. Results for 3/14/85, a two-layer model is used. The slight difference in the shapes of the calculated curves for the two equivalent spheres results from the difference between snow densities for section data and field data.

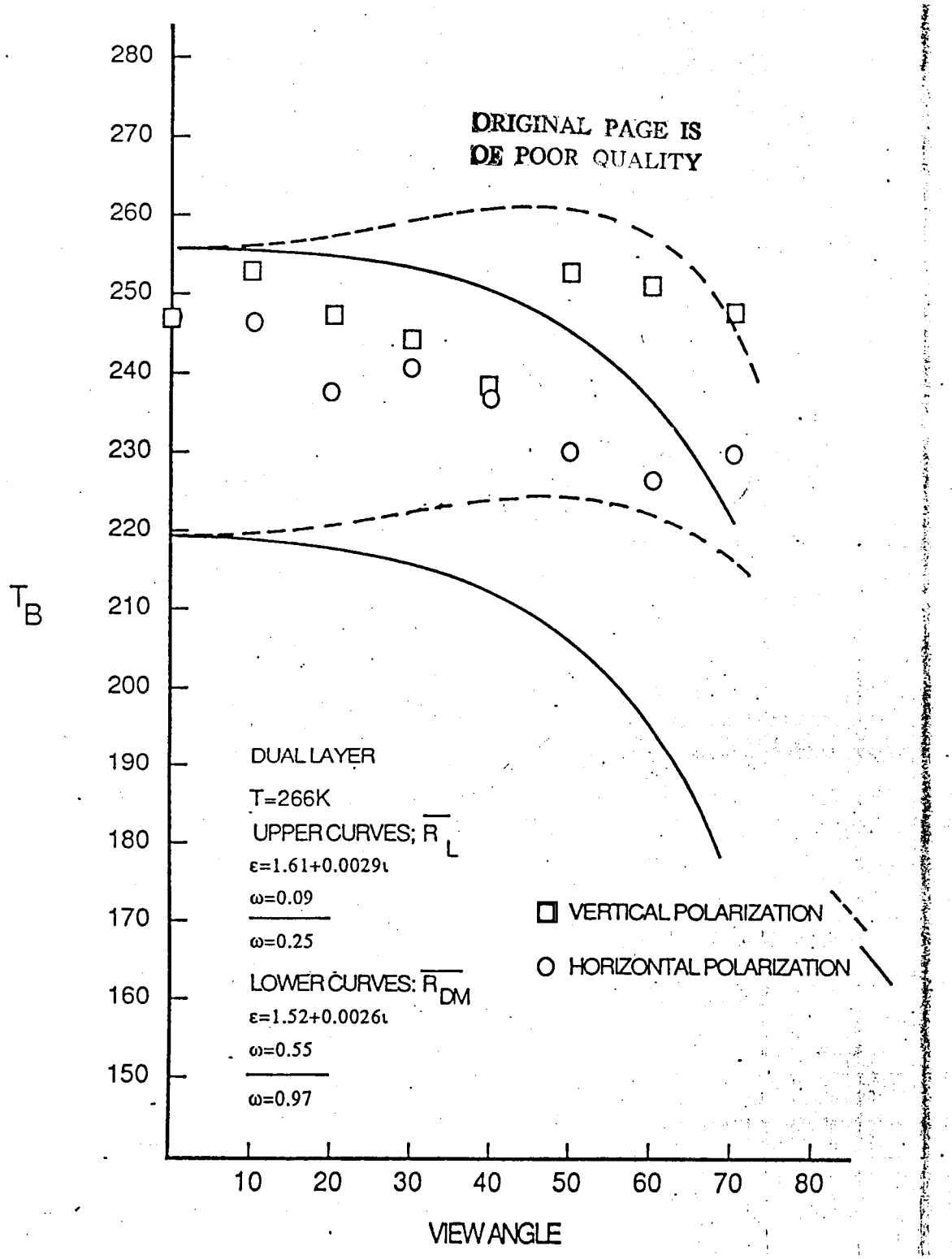

Figure 8. Results from 3/15/85. Average snow temperature increased from previous day.

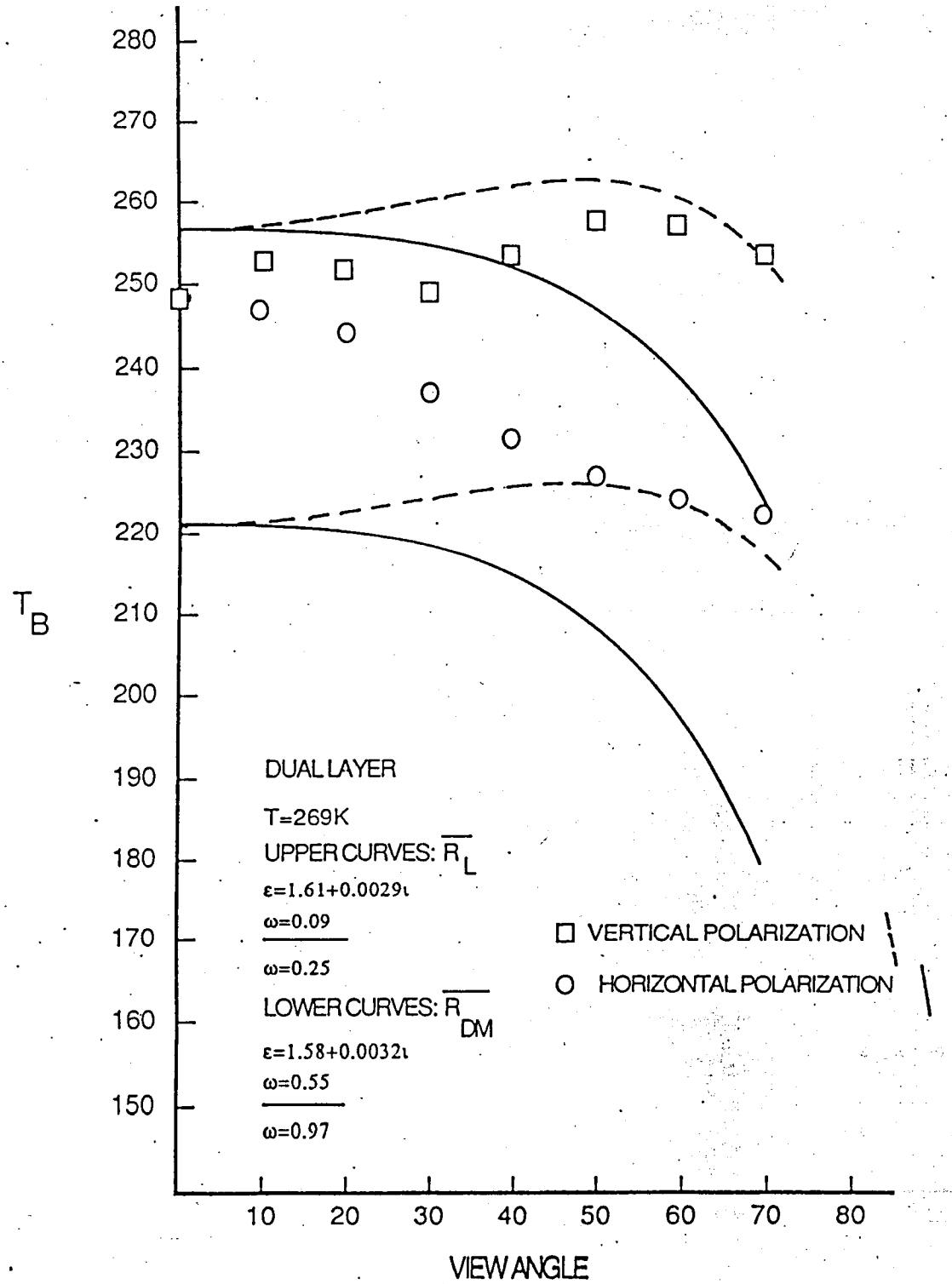

Figure 10. Results from 2/11/85, refractive index of spheres has been adjusted, densities near the snow surface are used to calculate ε.

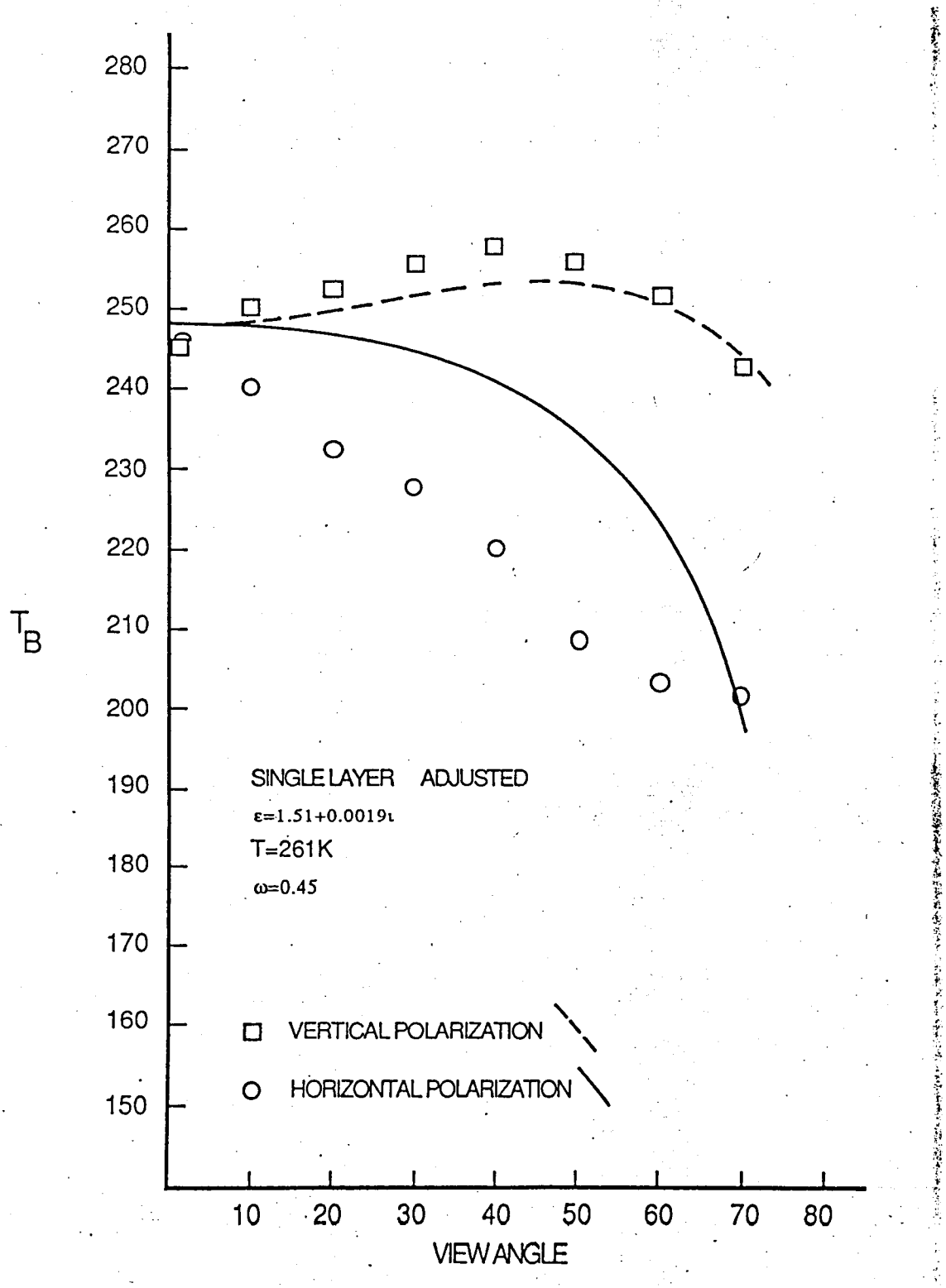

Figure 11. Results from 3/14/85 using refractive index adjustment.

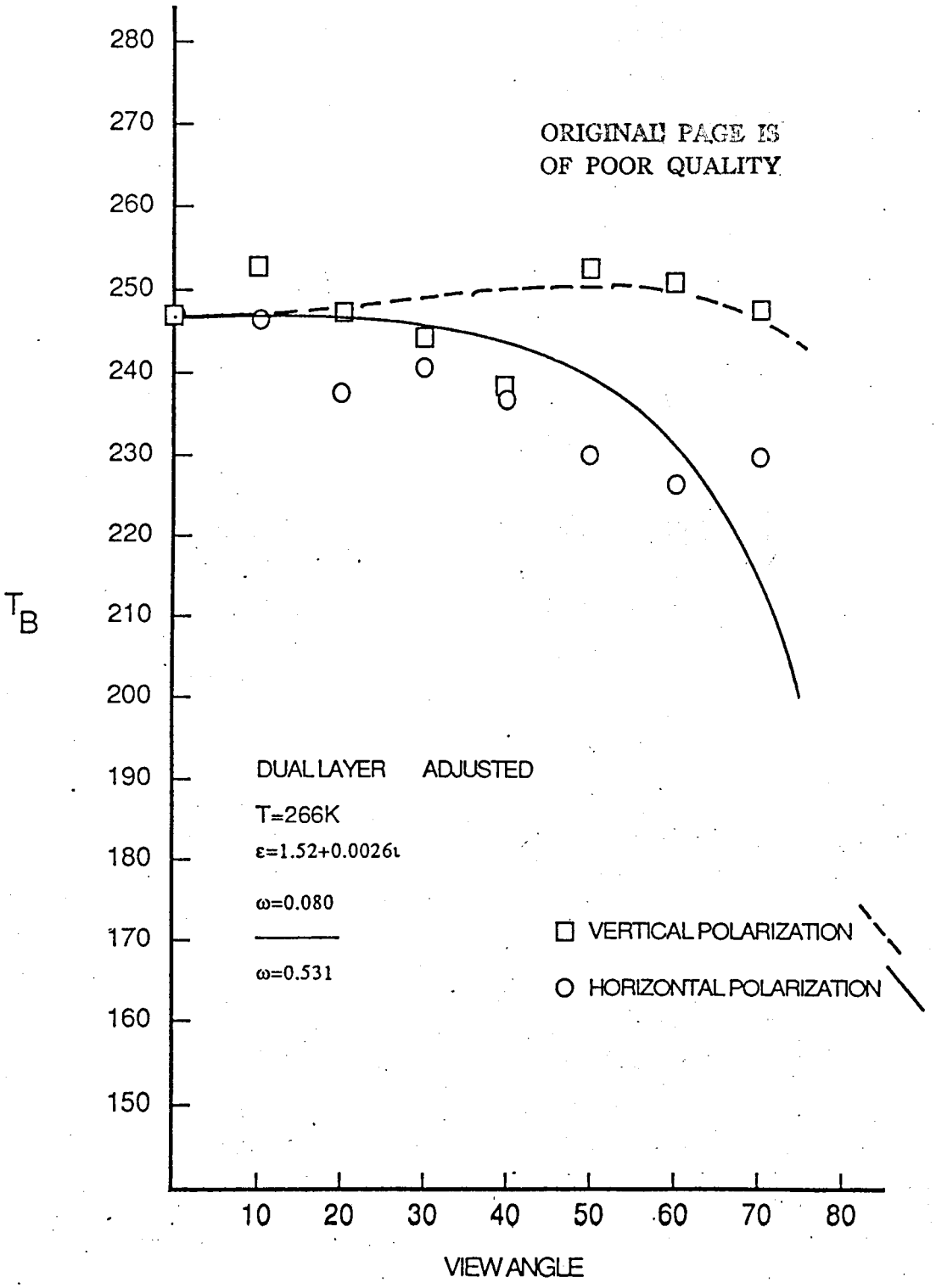

Figure 12. Results from 3/15/85, ε calculated using surface density.

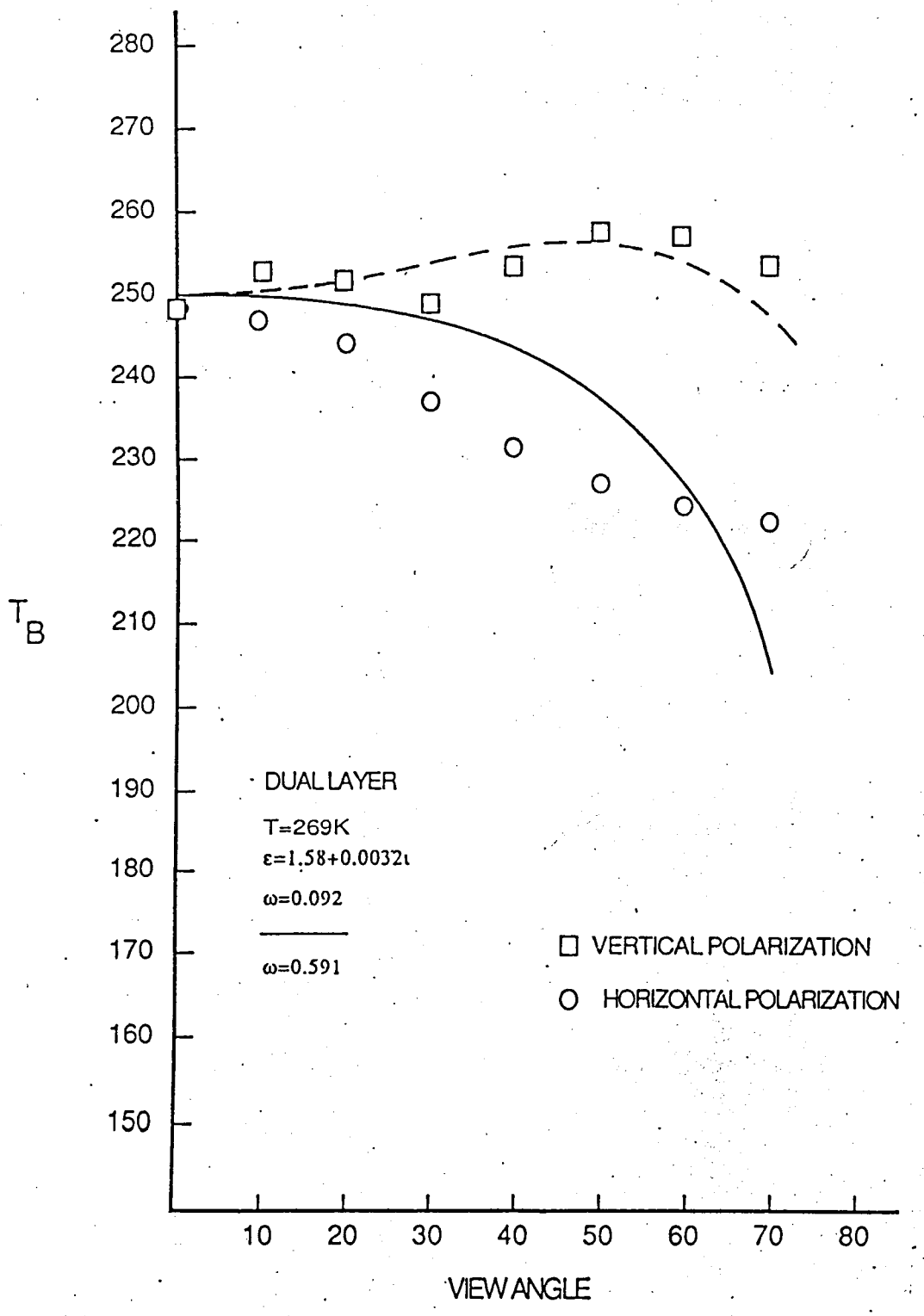

Figure 9. Results from 2/10/85, refractive index of spheres has been adjusted, densities near the snow surface are used to calculate ε. The model does not account for horizontally polarized signal.

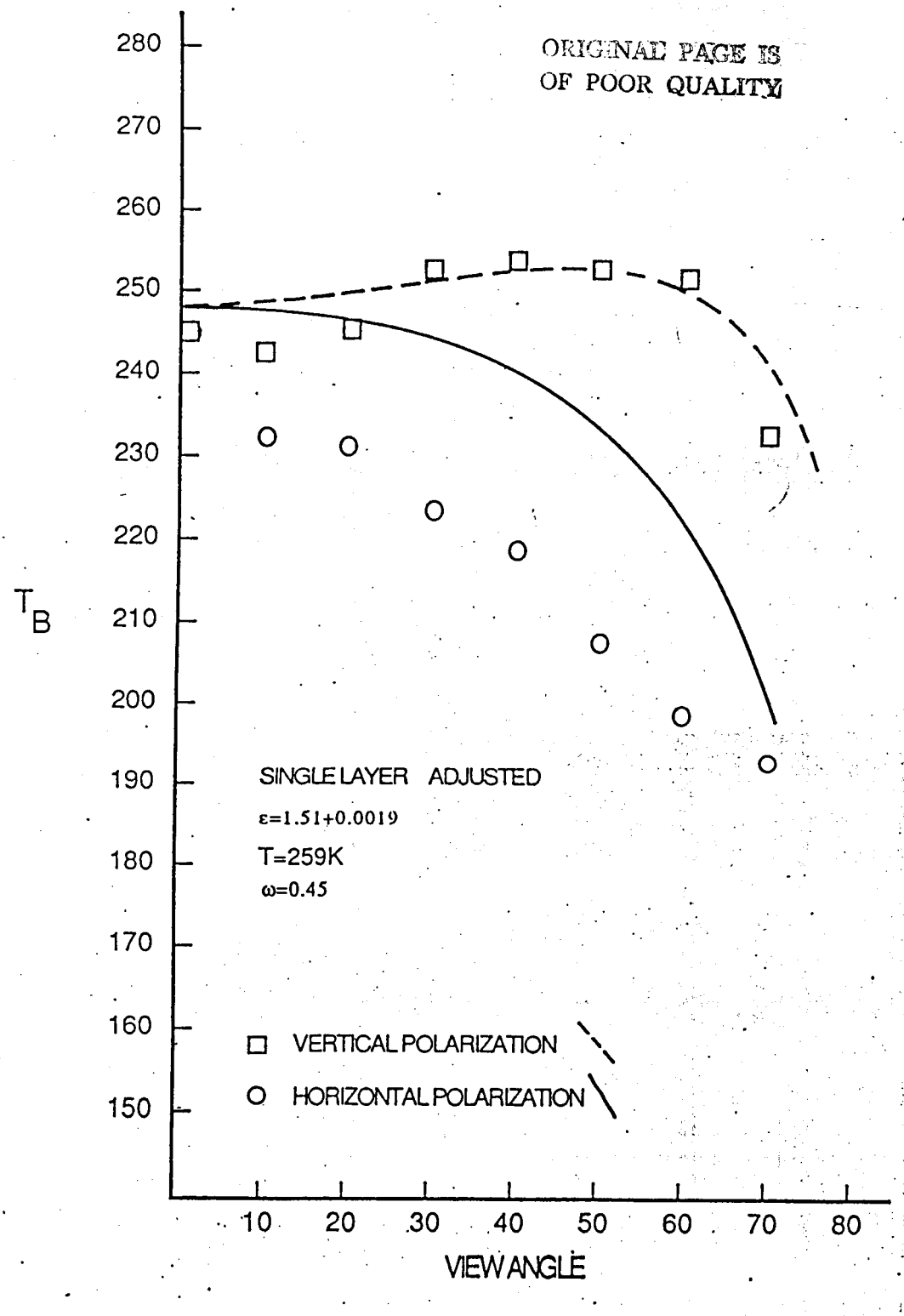

Figure 13. Results from 3/20/85, showing difference in the geometry of liquid water specified in the model. Upper curves are obtained by using a concentric–sphere configuration and the lower curves by using separate spheres of ice and water. Measurements and calculations are for low water content.

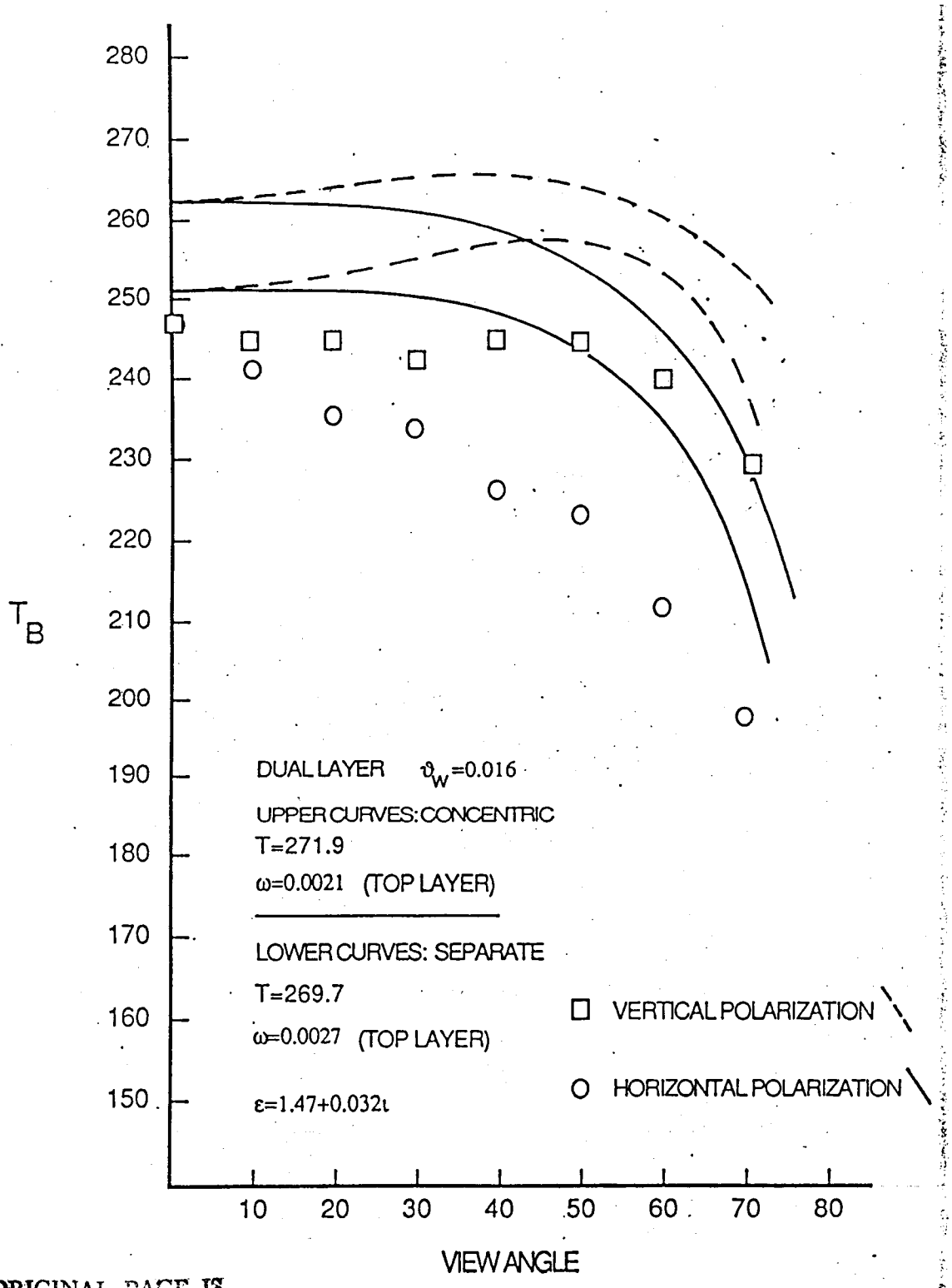

Figure 14. Results from 3/20/85, showing difference in liquid geometry in model, at greater water content. The upper curves result from concentric–shell geometry and the lower curves from separate– sphere geometry.

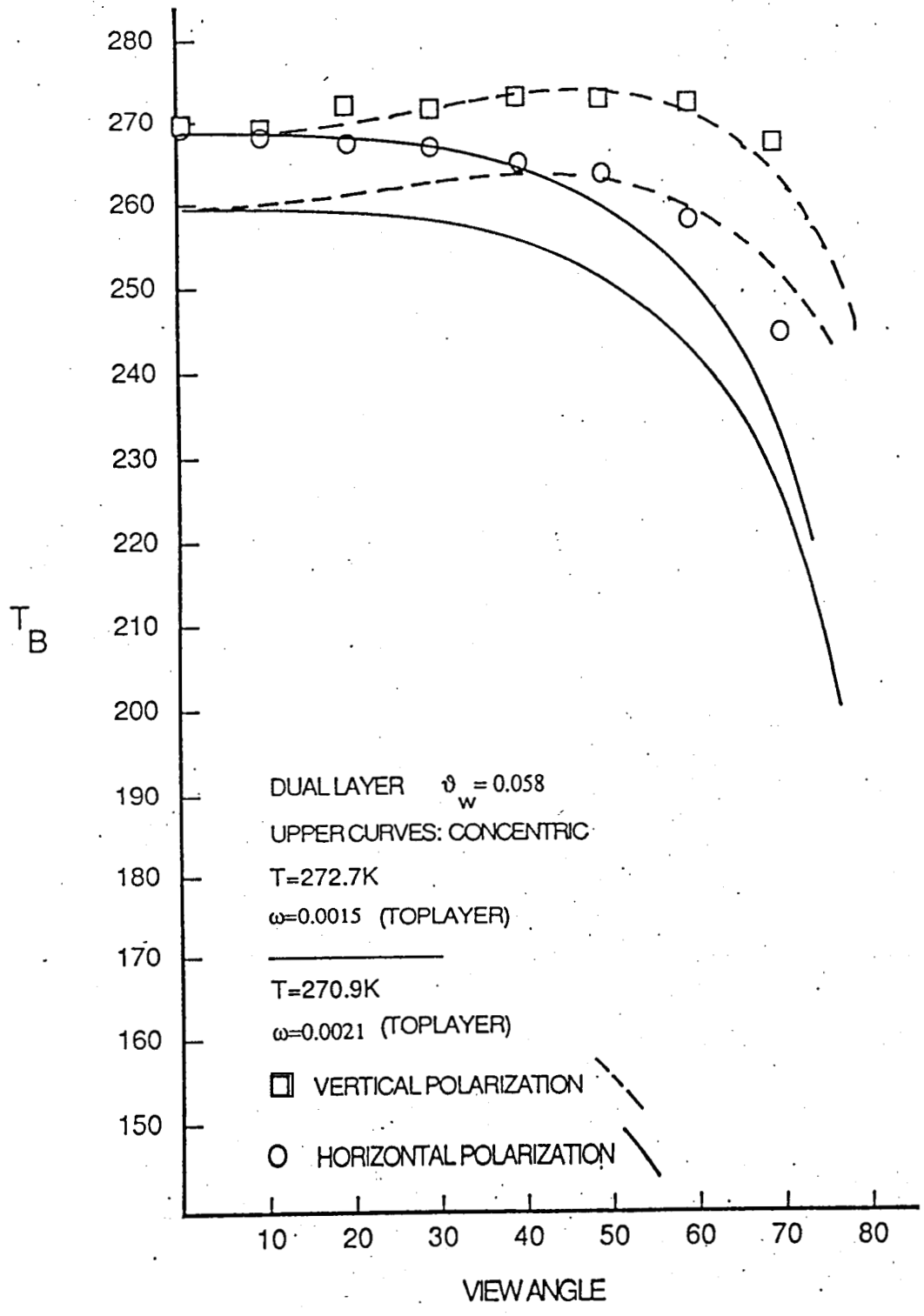

Figure 15. Results from 4/28/85, wet spring snow. The concentric–shell geometry gives higher emissivity, hence better results.

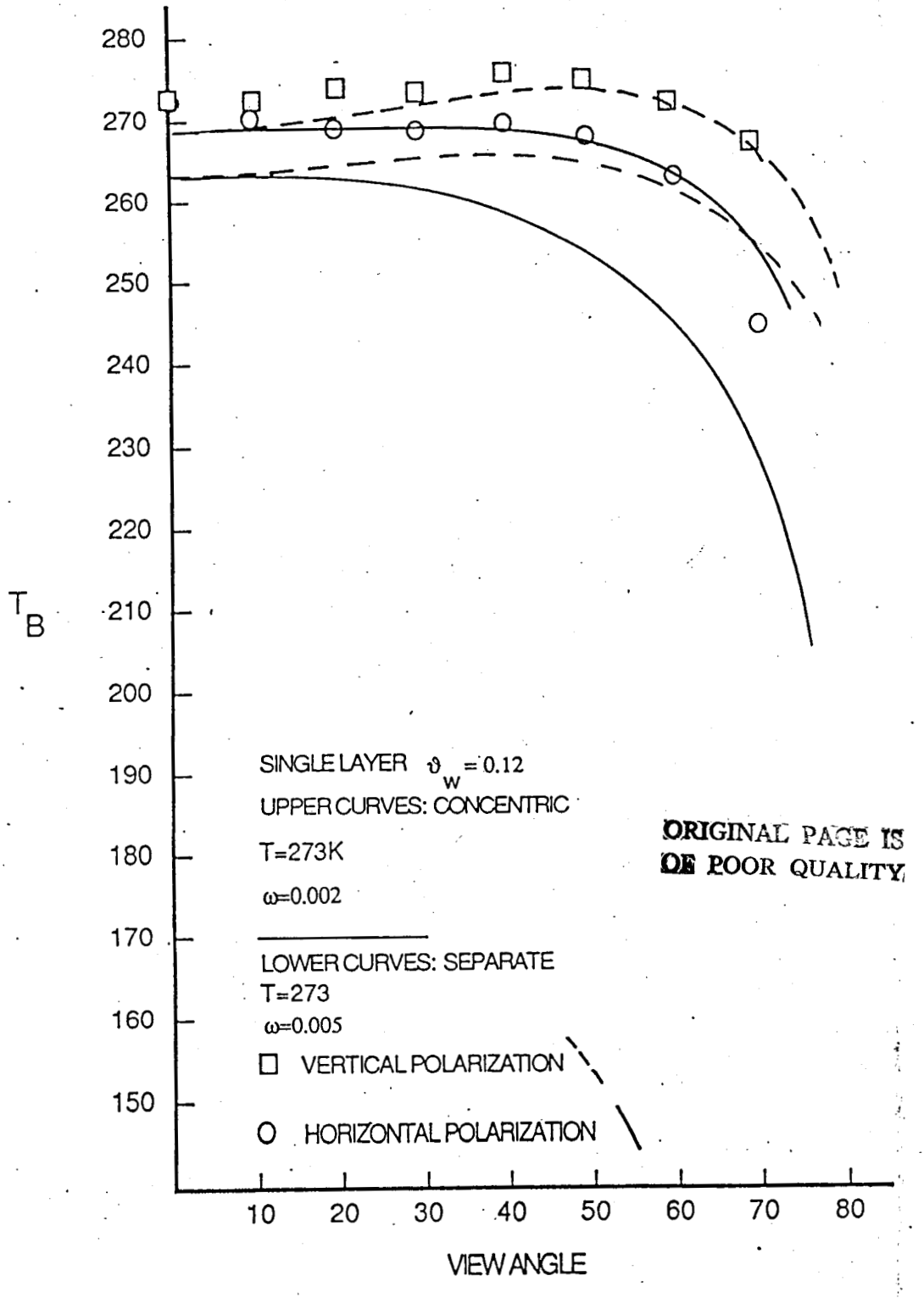

SUMMARY

The period funded by NASA grant NAG 5-328 was from July, 1983 to September, 1987. The following experimental objectives were realized. In this study snow reflectance was measured for the visible and near-infrared wavelength range $0.3 \overset{1.1}{\mu m}$ with two different instruments. Stereological measurements were made from sections prepared from snow specimens, temperature profiles in the snow cover were monitored, snow wetness was measured, and the traditional snow pit observations were made (e.g. density). Measurements of microwave brightness temperature at 35GHz were acquired at a variety of angles at horizontal and vertical polarization during snow accumulation, metamorphism and melt. These radiometric measurements were compared with theoretical model calculations, whose input parameters were derived from measurements of snow properties.

A summary of the total budget expenditures can be found in Table 4.

Total Budget of Grant No. NAG 5-328	
Wages & Benefits	$78,591.95
Supplies and Expense	$11,156.19
Domestic Travel	$12,342.86
Sub-total of Direct Costs	$102,091.00
Overhead	$29,294.00
Total of All Sub Accounts	$131,385.00

We would like to also acknowledge the generous support of **Mammoth Mountain Ski Area** and its owner/operator Dave McCoy, whose support and cooperation made this study logistically possible.

THE SPECTRAL BIDIRECTIONAL REFLECTANCE OF SNOW

Jeff Dozier
University of California, Santa Barbara, CA, USA
and
Jet Propulsion Laboratory, California Institute of Technology, Pasadena, CA, USA

Robert E. Davis
Sierra Nevada Aquatic Research Laboratory, Mammoth Lakes, CA, USA

A. T. C. Chang and Ken Brown
NASA Goddard Space Flight Center, Greenbelt, MD, USA

ABSTRACT/RESUME

A radiative transfer model for the bidirectional reflectance-distribution function (BRDF) shows that snow is moderately anisotropic in the near-infrared wavelengths. Although the directional-hemispherical albedo of snow decreases as the grains become larger, the forward scattering also increases, with the result that the illumination and viewing geometry must be considered when interpreting physical properties of the surface layer of the snow pack from remote sensing data. Measurements of the BRDF for a variety of snow conditions were made throughout the winter and spring seasons with a SE-590 spectroradiometer, for wavelengths from 0.38 to 1.11 μm. Coincident with these the surface grain properties were analyzed by stereological methods. The data show that Mie scattering calculations using an 'equivalent' spherical radius match the directional-hemispherical reflectance, but the BRDF usually shows a small peak in the backscattered direction that would not occur from spherical grains. The sphere with the same surface-to-volume ratio as the ice grains is used as the equivalent sphere.

Keywords: snow, optical properties, remote sensing.

1. INTRODUCTION

Why are we interested in the spectral and angular reflectance of snow?

We need to estimate the albedo of snow from satellite in order to estimate the net solar radiation flux at the surface, given by the convolution of the spectral distribution of the incoming radiation and the spectral albedo:

$$S_{\text{net}} = \int_0^{\infty} [\cos\theta_0 R_s(\lambda,\theta_0) S_s(\lambda) + R_d(\lambda) S_d(\lambda)]\, d\lambda \qquad (1)$$

S_s and S_d are the spectral beam and diffuse irradiance at wavelength λ, and R_s and R_d are the spectral direct and diffuse albedo. θ_0 is the solar illumination angle.

The spectral albedo for direct and diffuse irradiance can be modeled from a knowledge of the snow's physical properties (Ref. 1). However, from satellite or aircraft we can measure only a part of the spectral BRDF (bidirectional reflectance-distribution function), at a few wavelengths and usually only one solar-viewing orientation. We therefore need to know the spectral BRDF of snow as a function of its physical properties. We can use this BRDF as a boundary condition in an atmospheric radiation model, to predict the at-satellite radiance as a function of surface snow properties and the atmospheric profile. In this paper we examine the spectral BRDF of snow.

2. HYPOTHESES AND ASSUMPTIONS

We adopt the following hypotheses and assumptions in our model of the reflectance of snow. The difference between *hypotheses* and *assumptions* is that the hypotheses are tested by comparing measurements of snow properties and snow reflectance with theoretical models of the reflectance. In contrast, the assumptions are not tested.

Hypothesis 1. The reflectance of snow is modeled as a multiple scattering problem, as first proposed by Bohren and Barkstrom (Ref. 2) and reviewed in detail by Warren (Ref. 1). The models proposed and described in these papers calculate the directional-hemispherical reflectance of snow, i.e. the reflectance to direct irradiance, where the reflected radiation is integrated over the entire upward hemisphere (Ref. 3). The calculations match measured spectra (e.g. Ref. 4), but the reflectance measurements were seldom accompanied by rigorous measurements of snow properties.

Hypothesis 2. Scattering properties of irregularly-shaped grains are mimicked by Mie calculations for an 'equivalent sphere'. Possible candidates for the equivalent sphere are the sphere with the same surface-to-volume ratio, the same projected area, same volume, or same surface area. Although snow grains are seldom spherical, they are usually not oriented, so the assumption that their scattering properties can be mimicked by some spherical radius r is reasonable when we want to describe the general spectral properties. When we want details about the angular characteristics of the reflectance, the spherical hypothesis could become more critical.

Hypothesis 3. Because the complex indices of refraction of ice and water are similar in the wavelength range from 0.4 to 2.5 μm, liquid water *per se* has little effect on the optical properties of snow. Instead liquid water causes grain clusters (Ref. 5), which behave optically as large single grains.

Assumption 1. Near-field effects are assumed unimportant. The fact that the ice grains in a snowpack touch each other should not affect the snow's reflectance, because the center-to-center spacing is still much larger than the wavelength. That is, snow reflectance is independent of density up to about 650 $kg\,m^{-3}$. Reflectance measurements carried out over a field season and simply analyzed statistically *will* show a significant inverse relationship between density and reflectance, but the physical model shows that the explanation for changes in reflectance lies in other properties of the snow cover, namely an increase in grain size and in the amount of contaminants near the surface. Measurements of snow reflectance, before and after artificially compacting the snow by driving a snowmobile over it, show no change in reflectance (Ref. 6). In Figure 1, the two representations of snow would have the same reflectance, even though their densities are different.

Assumption 2. The effect of absorbing impurities (dust, soot) is increased when they are inside the ice grains, because refraction focuses light on the impurity and therefore increases the probability that a photon will hit it. Unfortunately, analytical modeling of this situation is restricted either to treating the ice and the dust or soot as separate spheres, which gives the smallest effect, or as concentric spheres with the impurity in the center, which gives the largest effect. A proposed theoretical treatment of randomly located dust or soot (Ref. 7) apparently has mathematical and physical inconsistencies (Ref. 8). Figure 2 shows the two possible configurations.

3. OPTICAL PROPERTIES OF ICE FROM 0.4 TO 2.5 μm

The most important optical property of ice, which causes spectral variation in the reflectance of snow in visible and near-infrared wavelengths, is that the absorption coefficient (i.e. the imaginary part of the refractive index) varies by seven orders of magnitude at wavelengths from 0.4 and 2.5 μm. Normally the index of refraction is expressed as a complex number $n + i\,k$. Figure 3 shows both the real and imaginary parts of the refractive index for ice and water. The important properties to note are: (1) the spectral variation in the real part n is small, and the difference between ice and water is not significant; (2) the absorption coefficients k of ice and water are very similar, except for the region between 1.55 and 1.75 μm, where ice is slightly more absorptive; (3) in the visible wavelengths k is small and ice is transparent; and (4) in the near-infrared wavelengths ice is moderately absorptive, and the absorption increases with wavelength.

The right-hand graph of Figure 3 shows the absorption is a slightly different manner. Transmission of light along distance s through a pure substance decays as $\exp(-4\pi k\, s\,/\lambda)$. The right-hand graph shows the e-folding distance for ice as a function of wavelength, i.e. the distance through which light will propagate through pure ice before its intensity is reduced to e^{-1} times its initial value.

4. SPECTRAL PROPERTIES OF THE REFLECTANCE OF SNOW

Given the hypotheses and assumptions described earlier, the scattering properties for an ice sphere of appropriate radius r can be calculated by the Mie equations (Ref. 9), the complex angular momentum approximation (Ref. 10), or, for larger grains, by geometric optics (Ref. 11). Then the radiative transfer equation (Ref. 12) can be used to calculate the multiple scattering and absorption of the incident radiation.

$$\mu \frac{dL(\tau,\mu,\phi)}{d\tau} = -L(\tau,\mu,\phi) + J(\tau,\mu,\phi) \qquad (2)$$

L is radiance at optical depth τ in direction θ, ϕ; ϕ is the azimuth; θ is the angle from zenith, and $\mu = \cos\theta$. J is the source function; it results from scattering of both direct and diffuse radiation or, at thermal wavelengths, emission.

In our examination of the spectral properties of snow, it is computationally time-consuming to calculate the angular distribution of the reflected radiation. But it is comparatively simple to examine the reflectance integrated over all angles, and these calculations show the interesting spectral properties Therefore, in this section we restrict discussion to the spectral 'directional-hemispherical' reflectance (Ref. 3). This reflectance is defined as the ratio of all of the reflected radiation divided by the incoming solar beam:

$$R_s(\theta_0) = \frac{\int_0^{2\pi}\int_0^1 \mu L(\mu,\phi)\, d\mu\, d\phi}{\mu_0 S_0} = \frac{F_\uparrow}{\mu_0 S_0} \tag{3}$$

where θ_0 is the incident illumination angle, $\mu_0 = \cos\theta_0$, and S_0 is the direct illumination, measured on a plane normal to the solar beam.

We can solve this kind of problem analytically with the 'two-stream equations' for radiative transfer in a homogeneous medium (Ref. 13):

$$\frac{dF_\uparrow(\tau)}{d\tau} = \gamma_1 F_\uparrow(\tau) - \gamma_2 F_\downarrow(\tau) - \gamma_3 \omega_0 S_0 e^{-\tau/\mu_0} \tag{4a}$$

$$\frac{dF_\downarrow(\tau)}{d\tau} = \gamma_2 F_\uparrow(\tau) - \gamma_1 F_\downarrow(\tau) + \gamma_4 \omega_0 S_0 e^{-\tau/\mu_0} \tag{4b}$$

where $F_\uparrow$ and $F_\downarrow$ are upward and downward flux, ω_0 is the single-scattering albedo (i.e. the ratio of extinction by scattering to total extinction), and γ_i are parameters to approximate scattering function. The Mie equations are used to calculate ω_0 and g, the scattering asymmetry parameter, and the γ_i are functions of ω_0, g, and μ_0. To estimate the optical depth coordinate τ as a function of physical properties, we also need Q_{ext}, the extinction efficiency.

The total optical depth of a snowpack, τ_0, is a function of the extinction efficiency and the snow water equivalence W. The snow water equivalence W is the product of mean snow density, ρ_{snow}, and depth d.

$$\tau_0 = \frac{3 W Q_{ext}}{4 r \rho_{ice}} = \frac{3 \rho_{snow} d Q_{ext}}{4 r \rho_{ice}} \tag{5}$$

For the optical depth to be dimensionless, W is in $kg\,m^{-2}$ and r is in meters.

One solution to the twostream equations uses the delta-Eddington approximation to the γ_i parameters (Ref. 14), i.e.

$$\omega^* = \frac{(1-g^2)\,\omega_0}{1-g^2\,\omega_0}$$

$$g^* = \frac{g}{1+g}$$

$$\gamma_1 = \frac{7-\omega^*(4+3g^*)}{4}$$

$$\gamma_2 = -\frac{1-\omega^*(4-3g^*)}{4}$$

$$\gamma_3 = \frac{2-3g^*\mu_0}{4}$$

$$\gamma_4 = 1-\gamma_3$$

Then the twostream equations (4a,b) can be solved for the directional-hemispherical reflectance of snow. For deep snowpacks, 'semi-infinite', the underlying surface has no effect. The reflectance R_s is a function of the illumination angle θ_0.

$$R_s(\theta_0) = \frac{\omega^*}{1+P}\;\frac{1-b^*\xi\mu_0}{1+\xi\mu_0} \qquad 6)$$

The other variables are

$$\xi = [3(1-\omega^* g^*)(1-\omega^*)]^{1/2}$$

$$P = \frac{2\xi}{3(1-\omega^* g^*)}$$

For shallower snowpacks, the optical depth and the reflectance of the substrate, R_0, are needed.

$$R_s(\theta_0) = \frac{\omega^*[1+g^*/(1-\omega^* g^*)] - [\omega^* g^*/(1-\omega^* g^*)](Q^+ - Q^-)}{Q^+(1+P) - Q^-(1-P)} \qquad (7)$$

The additional variables needed for the finite-depth snowpack are

$$\tau_0^* = (1-\omega_0 g^2)\,\tau_0$$

$$\gamma = \frac{1-R_0}{1+R_0}$$

$$Q^{\pm} = (\gamma \pm P)\exp(\pm\xi\tau_0^*)$$

How thick is a semi-infinite snow pack? For practical purposes, we define it as a snow pack whose directional-hemispherical reflectance is within 1% of that at $\tau_0=\infty$. For a solar zenith angle of 60°, Table 1 shows the minimum values in millimeters of water equivalence.

Table 1. Snow-Water Equivalence (mm) of Semi-Infinite Snow Pack

λ	grain radius (μm)		
(μm)	50	300	1000
0.45	17	63	145
0.7	10	37	80
0.9	5	15	30
1.6	<1	<1	1

Figure 4 shows the spectral reflectance of pure, deep snow for visible and near-infrared wavelengths, for snow grain radii from 50 to 1,000 μm, representing the range for the finest new snow to coarse spring snow. Because ice is so transparent in the visible wavelengths, increasing the grain size does not appreciably affect the reflectance. The probability that a photon will be absorbed, once it enters an ice grain, is small, and that probability is not increased very much if the ice grain is larger. In the near-infrared, however, ice is moderately absorptive. Therefore, the reflectance is sensitive to grain size, and the sensitivity is greatest at 1.0 to 1.3 μm. Because the ice grains are strongly forward-scattering in the near-infrared, reflectance increases with illumination angle (Figure 5), especially for larger grains.

The presence of liquid water in the snow should not by itself affect the reflectance. Except where meltwater ponds in depressions when melting snow overlies an impermeable substrate, liquid water content in snow rarely exceeds 5 or 6%. This small amount of water does not appreciably affect the bulk radiative transfer properties, except possibly in those wavelength regions where the absorption coefficients are appreciably different. Instead, the changes in reflectance that occur in melting snow result from the increased crystal sizes and from an effective size increase caused by the two- to four-grain clusters that form in wet, unsaturated snow (Refs. 5,15). These apparently behave optically as single grains, causing decreased reflectance in near-infrared wavelengths. O'Brien and Munis (Ref. 4) observed the spectral reflectance of a snow sample to be lower after warm air had been blown over it, but that the reflectance did not increase when the snow was refrozen.

There is no explicit dependence on density, at least for the semi-infinite snowpack. Although Bergen (Ref. 16) has proposed a semiempirical formulation with a density term for snow reflectance, in practice the natural increases in density are usually accompanied by increases in grain size.

5. MEASUREMENTS OF ANGULAR REFLECTANCE OF SNOW

Measurements of the spectral BRDF of snow were made at Mammoth Mountain (elevation 2900 m) in the Sierra Nevada, California, during the winter and spring of 1987. The spectroradiometer we used was a Spectron Engineering SE-590, whose characteristics are given in Table 2.

Table 2. Characteristics of SE-590

spectral range	0.368–1.11 μm
spectral sampling	< 3 nm
spectral resolution	5–10 nm
field-of-view	7°

The geometry of measurements covered most of the upward hemisphere. For each of the following angles, spectral measurements were made. We assumed that the BRDF would be azimuthally symmetric. After each snow measurement, a spectral measurement of a halon target at 0° nadir angle was made, in order to characterize the irradiance (Ref. 17). Because of the clear days at high altitude the diffuse irradiance was minimal.

Azimuth angles from sun: 0 45 90 135 (165) 180
Nadir viewing angles: 0 15 30 45 60 75

Figure 6 shows the geometry of the measurements.

Table 3 shows the range of snow properties and viewing geometry observed

Table 3. Range of Snow Properties and Viewing Geometry

snow type	powder, old EQ, firnspiegel, corn
age of top layer	1 to 34 days
thickness of top layer	170 to 300 mm
density	150 to 457 kg m^{-3}
snow water equivalence (top layer)	45 to 148 mm
grain radius	60 to 500 μm
crystal form	dendrite, cluster, firnspiegel
wetness (volume fraction)	0.00 to 0.06
solar zenith angle	21° to 58°
viewing angle from nadir	0° to 75°
viewing azimuth from sun	0° to 180°

Data from selected days are presented in Figures 7 through 9. For each azimuth from 0–180° (with reference to solar azimuth) the spectral BRDF was measured for viewing angles 0–75° from nadir. In each spectral plot, the top line is at 75° viewing angle, and the bottom line is at 0°. Other specific information is given in each figure caption.

6. DISCUSSION

Interpretation of the grain characteristics was made mainly from reflectance at wavelengths from 0.80 to 1.05 μm. At shorter wavelengths reflectance is not so sensitive to grain size, and contaminants have more effect. For wavelengths close to 1.1 μm we do not trust the sensor as well, as we are approaching the limits of sensitivity of the silicon detectors.

The results show that the directional-hemispherical reflectance is explained by a radiative transfer model. Mie calculations for an equivalent sphere are used for the scattering properties of the ice grains, using the spherical radius with the same surface-to-volume ratio, measured from stereological sections. The same theory also explains the angular characteristics, except that there is a small peak in the backscattered direction, which is not predicted by the radiative transfer model. Steffen (Ref. 18) noted the same peak in his measurements at 0.4 to 0.5 μm.

The major caveat we must remember is that the spectral range up to 1.1 μm contains only a small part of the variation in the optical properties of ice. Therefore it would be very useful to also make measurements in the spectral range from 1.1 to 1.4 μm, 1.5 to 1.8 μm, and 2.1 to 2.3 μm. Here we would expect more angular variation and more sensitivity to grain radius.

7. REFERENCES

1. Warren, S. G., 1982, Optical properties of snow, *Rev. Geophys. Space Phys.*, 20, 67-89.

2. Bohren, C. F. and Barkstrom, B. R., 1974, Theory of the optical properties of snow, *J. Geophys. Res.*, 79, 4527-4535.

3. Nicodemus, F. E., Richmond, J. C., Hsia, J. J., Ginsberg, I. W., and Limperis, T., 1977, *Geometrical Considerations and Nomenclature for Reflectance*, Nat. Bureau Stds. Monogr. 160, 52 pp., U. S. Dept. Comm., Washington, DC.

4. O'Brien, H. W. and Munis, R. W., 1975, Red and near-infrared spectral reflectance of snow, Res. Rep. 332, 18 pp., U. S. Army Cold Regions Res. Engrg. Lab., Hanover, NH.

5. Colbeck, S. C., 1979, Grain clusters in wet snow, *J. Colloid Interface Sci.*, 72, 371-384.

6. Bohren, C. F. and Beschta, R. L., 1979, Snowpack albedo and snow density, *Cold Regions Sci. Technol.*, 1, 47-50.

7. Chýlek, P., Ramaswamy, V., and Srivastava, V., 1983, Albedo of soot-contaminated snow, *J. Geophys. Res.*, 88, 10,837-10,843.

8. Bohren, C. F., 1986, Applicability of effective-medium theories to problems of scattering and absorption by nonhomogeneous atmospheric particles, *J. Atmos. Sci.*, 43, 468-

475.

9. Wiscombe, W. J., 1980, Improved Mie scattering algorithms, *Appl. Opt.*, 19, 1505-1509.

10. Nussenzveig, H. M. and Wiscombe, W. J., 1980, Efficiency factors in Mie scattering, *Phys. Rev. Lett.*, 45, 1490-1494.

11. Bohren, C. F., 1987, Multiple scattering of light and some of its observable consequences, *Amer. J. Physics*, 55, 524-533.

12. Chandrasekhar, S., 1960, *Radiative Transfer*, 393 pp., Dover, New York.

13. Meador, W. E. and Weaver, W. R., 1980, Two-stream approximations to radiative transfer in planetary atmospheres: a unified description of existing methods and a new improvement, *J. Atmos. Sci.*, 37, 630-643.

14. Wiscombe, W. J. and Warren, S. G., 1980, A model for the spectral albedo of snow, I, Pure snow, *J. Atmos. Sci.*, 37, 2712-2733.

15. Colbeck, S. C., 1986, Classification of seasonal snow cover crystals, *Water Resour. Res.*, 22, 59S-70S.

16. Bergen, J. D., 1983, Observations on the relation of the short-wave reflectivity of recently deposited snow to its physical properties, *J. Clim. Appl. Meteorol.*, 22, 193-200.

17. Schutt, J. B., Holben, B. N., Shai, C. M., and Henninger, J. B., 1981, Reflectivity of TFE – a washable surface – compared with that of $BaSO_4$, *Appl. Opt.*, 20, 2033-2035.

18. Steffen, K., 1987, Bidirectional reflectance of snow at 500-600 nm, in *Large Scale Effects of Seasonal Snow Cover*, edited by B. E. Goodison, R. G. Barry, and J. Dozier, IAHS Publ. No. 166, pp. 415-420, Intl. Assoc. Hydrol. Sci., Wallingford, UK.

Acknowledgements

This work has been supported by the National Aeronautics and Space Administration, through the University of California, Santa Barbara, the NASA Goddard Space Flight Center, and the Jet Propulsion Laboratory, California Institute of Technology. Reference herein to any specific commercial product, process, or service by trade name, trademark, manufacturer, or otherwise, does not constitute or imply its endorsement by the United States Government, the University of California, or the California Institute of Technology.

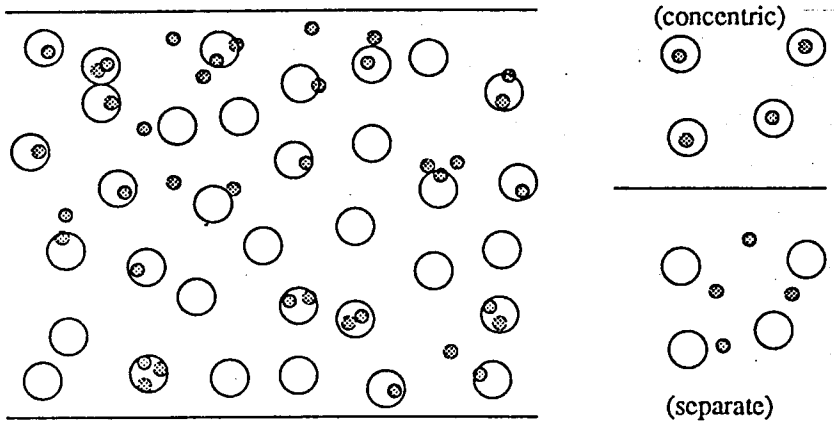

Figure 2. Absorbing impurities can be modeled either as separate or as concentric spheres. The concentric-sphere configuration has the maximum effect, becauses refraction focuses light on the absorber.

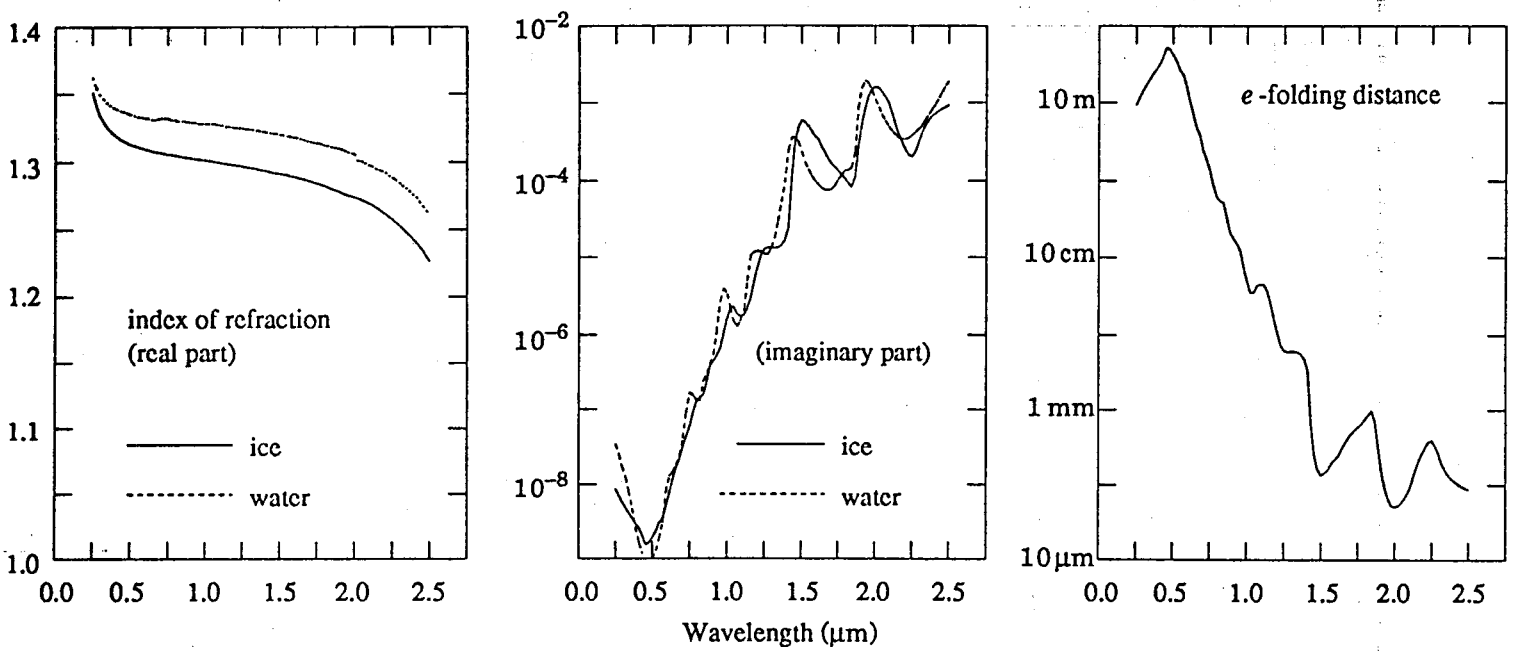

Figure 3. Complex refractive index ($n + i\,k$) and absorption properties of ice. Left: real part of refractive index (n). Middle: imaginary part of refractive index (k). Right: e-folding distance ($\lambda/4\pi k$), at which intensity is reduced to e^{-1}.

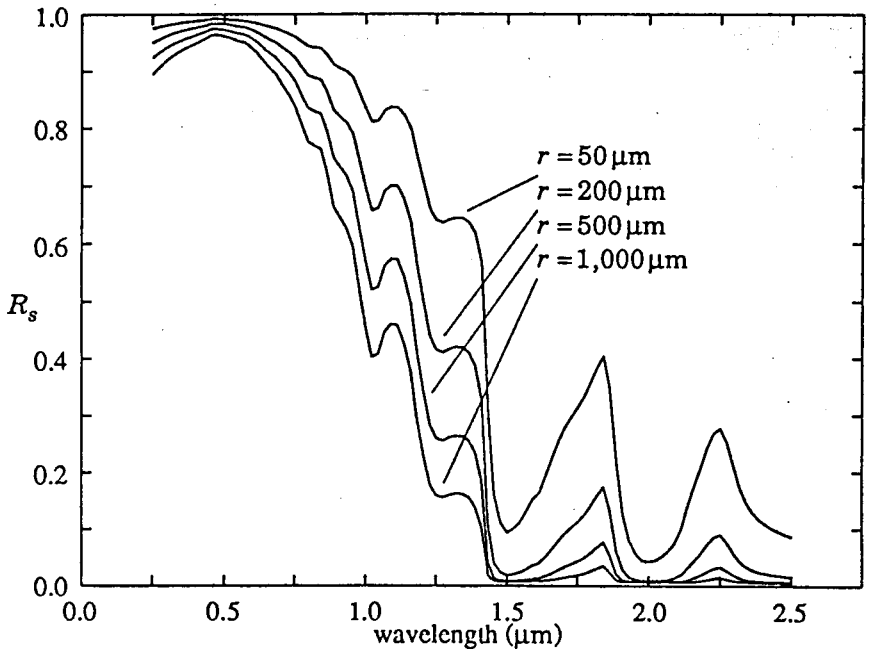

Figure 4. Directional-hemispherical reflectance R_s of snow at illumination angle $\theta_0 = 60°$ for wavelengths from 0.4 to 2.5 μm and grain radii r from 50 to 1,000 μm.

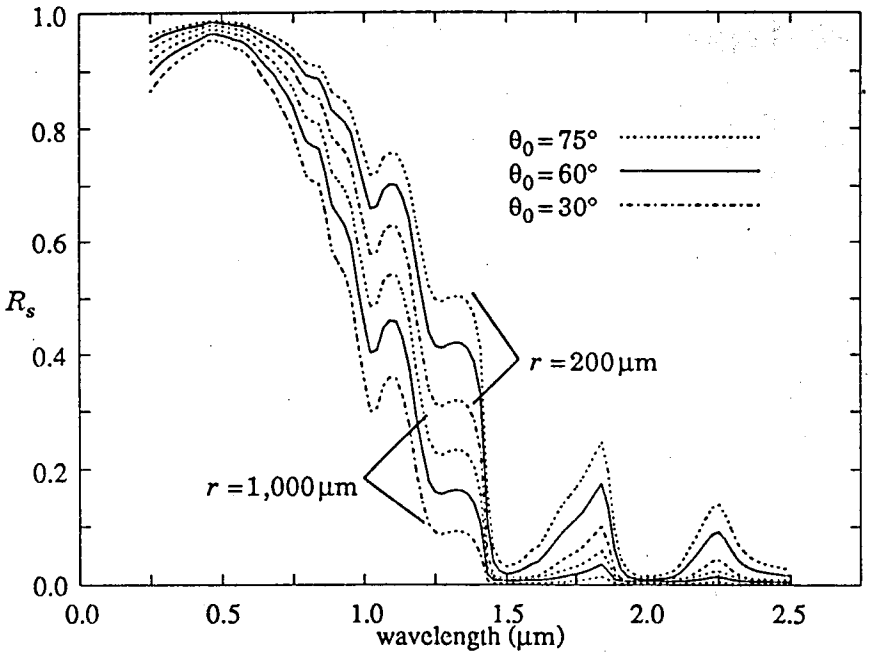

Figure 5. Directional-hemispherical reflectance R_s of snow at illumination angles $\theta_0 = 30°$, 60°, and 75°, for wavelengths from 0.4 to 2.5 μm and grain radii $r = 200\,\mu m$ and 1,000 μm.

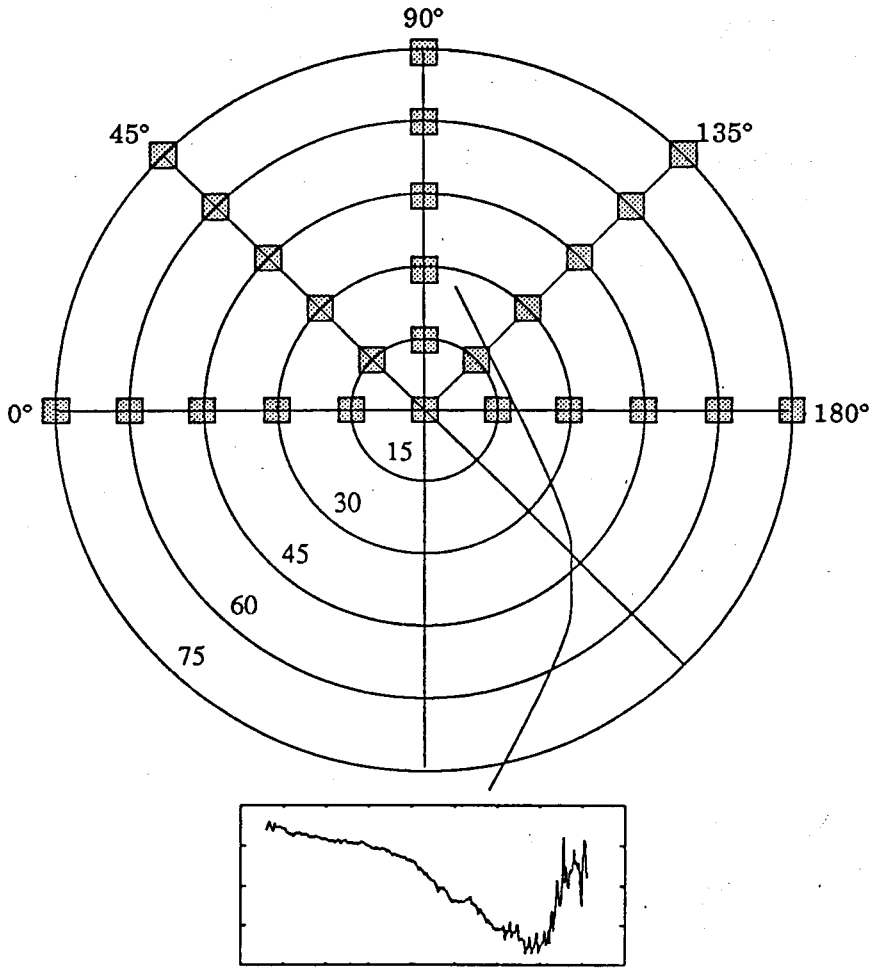

Figure 6. Viewing geometry of measurements. Spectral measurements were made at each of the indicated points on the polar diagram.

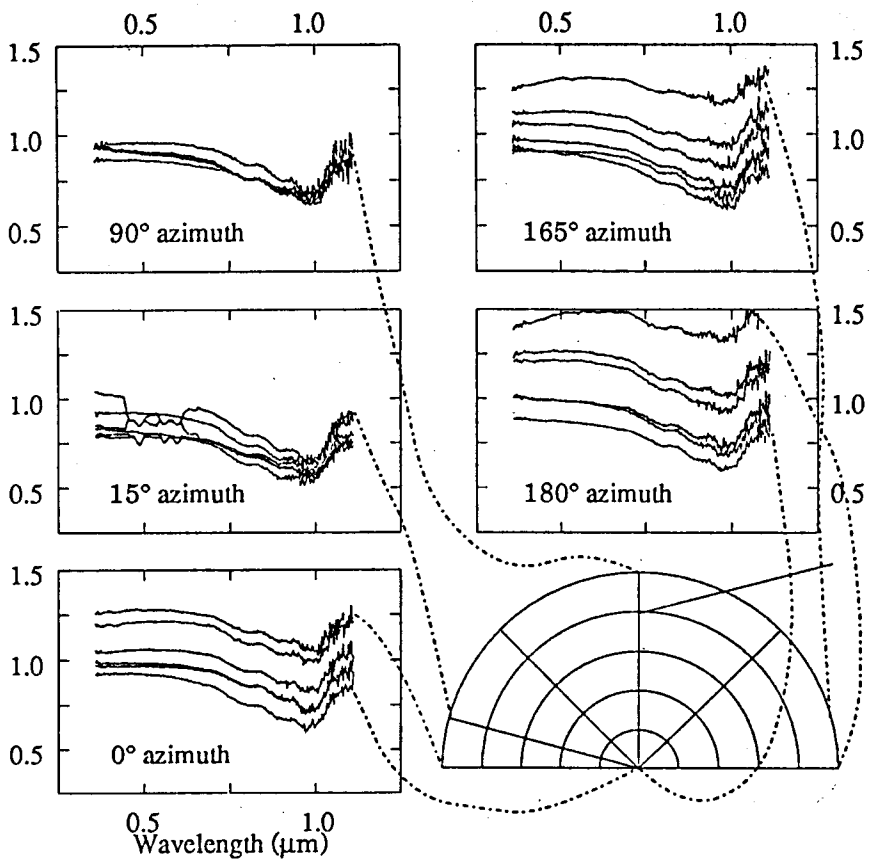

Figure 7. Spectral BRDF (×π) on March 30 ($\theta_0 = 50°$): 15 days since last snowfall; density 326 kg m^{-3}; equivalent spherical grain radius 190 μm; wetness of surface layer 3%.

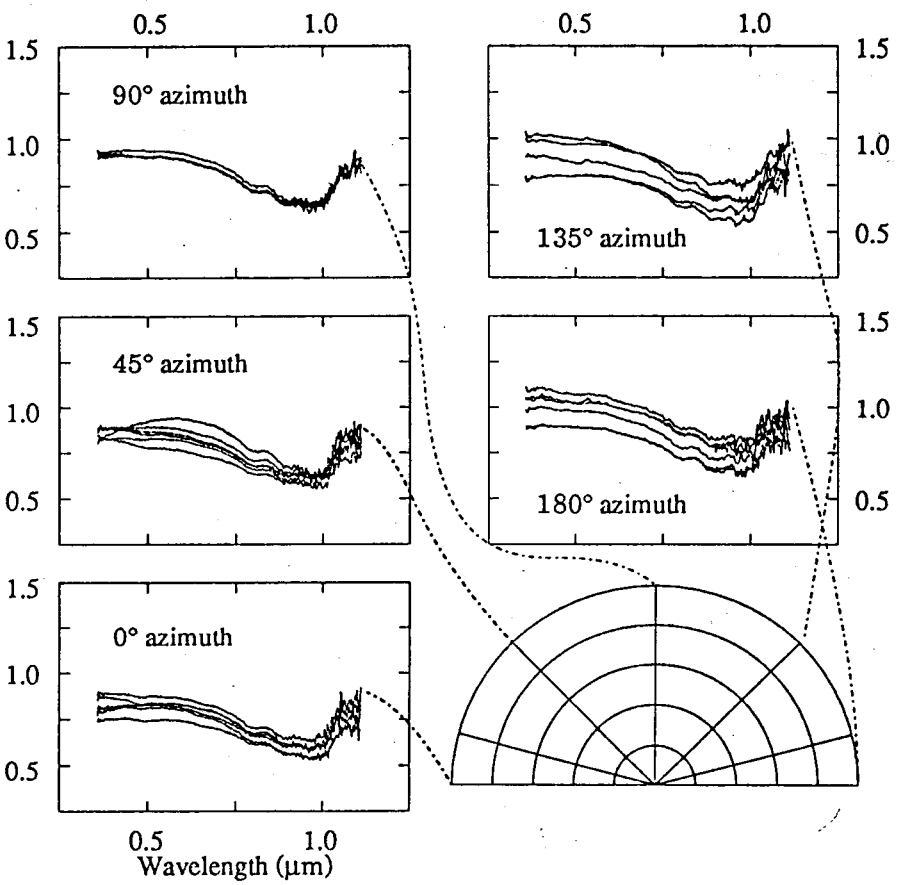

Figure 8a. Spectral BRDF ($\times\pi$) on April 22 ($\theta_0 = 40°$): 20 days since last snowfall; density 461 kg m^{-3}; equivalent spherical grain radius 380 μm; wetness 2%.

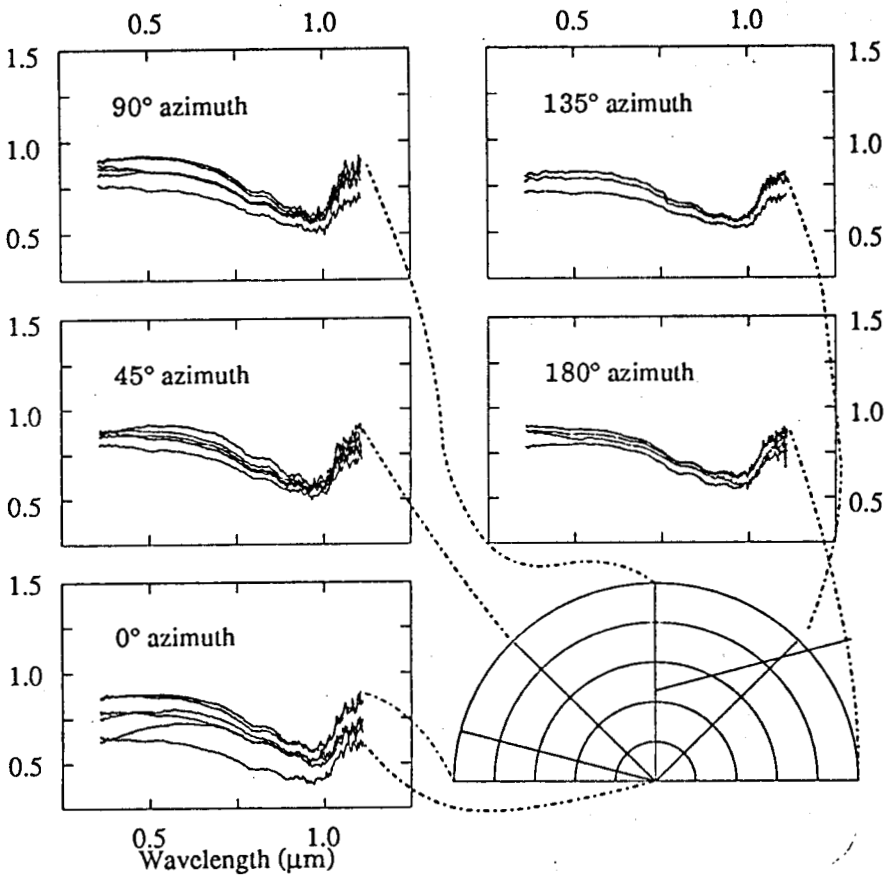

Figure 8b. Spectral BRDF ($\times\pi$) on April 22 ($\theta_0 = 30°$): 20 days since last snowfall; density 461 kg m^{-3}; equivalent spherical grain radius 380 μm; wetness 4%.

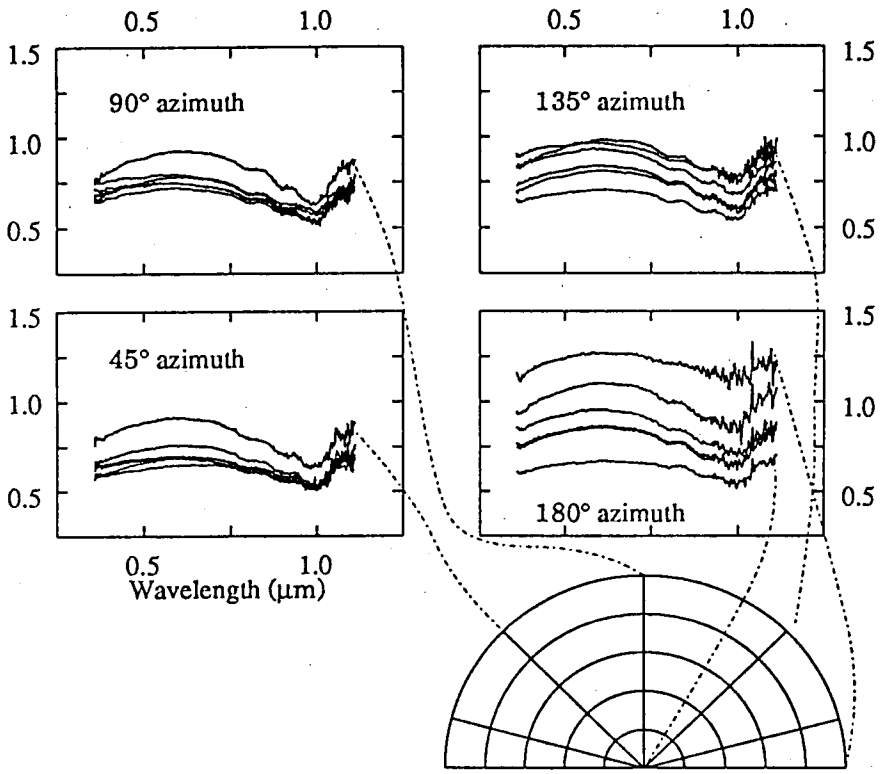

Figure 9a. Spectral BRDF (×π) on May 6 ($\theta_0 = 50°$): 34 days since last snowfall; density 547 kg m^{-3}; equivalent spherical grain radius 440 μm; wetness 1%.

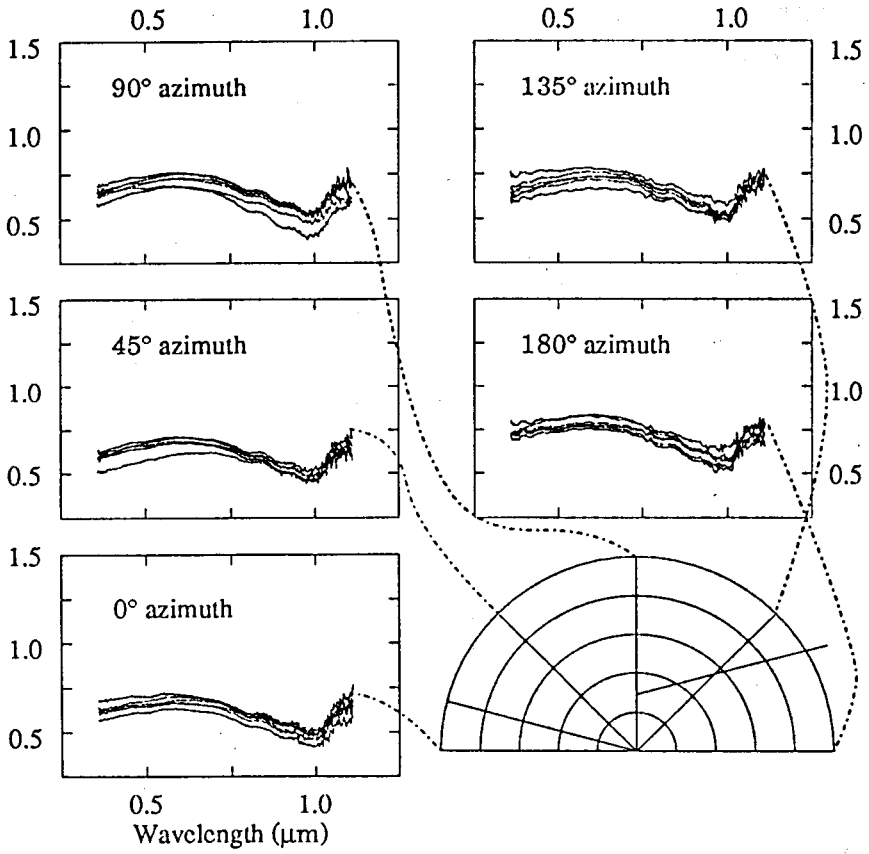

Figure 9b. Spectral BRDF ($\times\pi$) on May 6 ($\theta_0 = 30°$): 34 days since last snowfall; density 547 kg m^{-3}; equivalent spherical grain radius 440 μm; wetness 3%.

Draft 8/21/86

Reflected Solar Radiation from Snowpack

A.T.C. Chang[1], J. Dozier[2], K.S. Brown[1] and R.E. Davis[2]

1. Goddard Space Flight Center, Greenbelt, Maryland
2. Geography Department, University of California, Santa Barbara, California

ABSTRACT

Reflected solar radiation is a major and often varying parameter contributing to the net radiation budget over the earth's surface. Snowpacks, which cover approximately 40 million km^2 of the earth's surface in high winter, reflect about 80% of the incident solar radiation. Depending on surface roughness, snow crystal size, and contaminates, snow reflentances can vary widely. Accurate evaluation of the net radiation over snow fields requires detailed knowledge of the bidirectional reflectance distribution function (BRDF) and its relationship to typical snow conditions. From this knowledge and remote sensing data it may be possible to obtain timely reflected solar radiation distributions over large snow areas when the snow BRDF can be fitted to discrete band multispectral radiometer data.

In the past, the snow BRDF has received very little attention. Yet these measurements when coordinated with snow condition and runoff data can significantly improve our understanding of snowmelt processes, water survey, and climate modeling. A field experiment designed to further our understanding of the snow reflectance relationship has

been carried out at a test site near Mammoth Lakes, California. Snow reflentance , snowpack characteristics, and snowmelt were measureed simultaneously. The most critical engineering factor of the initial investigation was the instrument measuring speed. This effect complicates the extraction of snow reflectance due to atmospheric and solar angle changes. Preliminary results from the observed data appear to match model calculations. The measured reflectances from new snow (r=0.1mm) are within 5% of the model calculations and from old snow about 10%. This is because the model calculations did not take into account the effect of the contaminents accumulated in the snow due to aging.

INTRODUCTION

Reflected solar radiation is a dominant component of the energy balance over snowpacks. It has been established from theoretical studies that this component varies with snow and bidirectional conditions and cause large changes in reflectivity within the spectral region from 400 to 1800 nm (Wiscombe and Warren, 1981; Choudhury and Chang, 1979). Approximately 90% of the solar spectral irradiance lies within this region. Under typical weather conditions, the reflectivity can fall from 90% to 50% in a matter of days. During this period there is a significant change in the local global energy balance which of course is predominately driven by the upwelling radiation. At the same time, snow properties are making a transformation impacting the

snowmelt runoff estimates. The in-situ reflectance measurements will improve the modeling of the net solar budget if the snow conditions can be taken into account. Of course, a direct and fundamental goal is to build a snowpack runoff model for vital hydrological research in projecting water resources. For these reasons, it is necessary to observe and understand the relationship between snow condition and snow spectral reflectance.

The goal of this program is to use this information to aid in the projection of water resources estimates for areas like Southern California which rely on snowmelt for potable water supplies or areas like Colorado which use containment systems to regulate the rate of outflow from large masses of snowpack. Additoinal applications for the data in climatic reaearch are promising. The condition of the land surface plays a predominate role in the seasonal variance of solar radiation and atmospheric heat transport. The modeling of reflectivity with respect to snow condition could improve the climate anomally investigations. In pursuit of this goal, a field experiment was conducted at a California test site near Mammoth Lakes area to collect data for determining the bidirectional reflective properties of snowpack with respect to varying snow conditions.

The experiment attempted to initially evaluate the measuring apparatus, a spectroradiometer operated under unusually severe field conditions at the snow site. Very little emphasias has been given this type of experiment in

the past, most measurements have not focused on the snow state aspects vital to this investigation nor has an apparatus been especially developed for use in the hostile environment. Most measurements have been conducted in the the laboratory with laboratory equipment. An added difficulty was that this demonstration was made in a test site located at an elevation of 3km in open terrain subject to heavy yearly snow activity.

INSTRUMENTATION

Scientific requirements for a field instrument measuring snow reflectivity are similar to those for investigating solar spectral irradiance. In the range from 400 to 2500 nm where 90% of the extraterrestial solar radiation is found snow reflectivity changes with surface conditions. Hence an instrument originaly developed to measure solar irradiance from an aircraft platform appeared to be a reasonable choice for initial studies. The instrument was called the Solar Energy Monitor In Space (SEMIS) aircraft model (Thekakera, 1976). It's general specifications include; a spectral range from 500 to 2500 nm; 7 degrees field of view; prism monochrometric dispersion; and dual channel detection. When operating from a fixture in the snowfield the sample area 25 cm in diameter. The time to complete scaning the spectral range is twenty minutes, ten minutes to make a scan and ten to back up to the start position. Overall size complete with

ruggedized case, is approximately 50cm x 30 cm x 20cm, and total weight is 25 kg.

A diagram of the optical layout appears in Figure 1. Light from the target enters the system through an aperture slit. It strikes a collimating mirror and then it passes through a quartz prism. The dispersed monochromatic light leaving the prism is then refocused and exits the monochrometer through a slit which, like the entrance slit, is approximately 2 x 10 microns in size. The narrow band light from the monochrometer is modulated at 600hz by a tuning fork type chopper. The specular chopper blade not only chops the light but also acts as a dichroic, alternately bending the light onto the infrared detector when interrupting the straight through path to the visible detector.

Active thermal control of the detector packages limits signal gain deviations caused by large swings in temperature. Each detector element is packaged in its own hermetically sealed case on a thermalelectric wafer. The window is made of quality quartz glass. Also within the case are two thermistors. One is used in the circuit which dynamically cools the wafer and the other is used to check the assembly temperature. Heating and cooling are both performed by the thermoelectric device which keeps the assembly temperature between 0 and 2 C. The maximum signal to noise ratio in the visible and infrared channels are 250 at 880nm and 98 at 1800nm, as shown in Figure 2.

A scan of the spectrum occurs as the prism rotates dispersing monochromatic light onto the detectors. Prism rotation is driven by a stepper motor and cam. The complete cycle of the cam is approximately 20 minutes,ten of which is in the scanning phase and ten to return to the beginning of the spectral interval. During the scan the two detectors continiously respond to the monochromatic light and produce chopper modulated signals. These are demodulated synchronously, filtered and buffered. The analog outputs of detectors and the start of scan marker are acquired by a processor which converts the analog signals to digital counts. The digitizer sampling of the signal is controlled by timing with respect to the start of scan. The detector signals (0 to 5 Volts) are quantized to 12 bit code and their sample position corresponds to the spectral band position of the monichrometer at the time of sampling. These scan digital counts are stored as a file on a diskette with header data which records day and time and other test information.

CALIBRATION PROCEDURES

Conversion of the data from digital counts to the spectral irradiance in flux density units required a calibration of the response to controlled standards. Three calibration proceedures were required; (1) determine wavelength as a function of sample number referenced to the start of scan; (2) conversion of standard irradiance input

traceable to a National Bureau of Standards measured source; and (3) a check of the spectral response linearity.

Spectral wavelengths were assigned to the ordered position of the amplitude digital samples. For those near the start of scan, corresponding to wavelengths from 300 to 1000 nms, a low pressure mercury lamp was used to locate the standard emmission lines. At wavelengths in the near-infrared, discrete filters were used.

To convert counts to radiance, a Quartz Halogen lamp standard irradiance source was used. The input vs. output response curve from this test was shown in the previous section as figure 2. To relate the response curve at a particular spectral band to variations in detector gain, a linearity check has been run. The source for this test is an integration sphere illuminated internally by twelve lamps. As combinations of lamps are switched on the output radiance (input to the instrument) is raised. The plot of all points relates the liearity function at specific spectral frequencys.

Using the calibration data irradiance was computed. Figure 3 compares the calculated input solar spectral radiances for midaltitude winter atmosphere at 2900m, and typical reference measured radiances after calibration. The values of solar radiances are within 15% of the calculated input solar radiance. By comparing the position of the absorption lines, the errors of wavelength determined by the present method is less than 50 nm.

Reflectivity can be obtained in situ by referencing the sample target response to that of a standard reflence target. The standard target used in this field trial is formed from halon. This is a powder which has good stability and high overall reflective values in the range from 300 to 2500 nms (Weidner and Hsia, 1981). Besides its excellent diffuse characteristics, it is impervious to moisture under most of the field conditions. The target used is 30 x 30 cm.

FIELD OBSERVATIONS

During the winters of 1983-1984 and 1984-1985 field experiments were conducted in a testsite near the Mammoth Lakes, California. The spectroradiometer data were collected routinely with varying incidence angles and snow conditions. A complete set of bidirectional reflectivity observation for a particular arzimuth angle consists of spectral scans of the snow, spectral scan of Haylon target, and scans of a low pressure Mercury lamp. Scans of the snow were made at six angles, starting at nadir and extending out to 75 degrees. These scans were facilitated by the yoke mount assembly shown in Figure 4. The data was sequenced as follows, scan the halon target, scan the mercury lamp and then scans of the snow at the following angles: 0, 15, 30, 45, 60, and 75 degrees. The time for taking this set of data was 160 minutes. Solar zenith angle variation is obtained by data taken from different time of the day. The arzimuth angle variation was controlled by rotating the

radiometer mounting to lineup on compass headings. Since the time to obtain a complete set of angular reflectivity data was inordinately long, changes in solar irradiance were a problem. Incoming solar and reflected solar albedo were routinely measured along with other in situ measurements such as temperature, density, grain size and free water contents. Samples of the snow were removed from the local area for further analysis in the cold laboratory. The density, grain size and free water content were determined by laboratory techniques (Davis, 1986).

DISCUSSIONS AND PRELIMINARY RESULTS

During the winter of 1983-1984 efforts were concentrated on setting up and to evaluate the applicability of this instrument for snow reflectance measurements. The instrument seemed to function well in the cold weather. However the floppy disk units of the data system became intermittant when the air temperature was below -3 C. This problem was resolved by warming the drives with heating elements. In the winter of 1984-1985, many data sets were collected over different snow conditions for clear, partly cloudy and cloudy sky conditions with varying sun angles. Figure 5 shows a typical new snow reflectance for a clear sky. During the data collecting time the pyranometer's reading were almost constant. The reflectance result is quite comparable with the model calculations (snow radius = 0.1mm) reported by Choudhury and Chang (1979). Figure 6

shows snow reflectance from a old snow sample. The values are generally lower than thos shown in Figure 5. This is due to the change of snow crystal sizes which grow as the snow aging on earth's surface. The observed vaules are somewhat lower than the model calculations. This is because the model calculations did not take into account the effect of contaminants in the snow.

The major difficult of using this instrument in the field is that it takes approximately 10 minutes for the spectrometer to scan from 500 to 2500 nm. During the long data collecting cycle the solar input at the snow surface is subject to atmospheric variations (Byrd et al,1982). This variation of solar input might be corrected by utilizing the simultaneous pyranometer data taken during the data scanning period. To circumvent the difficulty of varying solar input one would conduct the experiment at night using artificial light sources. Thus the solar incidence angle, arzimuth angle and incidence angle can be totally controlled by artifical lighting. This experiment was carried out in the snow fields by using lamps mounted inside a 30 cm integrating sphere as light source. Due to low lamp efficiency and lack of sufficient electrical power to run all lamps, the reflected light level was too low to be detected by the spectroradiometer. In addition to the low light level, the uniformity of the artificial light spot was difficult to control. Due to these problems, the idea of using artificial light to replace the sun as light source

for reflectance measurements was not successful. It is difficult if not impossible to obtain bidirectional reflectance relationship using this instrument. Even though the measurements are accurate enough, the scanning time is the limiting factor for this instrument. Future instrument for the reflectance measurements should be possible to obtain the entire spectral responses in seconds.

REFERENCES

Byrd,R.E.,et al, 1982, "Solar Spectral Measurements In The Terrestrial Environment", Applied Optics, Vol 21, N0.8, 1430-1435.

Choudhury, B.J. and A.T.C. Chang, 1979, "Two stream theory of spectral reflectance of snow," IEEE Trans. GE, Vol. 17, 63-68.

Davis, R.E., 1986, "Snow property measurements correlative to microwave emission at 35 GHz," Ph.D. Dissertation, Geography Department, University of California, Santa Barbara.

Thekaekara,M.P., 1976, "Solar Energy Monitor In Space, (SEMIS)", SMM Proposal, Goddard Space Flight Center, Greenbelt, Maryland.

Weidner, V.R. and J.J. Hsia, 1981, "Reflection properties of pressed polytetraflouroethylene powder," J. Opt. Soc. Am. Vol. 71, 856-861.

Wiscombe W.J. and S.G. Warren, 1980, "A model for the spectral albedo of snow, 1, Pure snow," J. Atmos. Sci., Vol. 37, 2712-2733.

FIGURE CAPTIONS

(1) The optical layout of the Solar Energy Monitor In Space (SEMIS) spectroradiometer.

(2) The spectral responses curve for the visible and infrared detectors.

(3) Comparison of observed solar radiance and calculated solar radiance at 2900 m above sea level.

(4) York mounting assembly of the SEMIS spectroradiometer.

(5) Comparisons of observed and calculated reflectance of new snow (4/5/84).

(6) Comparisons of observed and calculated reflectance of old snow (4/27/85).

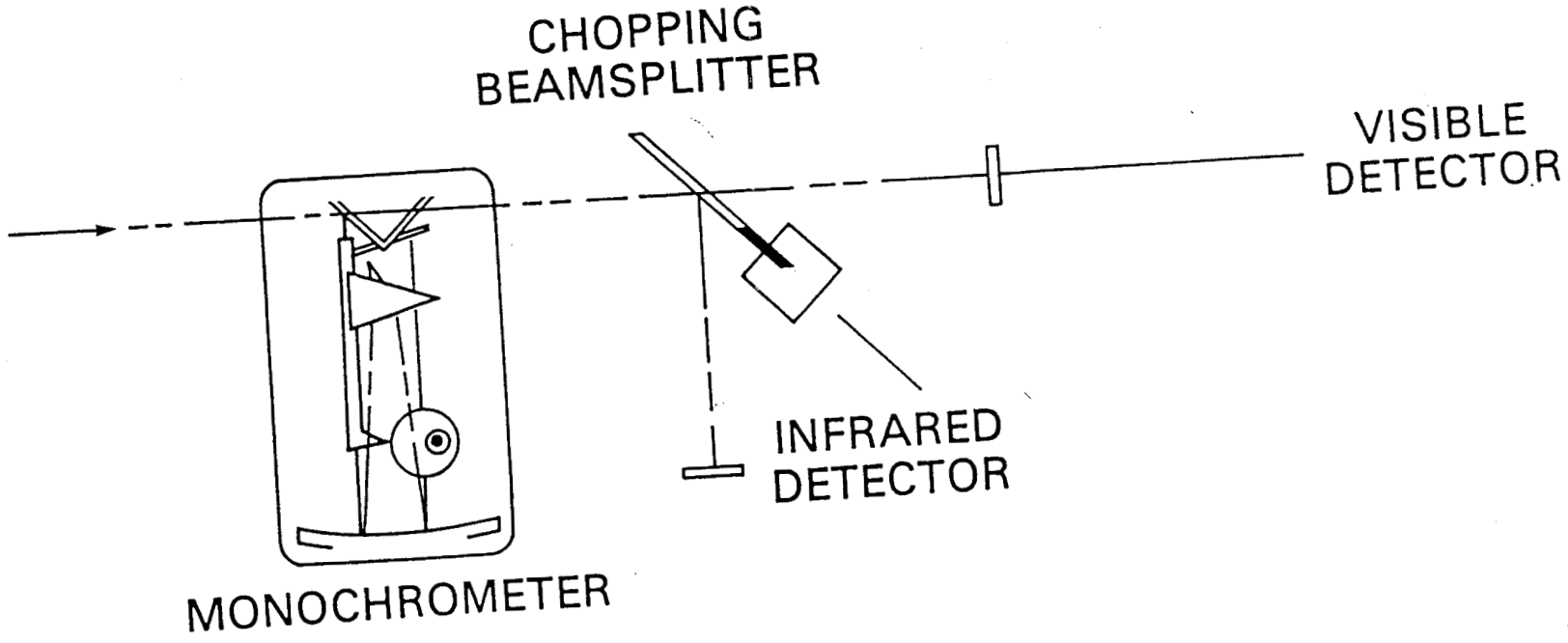
CHOPPING
BEAMSPLITTER
VISIBLE
DETECTOR
INFRARED
DETECTOR
MONOCHROMETER

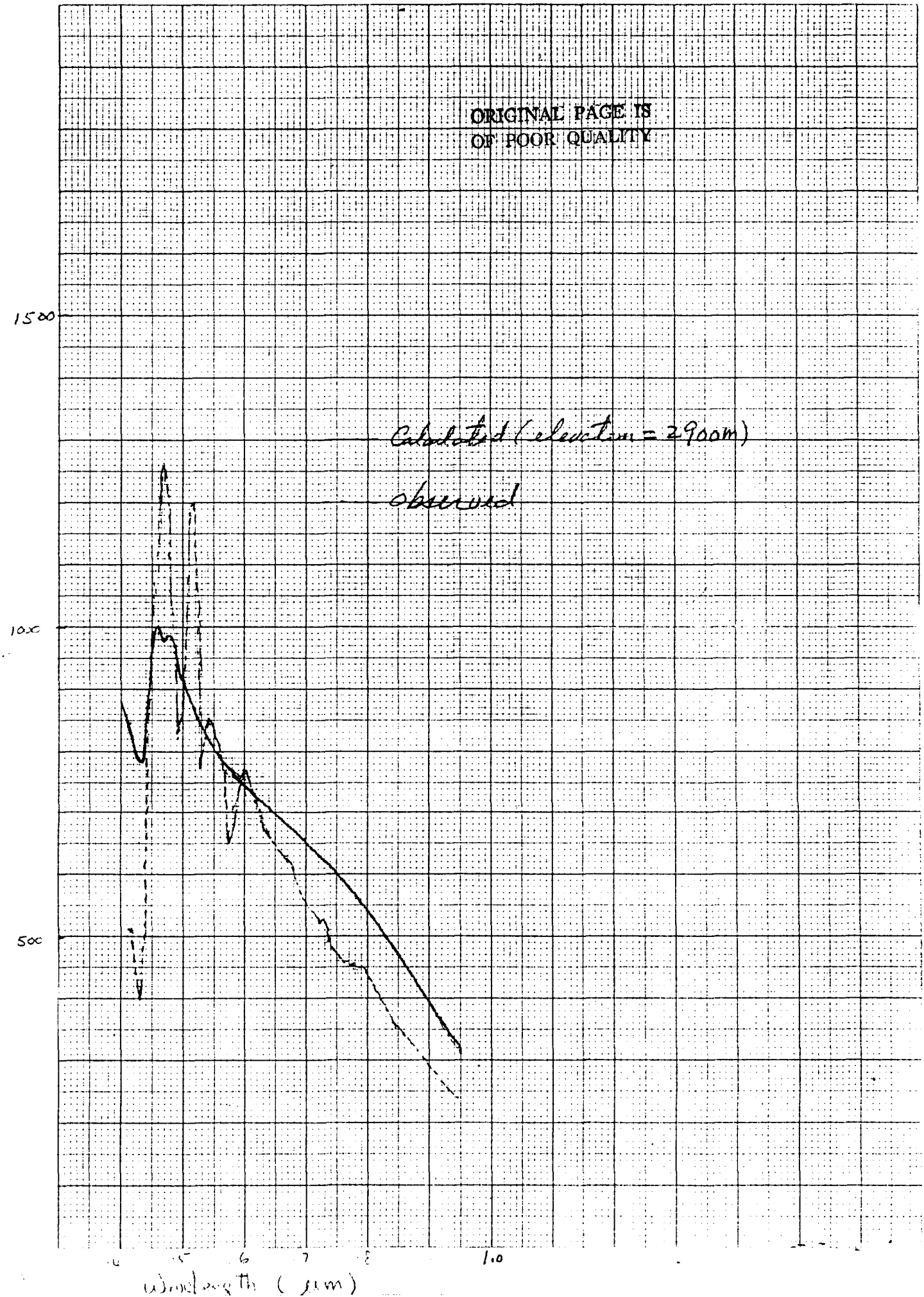

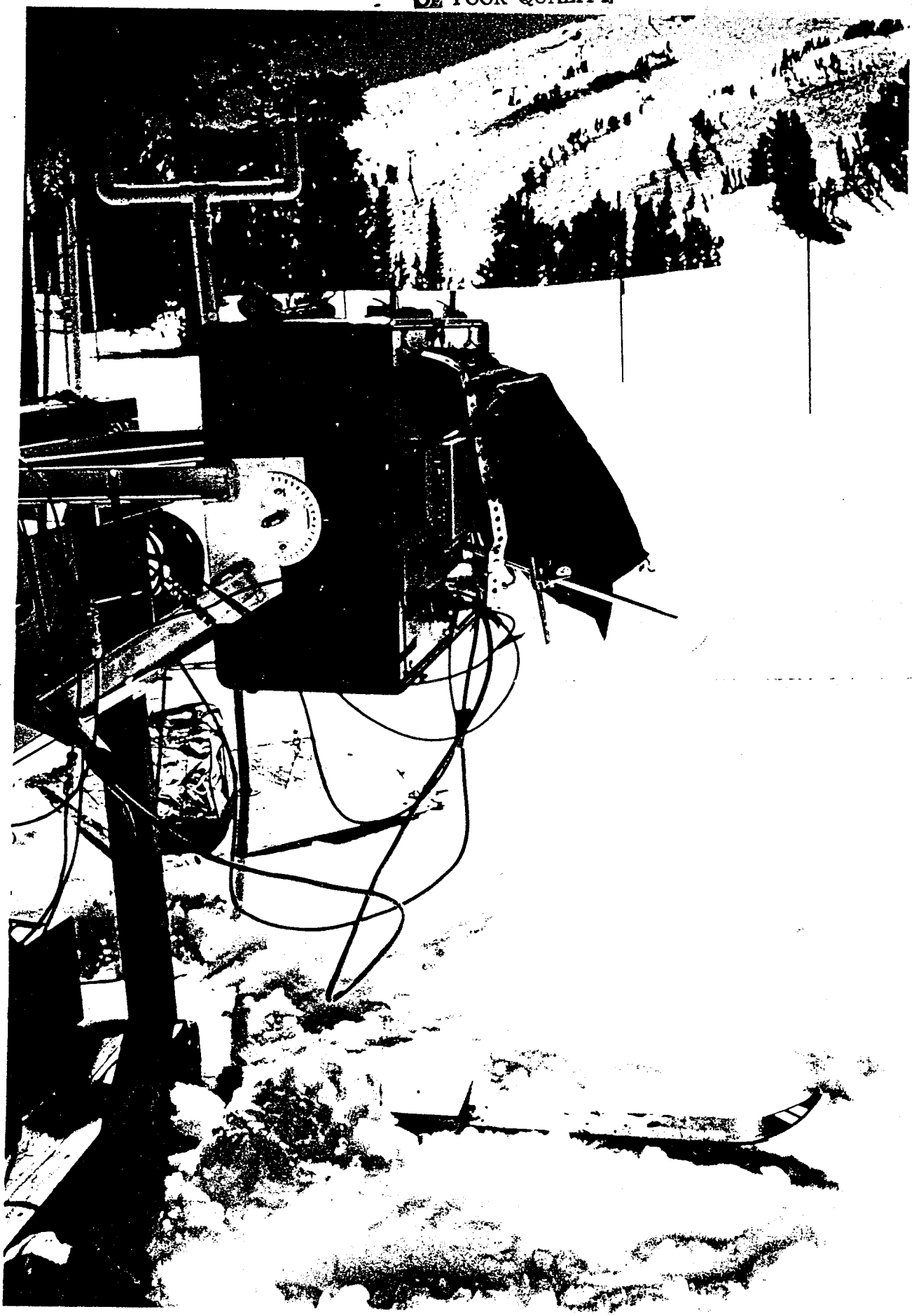

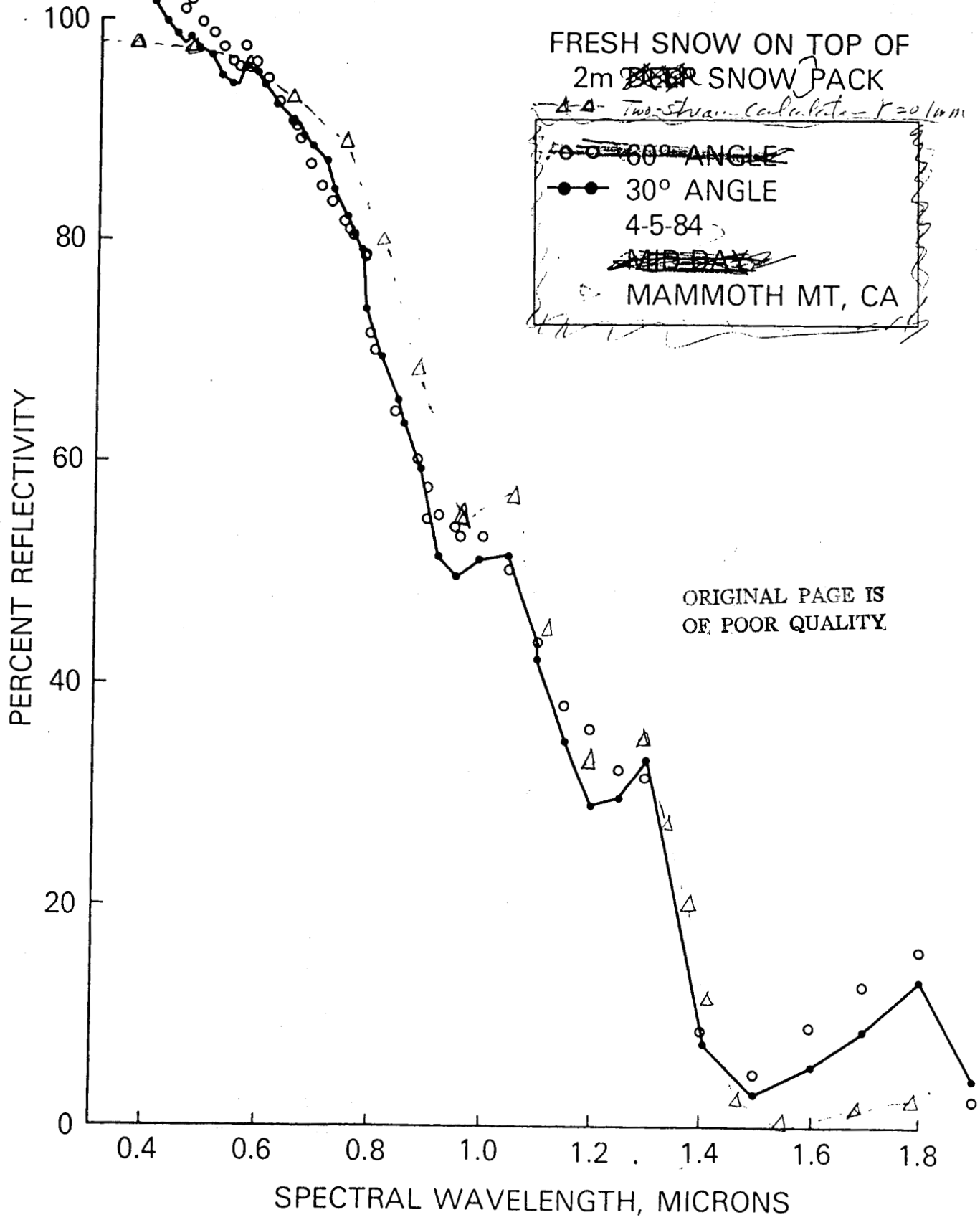

ORIGINAL PAGE IS
OF POOR QUALITY

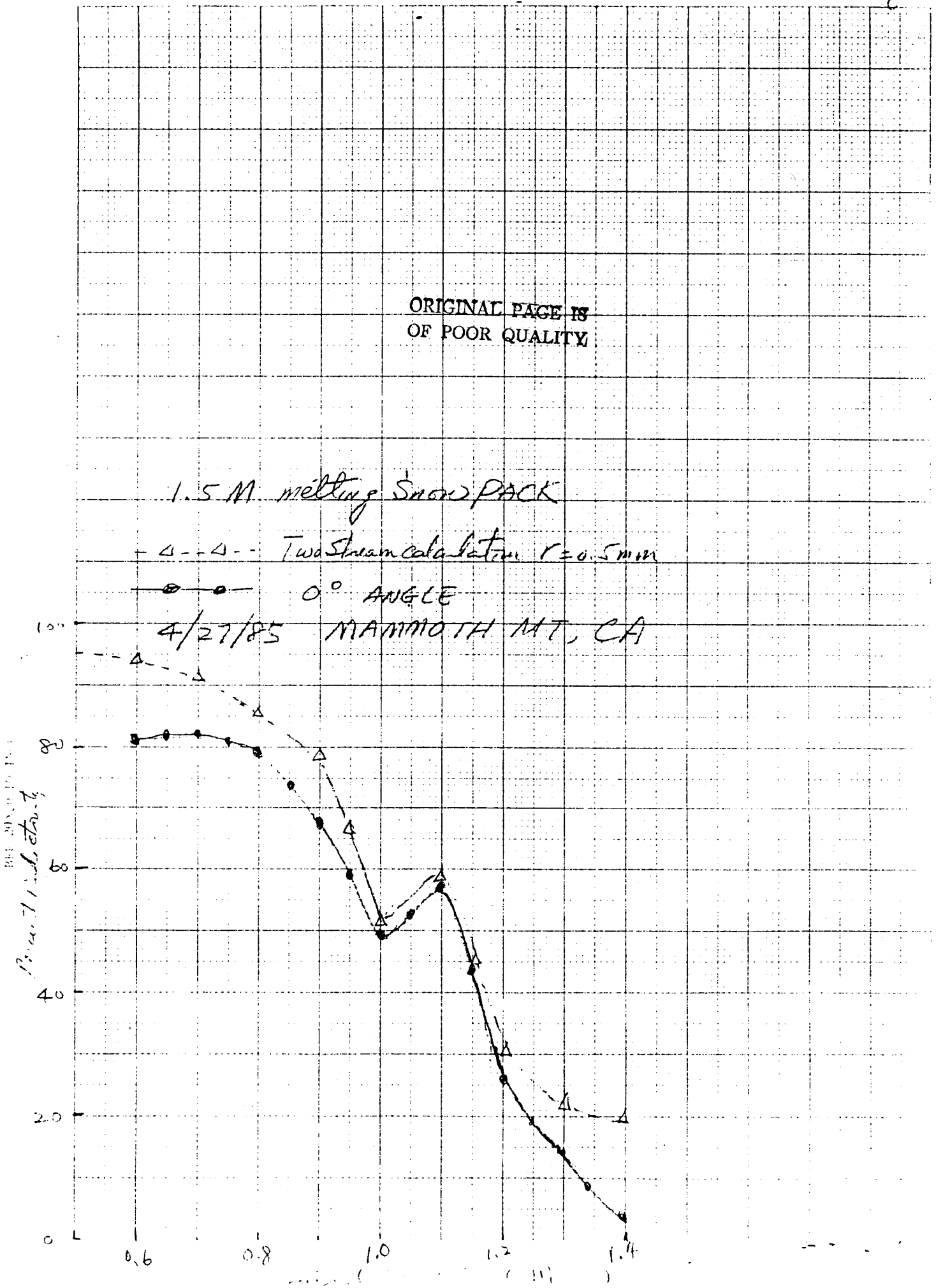

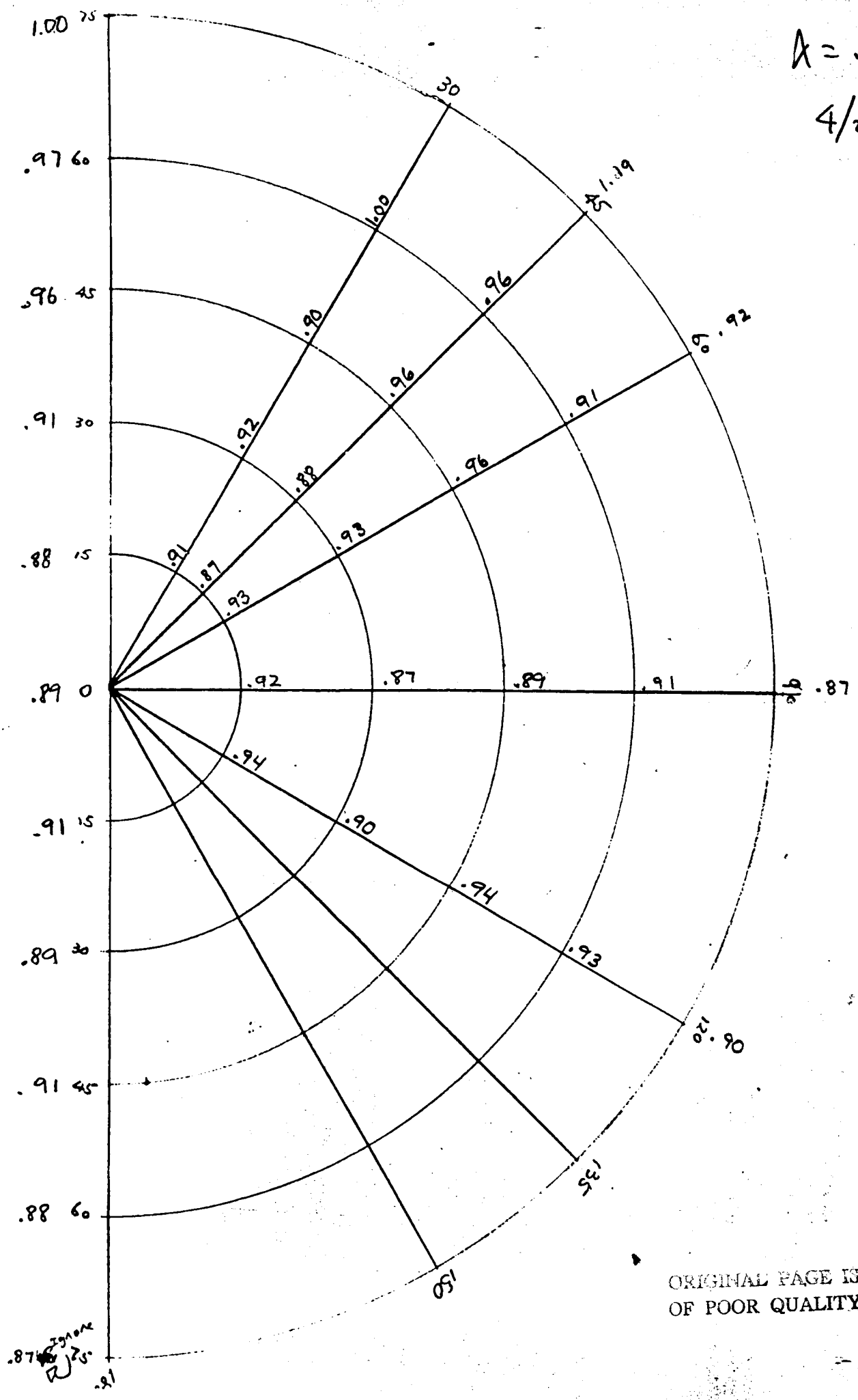

A = .5A

4/2

ORIGINAL PAGE IS
OF POOR QUALITY

$\lambda = .7\,w$

4/2

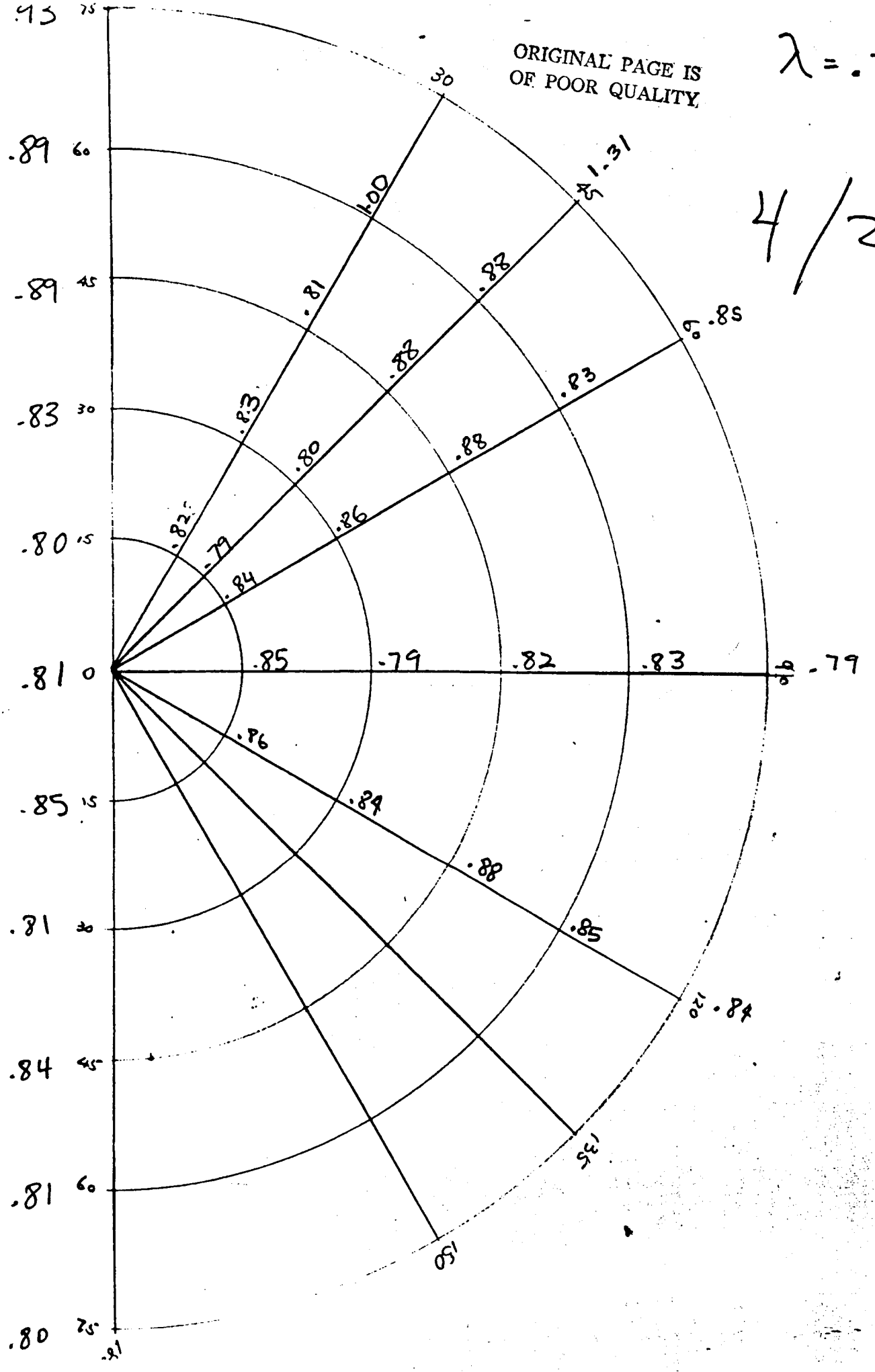

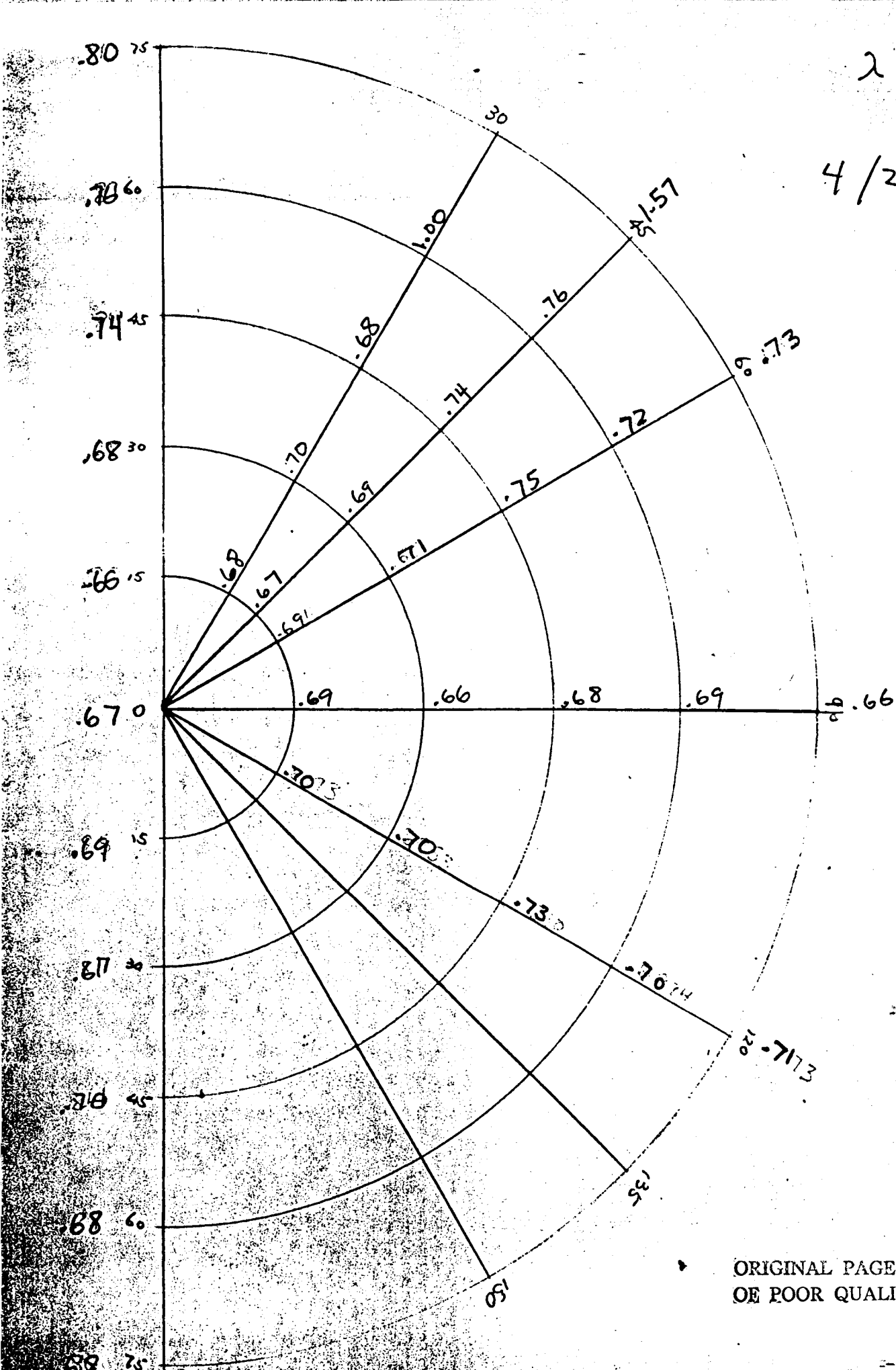

ORIGINAL PAGE IS
OE POOR QUALITY

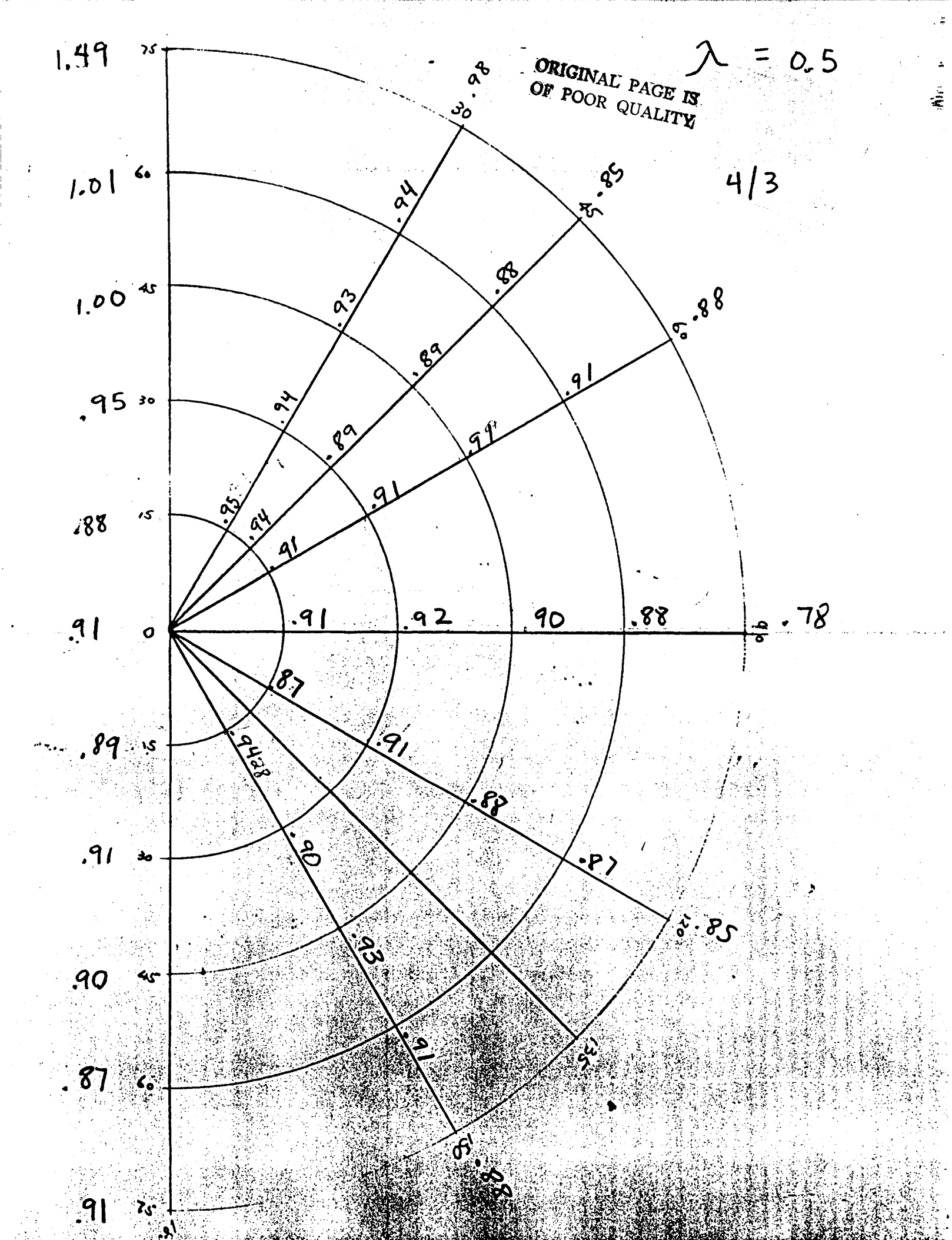
λ = 0.5
4/3
ORIGINAL PAGE IS
OF POOR QUALITY
1.49
1.01
1.00
.95
.88
.91
.89
.91
.90
.87
.91
75
60
45
30
15
0
15
30
45
60
75
90
105
120
135
150
165
180
.98
.85
.88
.78
.85
.88
.94
.93
.89
.94
.95
.94
.91
.91
.97
.91
.91
.92
.90
.88
.87
.91
.88
.87
.94
.90
.93
.91
.88

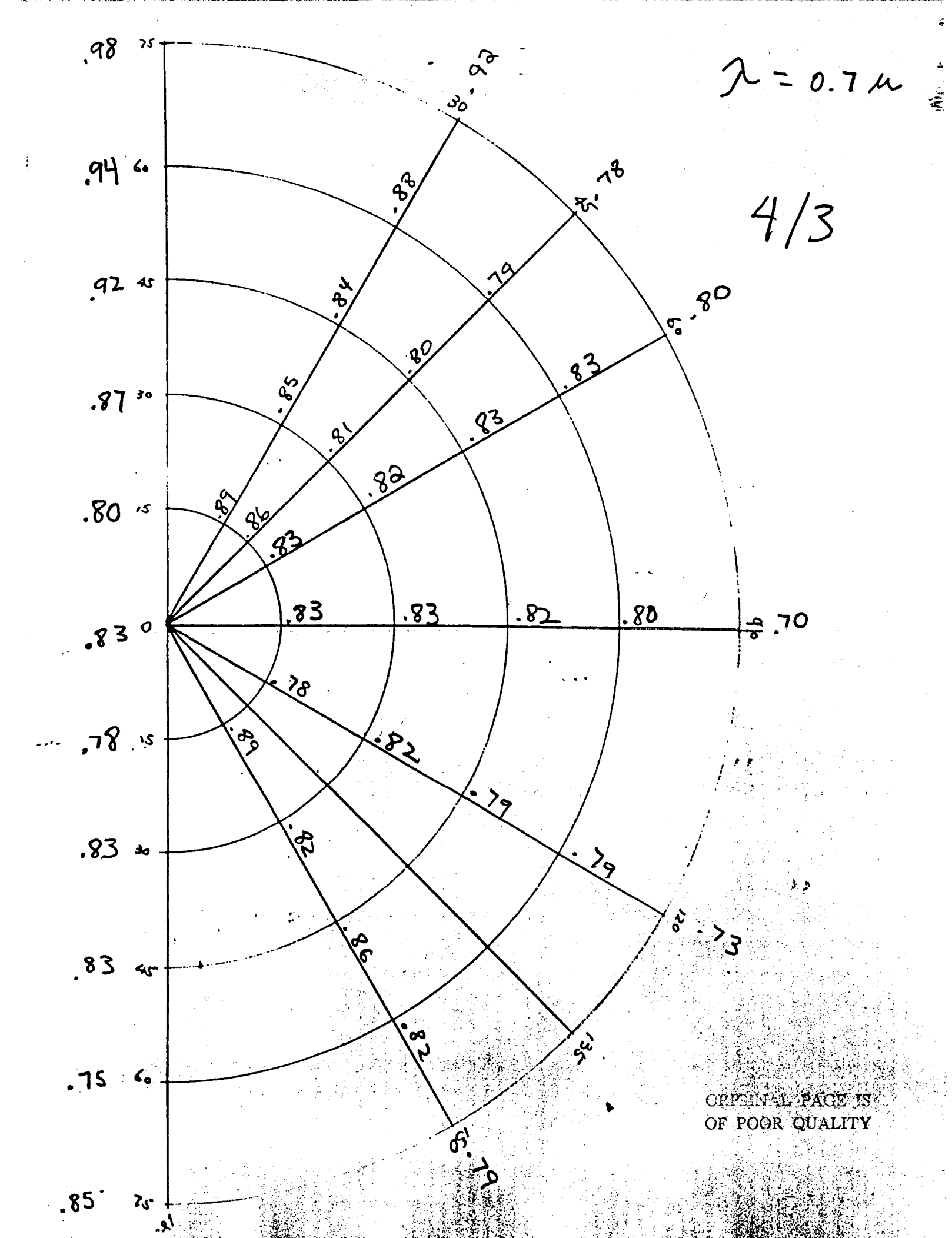
λ = 0.7 μ
4/3
.98
.94
.92
.87
.80
.83
.78
.83
.83
.75
.85
75
60
45
30
15
0
15
30
45
60
75
90
.92
.88
.84
.85
.81
.89
.86
.83
.78
.82
.89
.82
.86
.82
.79
.85
.79
.88
.79
.80
.80
.83
.83
.82
.83
.82
.80
.70
.79
.79
.73
120
135
150
OF POOR QUALITY

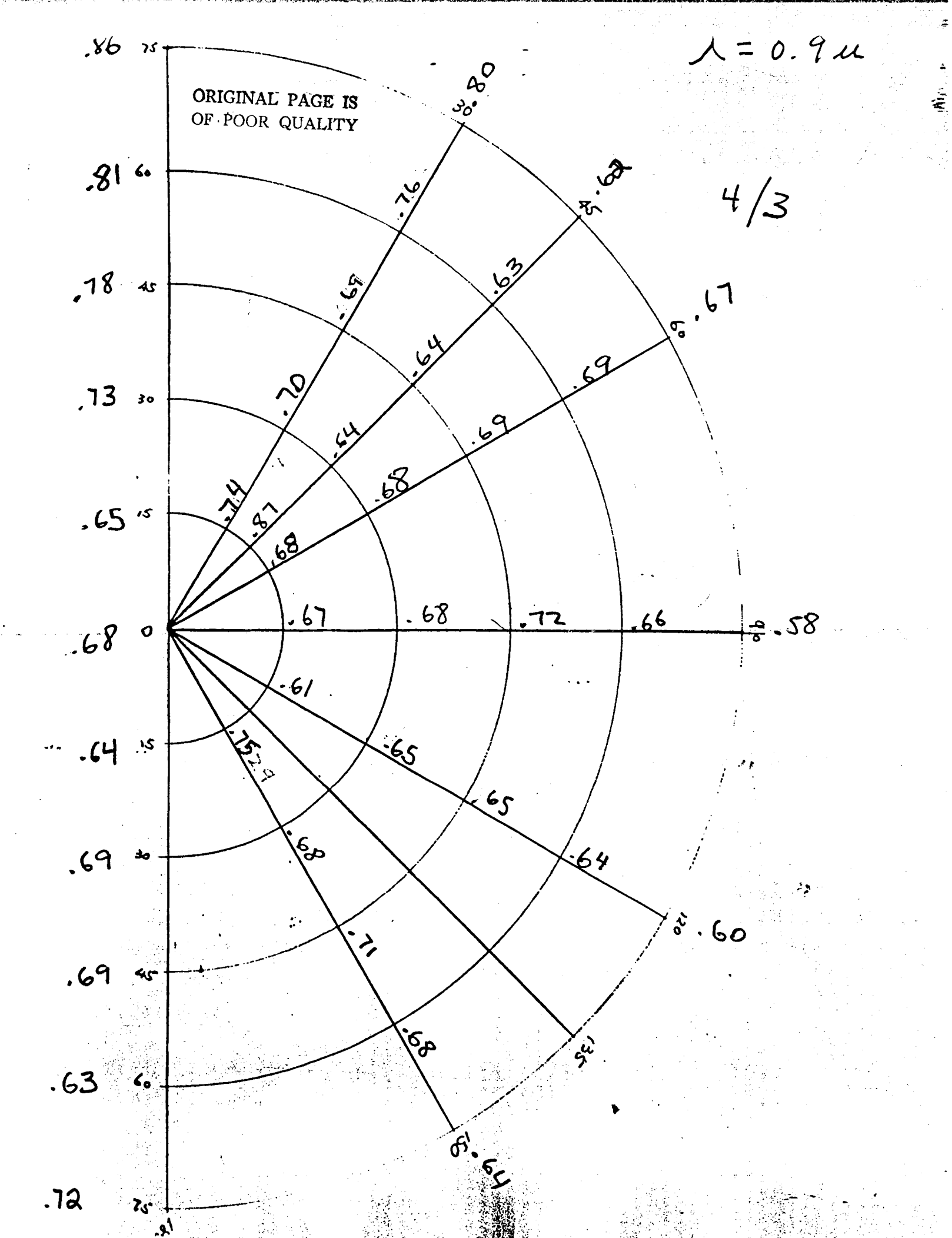
λ = 0.9 μ
4/3
ORIGINAL PAGE IS
OF POOR QUALITY
.86 75
.81 60
.78 45
.73 30
.65 15
.68 0
.64 15
.69 30
.69 45
.63 60
.72 75
.81
30° .80
45° .68
60° .67
90° .58
120° .60
135°
150° .64
.76
.69
.63
.70
.64
.54
.69
.74
.87
.68
.68
.67
.68
.72
.66
.61
.65
.65
.64
.68
.71
.68

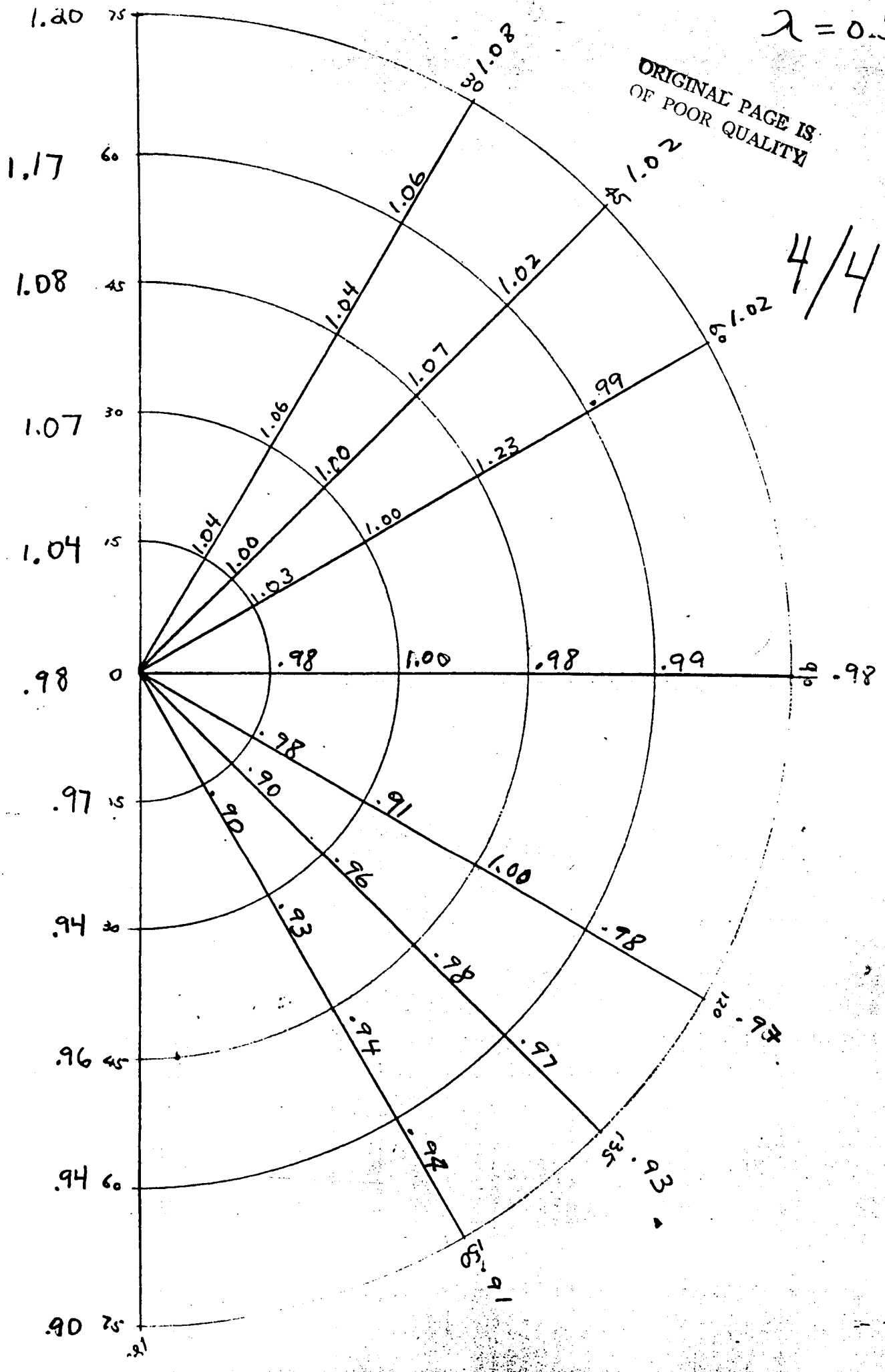
λ = 0.5 μ
ORIGINAL PAGE IS OF POOR QUALITY
4/4
1.20
1.17
1.08
1.07
1.04
.98
.97
.94
.96
.94
.90
75
60
45
30
15
0
15
30
45
60
75
90
105
120
135
150
165
180
1.03
1.02
1.06
1.04
1.07
1.02
1.06
1.00
1.23
1.04
1.00
1.00
1.03
.98
1.00
.98
.99
.98
.98
.90
.91
1.00
.92
.96
.98
.93
.97
.94
.94

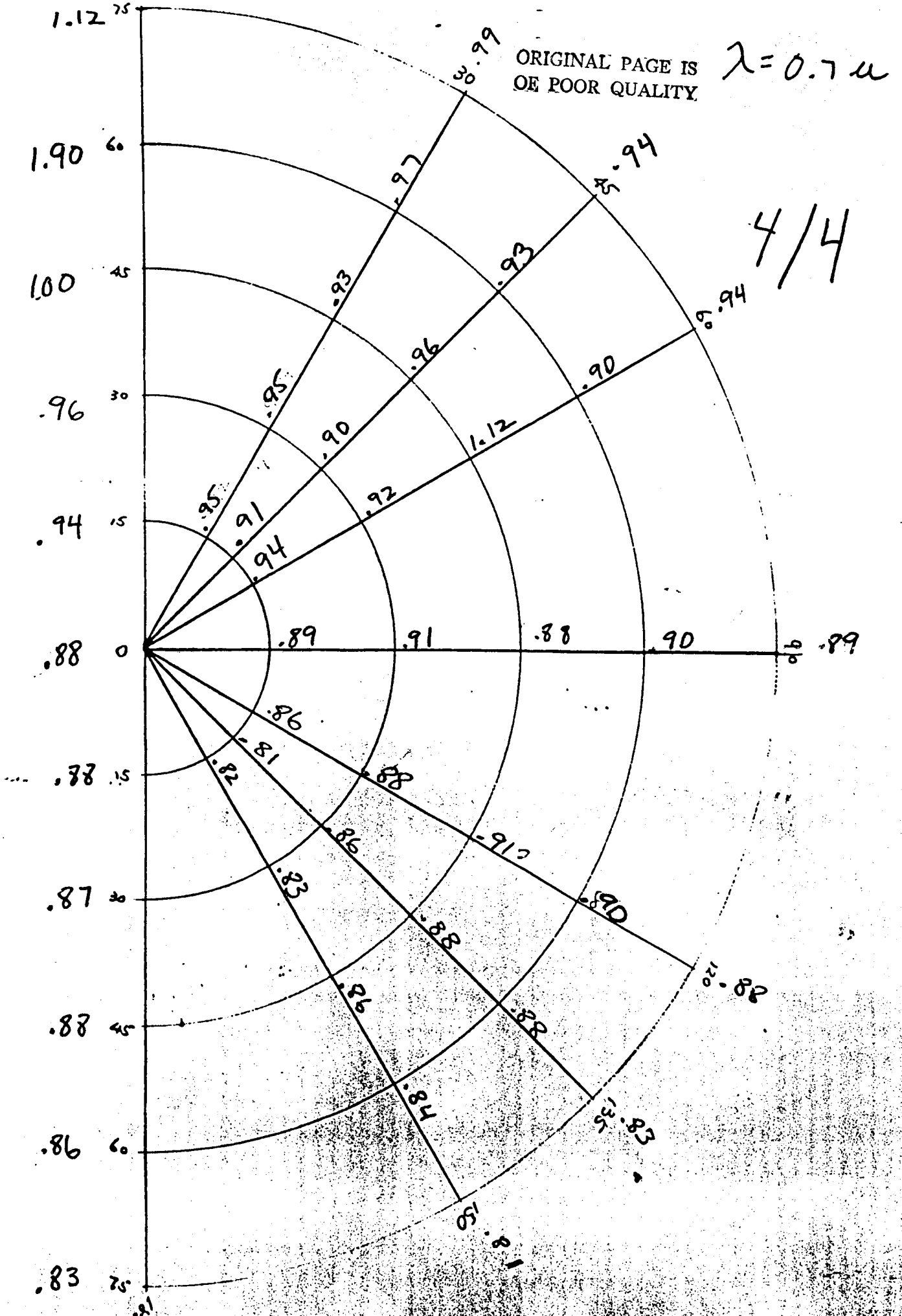
ORIGINAL PAGE IS
OE POOR QUALITY
λ=0.7 u
4/4
1.12
1.90
1.00
.96
.94
.88
.88
.87
.88
.86
.83
75
60
45
30
15
0
15
30
45
60
75
90
105
120
135
150
165
180
.99
.94
.94
.93
.93
.97
.96
.95
.90
.90
1.12
.95
.91
.94
.92
.89
.91
.88
.90
.89
.86
.81
.82
.88
.86
.91
.83
.90
.88
.88
.86
.84
.83
.81

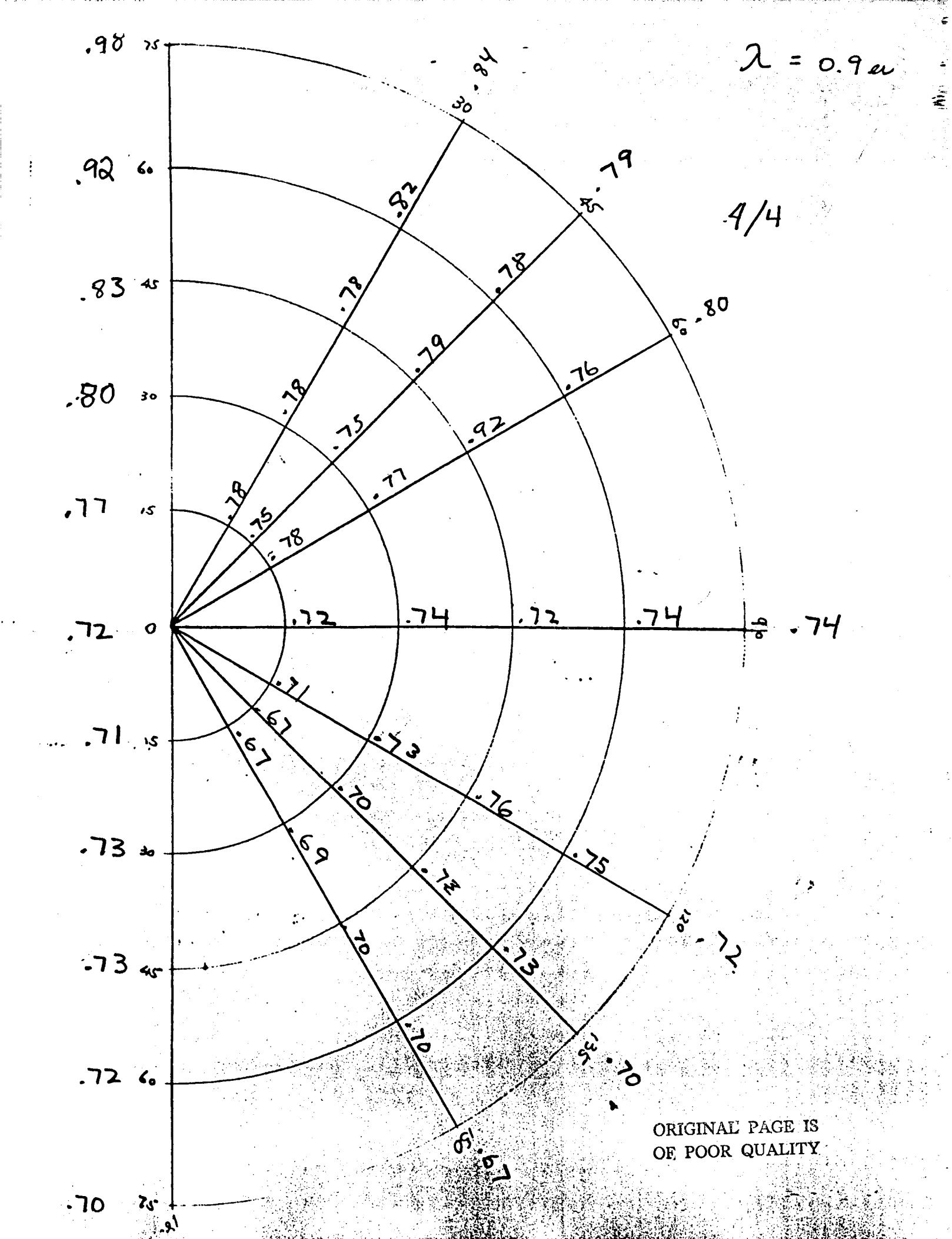

ORIGINAL PAGE IS
OF POOR QUALITY

$\lambda = 0.7$

4/6

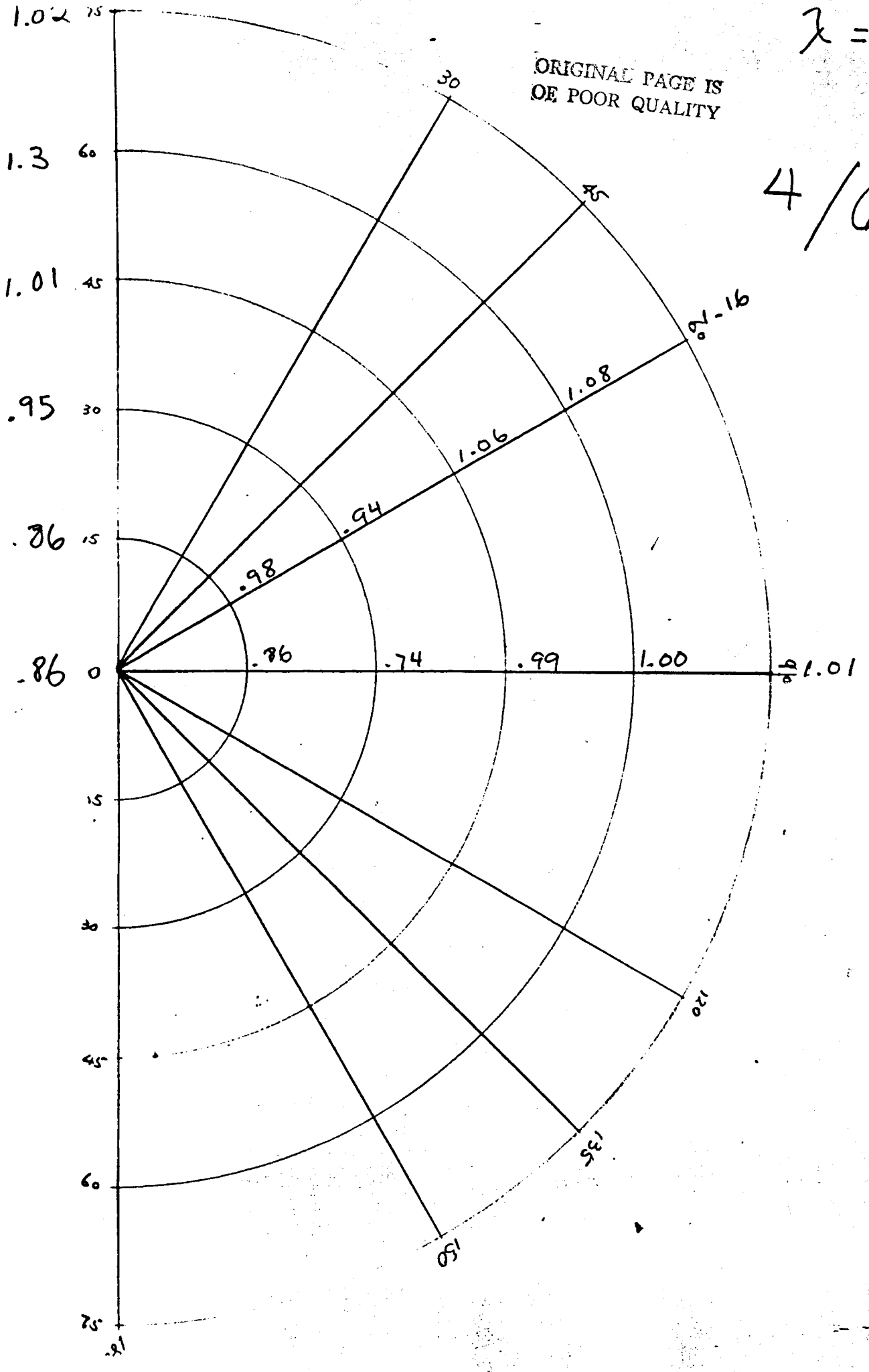

$\lambda = 0.9\mu$

4/6